DO NOT REMOVE FROM ROOM

except to make a copy

# ISENTROPIC ANALYSIS AND INTERPRETATION

## OPERATIONAL APPLICATIONS TO SYNOPTIC AND MESOSCALE FORECAST PROBLEMS

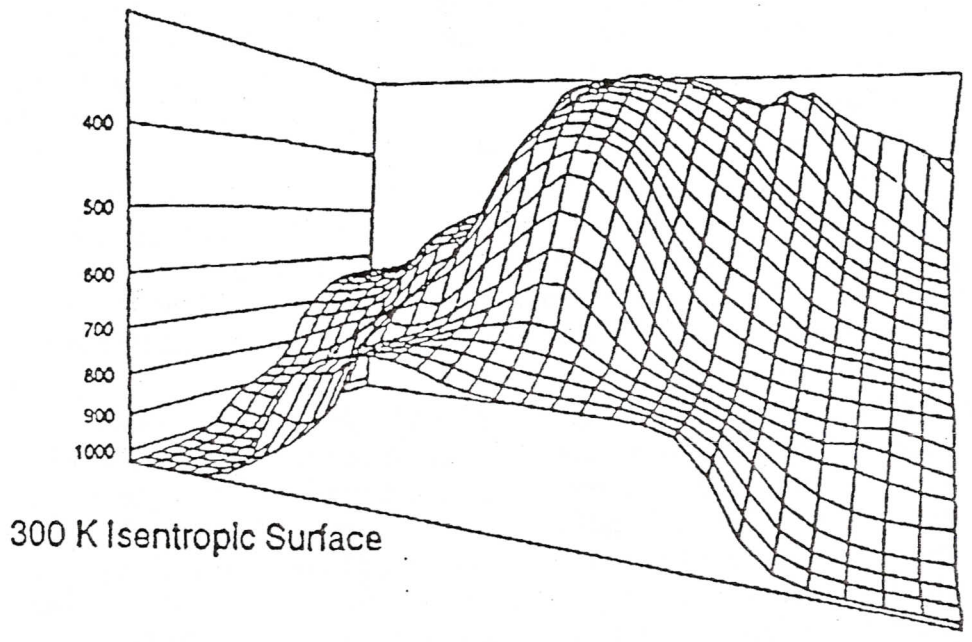


300 K Isentropic Surface

DR. JAMES T. MOORE
Saint Louis University

Department of Earth and Atmospheric Sciences
3507 Laclede Avenue
St Louis, Missouri 63103-2010

NATIONAL WEATHER SERVICE TRAINING CENTER
Kansas City, Missouri

JUNE 1993

# PREFACE

Before the changeover to pressure coordinates in the early 1940's, isentropic analysis was utilized extensively for diagnosing and forecasting weather systems. Since that time the advantages of the isentropic coordinate system and isentropic analysis techniques have been neglected in the curricula of both universities and training centers. The 1960's and 1970's saw a resurgence of isentropic analysis in the research community as it was well-suited to the needs of those studying atmospheric flow on both the synoptic and mesoscales of motion. This monograph has been written with the goal of presenting the isentropic viewpoint and methods of diagnosis in one volume that can be easily accessible to the practicing operational meteorologist. It is the author's hope that this information will help increase the use of isentropic analysis techniques in the field as a supplement to standard constant pressure analyses as forecasters attempt to diagnose and predict the three-dimensional flow associated with precipitation systems.

I would like to acknowledge that motivation for this paper came form Dr. Lawrence Wilson of the Atmospheric Environment Service in Canada who wrote a similar shorter paper for Canadian meteorologists. Several examples discussed in this text are borrowed from his training paper. Also, Anderson (1984) wrote a paper for the National Weather Service (NWS) Western Region describing isentropic analysis which is frequently referenced.

The author would like to thank Saint Louis University for offering a sabbatical leave during which time he was able to work on this manuscript. The people at the NSSFC were also very supportive and offered ideas on strengthening the text. Dr. Joe Schaefer, Director of the National Weather Service Training Center (NWSTC), Dr. Richard McNulty, Chief of the Hydrometeorology and Management Division of the NWSTC, and Mr. Pete Chaston, Technical Project Leader of the NWSTC were instrumental in implementing this material intc the NWS training program. Their support and enthusiasm for introducing isentropic analysis into the forecast routine through applications of material described in this text is deeply appreciated. Also, Dr. Dale Meyer, Mr. George Taniguchi, Mr. George Horn and Mr. Michael Squires of the Air Weather Service are to be thanked for their proofreading of the text. Last, but not least, the expert typing of Ms. Juanita Ryles, Ms. Jeanne Mueller and the assistance of Dr. Richard Molinaro at Saint Louis University are deeply appreciated.

TABLE OF CONTENTS

## ABSTRACT

A basic review of the isentropic coordinate system, including its advantages nd disadvantages for operational use, is presented. The primitive equations in sentropic coordinate form are discussed with an emphasis upon their physical neaning and interpretation. Isentropic analysis techniques for "horizontal" and ross sectional perspectives are described as aids for the diagnostic analysis of ynoptic scale weather systems. Numerous diagnostic parameters are discussed vhich can be excellent tools in identifying synoptic scale features helpful in forecast-ng cyclogenesis and regions susceptible to strong convection. The final section resents specialized applications of isentropic techniques to weather analysis and orecasting including: trajectory analysis, tropopause folding processes, conditional symmetric instability, short-term forecasting of severe convective threat areas, and aviation forecasting.

# I. INTRODUCTION

The motivation behind this paper is simple—I wanted to lay down the basic concepts of isentropic analysis and interpretation for those people in the "front lines" of meteorology, the practicing forecasters. Since the demise of the isentropic coordinate system in the 1940's, few academic institutions or training centers have taught isentropic meteorology as part of their synoptic or weather analysis and forecasting laboratory courses. More recently, that situation has been changing. However, there are several generations of meteorologists who have never been shown the advantages of isentropic analyses in diagnosing the current weather. Therefore, they are naturally reluctant to incorporate these charts into their daily forecasting scheme. The success of systems such as AFOS (Automation of Field Operations and Services) and McIDAS (Man-Computer Interactive Display Acquisition System) show that new and varied computer products can be incorporated into the operational environment. Most recently, the software written by Dr. Ralph Petersen of the Development Division at the National Meteorological Center (NMC) called Personal Computer-Gridded Interactive Display and Diagnostic System (PC-GRIDDS), has brought isentropic analysis into the operational environment. PC-GRIDDS enables forecasters to run *both* constant pressure and isentropic diagnostics on numerical model data sets. For the first time, forecasters can utilize *forecast* isentropic surfaces to interpret model output. However, if these products are to be efficiently and intelligently utilized, the end users (i.e., the forecasters) must be knowledgeable about the advantages and disadvantages of each new tool. As Doswell (1986) notes, we need to consider training at least as much as technology. The technology makes it very easy for us to create isentropic data sets and analyses. The training makes this not-so-new method of diagnosing atmospheric flow easy to use, understandable and useful.

Toward that end I will try to illustrate the advantages *and* disadvantages of isentropic analysis in the diagnosis of weather patterns *as a supplement to* standard constant pressure analyses. I will draw heavily on the work of other researchers (e.g., Danielsen, Reiter, Uccellini, Petersen, Namias, Rossby, Wilson, Anderson) who have proven isentropic analyses effectiveness in diagnostic work through numerous case studies. References will be given so that the adventuresome reader can delve into some of the topics we discuss in greater detail. For that reason this paper does not attempt to be an exhaustive guide for isentropic meteorology. Mathematics will be used but minimized for fear of boring or disenfranchising the reader. Emphasis instead will be placed upon *conceptualization* of ideas rather than heady dynamics. This is especially important in isentropic analysis since isentropic surfaces are truly three-dimensional, unlike the quasi two-dimensional pressure surfaces. Our experience at St. Louis University in the synoptic laboratory is that it takes several weeks for students to get over their two-dimensional, constant pressure biases to visualize three-dimensional isentropic flow. It is much like the transition for A. Square, the key character in *Flatland* by Edwin A. Abbott (1952), in going from Flatland to the three-dimensional world of *Sphere land* (Burger, 1965). This author encourages the reader to read both *Flatland* and *Sphere land* as they are useful exercises in visualization; references are given at the end of this paper.

Finally, I want to acknowledge that motivation for this paper came from Dr. Laurence Wilson of the Atmospheric Environment Service in Canada who wrote a similar shorter paper for Canadian meteorologists. Several examples discussed in this text are borrowed from his training paper. Also, Anderson (1984) wrote a paper describing isentropic analysis for the National Weather Service's (NWS) Western Region which is frequently referenced.

## II. ISENTROPIC COORDINATE SYSTEM

### A. Definition

One must first begin with the concept of an *adiabatic* process as applied to a fictitious parcel of air with a volume of roughly 1 $m^3$. During an adiabatic process an air parcel will experience no heat exchange with its environment; i.e., no heat is added or taken away from the parcel. In terms of the first law of thermodynamics we write,

$$dh = 0 = C_p dT - \alpha dP \tag{1}$$

Since $\alpha = RT/P$ we can write (1) as:

$$\frac{dT}{T} = \frac{R}{C_p}\frac{dP}{P} \tag{2}$$

Following Hess (1959), if we integrate from some temperature, T, and pressure, P, to a temperature, $\theta$, at 1000 mb, we obtain:

$$\theta = T\left(\frac{1000}{P}\right)^{\kappa} \tag{3}$$

where $\kappa = R/C_p$.

The temperature, $\theta$, is physically defined as the temperature that a parcel of air would have if it were compressed (or expanded) adiabatically from its original pressure to 1000 mb. It is known as *potential temperature* and is a conservative property for parcels of air with *no* changes in heat due to such processes as solar/terrestrial radiation, mixing with environmental air that has a different temperature, and latent heating/evaporative cooling. Although these restrictions would seem to make the application of this thermodynamic variable limited there is empirical evidence that such "diabatic" heating and cooling processes are usually secondary in importance for temporal scales on the order of the synoptic. Some people (such as the author) would also argue that one could extend this approximation to meso $\alpha$ (Orlanski, 1975) scales of motion under certain conditions.

Hess (1959) also shows that the entropy of an air parcel, $\phi$, is related to its potential temperature as:

$$\phi = C_p \ln\theta + \text{const} \tag{4}$$

So a parcel which moves dry adiabatically not only conserves its potential temperature but also its entropy. A surface composed of parcels whose potential temperatures are equal is described as an equal entropy or isentropic surface. In thermodynamics we are told that entropy is a measure of the disorder of a system. However, operational meteorologists have little use for this concept. Thus, aside from using the term *isentropic*, we meteorologists prefer to use *potential temperature* as a variable rather than *entropy*, which carries more of a mystical aspect!

In the troposphere the atmosphere is, on the average, stable; i.e., $-\partial T/\partial Z = \gamma_{envir} < 9.5^{\circ}C/km$, typically $\gamma_{envir} = 6.5^{\circ}C/km$. In such an atmosphere the potential temperature can be shown by (5) to *increase* with height.

$$\frac{1}{\theta}\frac{\partial\theta}{\partial z} = \frac{(\Gamma_d - \gamma)}{T} \qquad (5)$$

In (5) $\Gamma_d$ is the dry adiabatic lapse rate and $\gamma$ is the actual or environmental lapse rate. Under stable conditions $\gamma < \Gamma_d$, so $\partial\theta/\partial Z > 0$ meaning $\theta$ increases with height. If the lapse rate is neutral then $\gamma = \Gamma_d$ and $\partial\theta/\partial Z = 0$; i.e., $\theta$ is constant with height. If $\gamma > \Gamma_d$ the lapse rate is superadiabatic and $\theta$ decreases with height. Furthermore, as Rossby et al. (1937) note, the potential temperature also increases southward at about the same rate as the dry bulb temperature. So the troposphere may be envisioned as being composed of a great number of isentropic layers which gradually descend from cold polar regions to warmer subtropical latitudes. As one ascends from the troposphere into the stratosphere, where the atmosphere is very stable, isentropic surfaces become compacted in the vertical. This attribute makes them extremely valuable for resolving upper-level stable frontal zones in the presence of upper tropospheric wind maxima or jet streaks. Thus, in a stably stratified atmosphere; i.e., $-\partial T/\partial Z < 9.8^{\circ}C/km$, potential temperature can be an excellent vertical coordinate—especially since it increases with height, thereby avoiding the headaches of dealing with a vertical coordinate (namely pressure) which decreases with height.

Rossby et al. (1937) and later Blackadar and Dutton (1970) note that it is necessary to "tag" a parcel with more than its potential temperature since on an isentropic surface all parcels "look alike". A second natural "tag" would be mixing ratio or specific humidity, both quantities which are also conserved during dry adiabatic ascent/descent. Another possible "tag" (which will be discussed later) is *potential vorticity*. It should be no surprise, then, that the three-dimensional transport of moisture on a vertically sloping isentropic surface should display good spatial and temporal continuity. As will be shown later, this has important diagnostic and prognostic implications for the movement of both moist and dry tongues in low-middle levels of the troposphere.

Meanwhile, one might ask why isentropic analysis was ever abandoned if, as recognized way back in the 1930's, it showed such great promise? Perhaps even more importantly, why has it regained favor today?

### B. History of Isentropic Analysis

The rise and fall and subsequent rebirth of isentropic analysis for the study of synoptic scale systems is quite interesting. The historical perspective discussed by Bleck (1973) is summarized here. Apparently, as the story goes, in the 1930's once upper air observations became available there was quite a debate over what vertical coordinate system would be most useful for weather analysis and forecasting. German meteorologists and several European colleagues favored a constant pressure coordinate system while the British Commonwealth and the United States favored using a constant height system. But, several vociferous meteorologists (e.g., C. G. Rossby and J. Namias) urged the adoption of isentropic coordinates. Consider their arguments:

"It can hardly be doubted that the isentropic charts represent the true motion of the air more faithfully by far than synoptic charts for any fixed level in the free atmosphere. At a fixed level in the middle of the troposphere entire air masses may, as a result of slight vertical displacements, appear or diappear in the time interval between two consecutive charts, making that entire method of representation futile." (Rossby et al. 1937).

"While maps of atmospheric pressure at various levels have been found especially helpful in weather forecasting, the use of temperatures and humidities on such constant level charts has hardly done more than make atmospheric disturbances seem more complicated in vertical structure than surface weather analyses would indicate." (Namias, 1939).

One researcher (Spilhaus, 1938) even suggested, in a short paper for the Bulletin of the American Meteorological Society, that airplanes fly along isentropic surfaces using a "thetameter" to keep track of the potential temperature for the pilots!

According to Bleck (1973) the U. S. Weather Bureau did respond in the late 1930's to these arguments (and other advantages noted in the next section) and transmitted data needed for isentropic analysis over the weather teletype network. However, after a number of years (by the mid 1940's) this service was discontinued and a constant pressure coordinate was used. Bleck (1973) and Wilson (1985) note several reasons for this action.

(1) The second world war created an impetus for a standardization to a common vertical coordinate system and analysis procedures. The demands of the aviation community were for winds on constant pressure surfaces.

(2) In the pre-computer age isentropic charts were difficult and time-consuming to prepare within operational time constraints.

(3) Perhaps most significantly, the Montgomery streamfunction, which defines geostrophic flow on an isentropic surface, was being erroneously computed. This resulted in a geostrophic wind law on isentropic surfaces which did not work. Undoubtedly, this led to disenchantment with isentropic analysis and its eventual demise.

Reiter (1972) discusses the last problem in some detail. Briefly, the Montgomery streamfunction (which is basically equivalent to heights on a constant pressure surface, in terms of its relationship to the geostrophic wind) is defined by Montgomery (1937) as:

$$M = \Phi + C_p T_\theta \qquad (6)$$

In the early isentropic years M was computed by interpolating the two terms, $\Phi$ and $C_pT$, separately, using for $\Phi$ the conventional pressure-geopotential calculations (Bleck, 1973). As Danielsen (1959) discovered, the two terms in (6) are related through the hydrostatic equation in isentropic coordinates. Therefore, computing these terms independently resulted in unacceptable errors of as much as 20% in their sum (Wilson, 1985). Bleck (1973) believes that this lack of a workable geostrophic wind relationship contributed to the demise of isentropic analysis--especially in the operational community.

After Danielsen's (1959) discovery of this error in computing the Montgomery streamfunction, the path was cleared for a resurgence of isentropic analysis--at first notably in diagnostic work and later in predictive models. Some examples of research which used isentropic analysis techniques include:

(1) Studies of exchange processes between the stratosphere and troposphere, especially along "breaks" or "folds" in the tropopause (Danielsen, 1959, 1968; Reiter, 1972, 1975, Staley, 1960; Reed, 1955; Shapiro, 1980; Uccellini et al. 1985; and others).

(2) Studies of air flow associated with extratropical cyclones attempting to explain the characteristic cloud patterns observed by satellite imagery (Carlson, 1980; Carr and Millard, 1985; Danielsen, 1966; Danielsen and Bleck, 1967; Browning, 1986; and others).

(3) The construction of isentropic trajectories used to diagnose Lagrangian vertical motions and ageostrophic flow associated with jet streak activity (Danielsen, 1961; Petersen and Uccellini, 1979; Haagenson and Shapiro, 1979; Kocin et al. 1981; Moore and Squires, 1982; Uccellini et al. 1985; and others). The relationship of isentropic upslope flow to cloud patterns has been noted by many Satellite Field Service Stations (SFSS) in their daily messages.

(4) Utilization of isentropic analysis to obtain better resolution of winds and moisture in the vicinity of frontal zones above the surface for diagnostic work or model initialization (Petersen, 1986).

(5) Experiments in numerical weather prediction using models with equations formulated in isentropic coordinates (Eliassen and Raustein, 1968; Bleck, 1973; Homan and Petersen, 1985; Uccellini and Johnson, 1979; and others).

(6) Studies of frontogenesis in inviscid, adiabatic flow, notably by Hoskins and Bretherton (1972).

### C. Advantages of Isentropic Analysis

The advantages of using an isentropic perspective in diagnosing atmospheric flow have been discussed by Saucier (1955), Bleck (1973), Uccellini (1976), Wilson (1985) and Moore (1985). These advantages include:

(1) Over synoptic (and to a degree, subsynoptic) spatial and temporal scales, isentropic surfaces act like "material surfaces", (Rossby et al. (1937). That is, air parcels are thermodynamically "bound" to their isentropic surface in the absence of diabatic processes such as terrestrial/solar radiation, latent heating/evaporative cooling and

sensible heat exchanges in the planetary boundary layer. The only other thermodynamic surfaces that act as material surfaces are surfaces of equivalent potential temperature and wet bulb potential temperature, both conservative properties for either "dry" or "wet" parcels. However, the latter are unwieldy to use in diagnostic work since they are typically multi-valued with respect to pressure; i.e., they are folded in the vertical. The only times that an isentropic surface has a non-unique value of pressure is if the environment is neutral ($\partial\theta/\partial Z = 0$) or if it is unstable ($\partial\theta/\partial Z < 0$). This is illustrated by Fig. 1a and 1b.

Of the diabatic processes most apt to restrict the applicability of isentropic analysis, the release of latent heat is the most significant. As we would expect this takes place in saturated, ascending air. The problems with isentropic surfaces within the planetary boundary is that they are subject to greater diurnal cycles of solar/terrestrial heating/cooling which causes the isentropic surface to move up/down thereby losing its continuity. Thus, airflow in the troposphere is best diagnosed by choosing the most appropriate isentropic surface in the area of interest above the planetary boundary layer.

(2) Isentropic surfaces can vary with respect to height (Z) or pressure (P). In fact, the slope of an isentropic surface is much greater than a corresponding constant pressure surface over a given thermal gradient. Also, since isentropic surfaces slope *up* towards cold air their slope is opposite that of constant pressure surfaces which slope down towards cold air. Sample calculations across a 2—3°C $(100\ km)^{-1}$ temperature gradient in the lower to middle troposphere resulted in a 2—3 gpm $km^{-1}$ slope on an isentropic surface. The corresponding slope of the nearest constant pressure surface was $10^{-1}$ to $10^{-2}$ gpm $km^{-1}$. Thus, isentropic surfaces can have slopes of 1—2 orders of magnitude greater than the corresponding constant pressure surfaces! Therefore, "horizontal" flow along isentropic surfaces contains the *adiabatic* component of vertical motion which would otherwise be computed as a separate component in either a Cartestian or isobaric coordinate system. This will be explained in greater detail as it is important for understanding how vertical motions appear on isentropic surfaces.

Vertical motion with respect to pressure in isentropic coordinates is expressed as:

$$\omega = \left(\frac{\partial P}{\partial t}\right)_\theta + \vec{V}\cdot\vec{\nabla}_\theta P + \frac{\partial P}{\partial \theta}\frac{d\theta}{dt} \qquad (7)$$

$$\text{A} \qquad \text{B} \qquad \text{C}$$

As described by Moore (1986), terms A, B, C can be physically described as:

(A) Local pressure tendency: This represents the effect of an isentropic surface moving up or down at a specific point (local derivative). With standard rawinsonde data this term can be evaluated over a 12-hour period as a backward time derivative. However, that is really a poor estimate of a local time derivative.

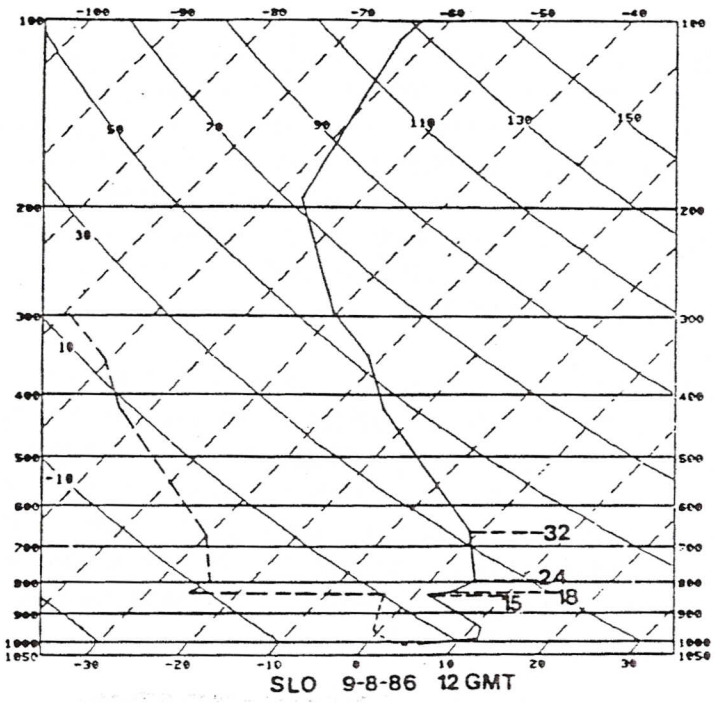


Figure 1a. Salem, IL (SLO) sounding for 1200 GMT, 8 September 1986. This skew-T, log P diagram shows how potential temperature changes in the vertical in the vicinity of a stable region. Numbers adjacent to the temperature sounding are potential temperature in °C.

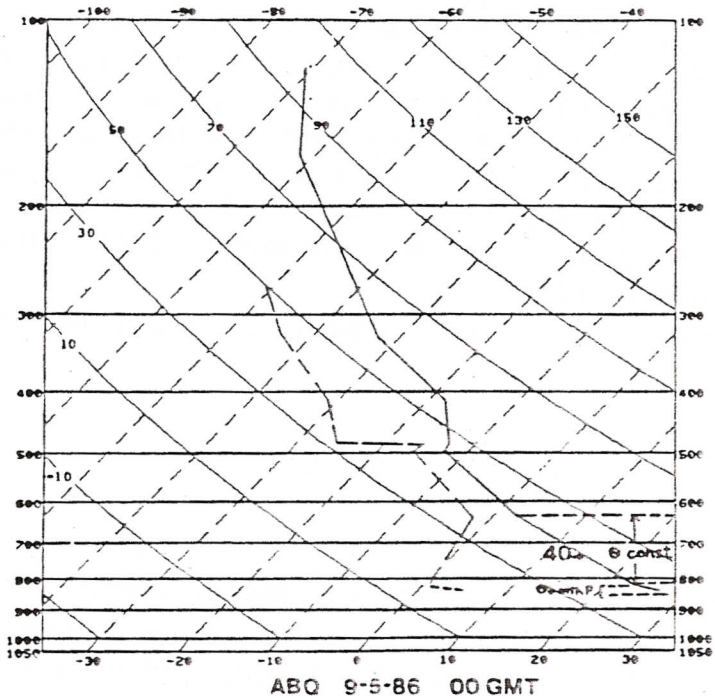


Figure 1b. Albuquerque, NM (ABQ) sounding for 0000 GMT, 5 September 1986. This skew-T, log P diagram shows how neutral and superadiabatic layers appear on a sounding. Note: 40=313°C=potential temperature of the layer; below that layer, lapse rate is superadiabatic.

(B) Advection of pressure on the isentropic surface: This term can be qualitatively evaluated by noting the cross-isobar flow on an isentropic surface. Air flowing from high to low pressure represents upward vertical motion ($\omega < 0$), while air flowing from low to high pressure indicates downward vertical motion ($\omega > 0$). Since an isobar on an isentropic surface is also an isotherm, this is equivalent to thermal advection. This can be proven easily by considering Poisson's equation (3) derived earlier:

$$\theta = T(\frac{1000}{P})^{\kappa} \tag{3}$$

If one considers an isobar (P) on an isentropic surface ($\theta$) it becomes clear that since P and $\theta$ are constant along that isobar, T must be also. Carrying this one step further--if we consider the equation of state,

$$P = \rho RT \tag{8}$$

One can see that since P and T are constant, so must be $\rho$, the density. Thus, an isobar drawn on an isentropic surface is also an isotherm and an isopycnic or isostere.

(C) Diabatic heating/cooling term: This term measures the contribution to vertical motion by diabatic processes such as those listed earlier, notably latent heating. When this term is non-zero, it forces the parcel to "jump" off the isentropic surface. In a stable atmosphere $\partial P/\partial\theta$ is $< 0$ since $\theta$ increases as P decreases. Therefore, the sign of term "C" depends totally upon the sign of the diabatic term, $d\theta/dt$, which is $> 0$ for heating and $< 0$ for cooling. Thus, diabatic heating will cause upward motion *with respect to the isentropic surface* and diabatic cooling will cause downward motion. This is the only true vertical motion *with respect to* the isentropic surface. Just as $w = dZ/dt$ measures vertical motion with respect to constant height surfaces and $\omega = dP/dt$ measures vertical motion with respect to constant pressure surfaces, $d\theta/dt$ is a measure of vertical motion with respect to an isentropic surface. Unfortunately, measuring $d\theta/dt$, especially within the confines of an operational environment, is not easy. Fortunately, at synoptic scales of motion and in the pre-severe storm or convective environment, it plays a secondary role in forcing changes in $\omega$. However, Moore (1986) has shown that once convection begins this term can be equal to or greater than terms A and B combined. It is modulated to a great extent by the static stability, $\partial P/\partial\theta$; i.e., in stable regions it is small, but in less stable regions it can be quite large.

If only term B of (7) is considered one can define the adiabatic vertical motion as:

$$\omega_{adiabatic} \approx \vec{V}\cdot\vec{\nabla}_{\theta}P \tag{9}$$

Wilson (1985) notes that the advection term and the local pressure tendency term are usually opposite in sign but that the advection term typically dominates, especially in regions of strong advection. He offers the following illustration:

Example:

Vicinity of Maniwaki, 0000 GMT January 14, 1980 300 K
Wind speed = 50 knots = 25 m $s^{-1}$ towards decreasing pressure
magnitude of $\nabla P$ = 50 mb / (3 deg latitude)
Pressure on 300 K surface at YMW at January 13/1200 GMT = 530 mb
Pressure on 300 K surface at YMW at January 14/0000 GMT = 610 mb
Pressure on 300 K surface at YMW at January 14/1200 GMT = 650 mb

This represents a warming trend over the 24 hour period.

$$\left(\partial P/\partial t\right)_\theta = (650 \text{ mb} - 530 \text{ mb})/24 \text{ hours} = +1.39 \ \mu\text{bars/s}$$

$$\bar{V}\cdot\bar{\nabla}P = V\frac{\partial P}{\partial n}\cos\theta$$

$$\bar{V}\cdot\bar{\nabla}P = 2500 \text{ cm/s} \times (50 \times 10^3 \ \mu\text{bars}) / (3^\circ\text{lat} \times (111 \text{ km}/1^\circ\text{lat}) \times 10^5 \text{ cm/km}) \times \cos 180^\circ$$

$$\bar{V}\cdot\bar{\nabla}P = -3.75 \ \mu\text{bars/s}$$

Also, $\partial P/\partial\theta \ d\theta/dt = 0$ for dry ascent
$> 0$ for moist ascent, solar heating, etc.
$< 0$ for evaporative cooling, terrestrial cooling, etc.

Therefore, $\omega$ = +1.39 μbars/s - 3.75 μbars/s = -2.36 μbars/s

This is a typical synoptic scale value for vertical motion. Normally, we would only have the t and t -12 hour maps which would permit us to estimate $\partial P/\partial t$ (i.e., use backward differencing). Note that if the air is saturated, the third term would amplify the vertical motion as latent heat would take the parcel up and off the isentropic surface. However, this effect would be compensated by increases in term A of (7) as the isentropic surface descends when diabatically heated.

Saucier (1955) notes that it is important to account for the horizontal motion of the isentropic surface. It can be shown that if a system translates without change of speed or shape, and does not fill or deepen, then term A in (7), the local pressure tendency, is equal to $-\bar{C}\cdot\nabla_\theta P$, where $\bar{C}$ denotes the velocity of the isentropic surface (system speed and direction), neglecting diabatic effects. Under these conditions (7) can be written:

$$\omega_{\text{adiabatic}} \approx (\bar{V}-\bar{C})\cdot\nabla_\theta P \qquad (10)$$

Thus, including $\bar{C}$ in the calculation of $\omega$ accounts for the vertical movement of an isentropic surface locally due to the "system" motion (this point will be further addressed in section III. D). In this form $\bar{V}-\bar{C}$ is a measure of the relative motion toward lower isentropic pressures (upslope flow) or higher isentropic pressures

(downslope flow). Typically, $| \bar{V} | > | \bar{C} |$, especially in mid-upper levels, meaning that the isentropic surface is being displaced horizontally more slowly than the air. In this way, the adiabatic vertical motion expressed by (10) is storm-relative. Storm-relative motions are often used in Doppler radar analyses of severe convective storms and are much more illuminating than the absolute wind vector field.

The natural question that arises is, how does one obtain a reasonable estimate for $\bar{C}$? It would seem most straightforward to obtain $\bar{C}$ from the 12 h displacement of the minimum (or maximum) value of the Montgomery streamfunction. However, at Saint Louis University, we have found that since a closed contour of M is not always available, following absolute vorticity maxima or minima, is more reliable. Thus, we compute $\bar{C}$ based in the previous 12 h movement of an absolute vorticity maximum (for cyclones) or minimum (for anticyclones). It is important to note that since all grid points on a U.S. map will use this $\bar{C}$ value, areas distant from the influence of the cyclone or anticyclone may not yield accurate results since their vertical motions should be referenced with respect to a different, perhaps approaching/leaving system.

Typically a forecaster would not compute vertical motion as above (although a computer could generate this product easily). However, it can quickly be estimated from the advection pattern by noting (a) the strength of the winds, (b) their component across the isobars, and (c) the strength of the isobar gradient.

(3) Because moisture transport on isentropic surfaces includes the vertical advection component, which is often missed or forgotten in pressure coordinates, moisture transport tends to display a more coherent pattern in space-time on isentropic surfaces than on standard 850 mb or 700 mb charts (Oliver and Oliver, 1951; Namias, 1938). Wilson et al. (1980) note that since isentropic parcels conserve their mixing ratio or specific humidity values one can forecast the motion of dry lines and moist tongues using the component of the wind perpendicular to the isohumes. Although we all try to do this on constant pressure charts it is really inappropriate since we have no way of estimating vertical advection on pressure charts.

The ability to track the three-dimensional motion of moisture is probably one of the greatest advantages of isentropic analysis. Air parcels not only conserve their potential temperature, but also their mixing ratio (or specific humidity) value while moving along an isentropic surface. Many a forecaster probably has seen patches of moisture "pop up" on 850 or 700 mb charts, especially during warm air advection (overrunning) situations. Undoubtedly this moisture is coming up from below the 850/700 mb surfaces—a process one cannot see within a constant pressure perspective. Isentropic uplifting typically represents not only vertical motion but moisture advection as well. Similarly, subsidence and drying out of air behind frontal systems (or associated with jet streak secondary circulations) can be seen quite nicely on isentropic analyses. Figure 2a-b illustrates how vertical motion *and* moisture advection can be visualized on an isentropic surface. In Fig. 2a, the geostrophic flow is parallel to the Montgomery streamfunction. On the western side of the short-wave trough, the flow is cutting across the isobars towards higher pressure — indicative of downward vertical motion. In the same area, dry air advection is

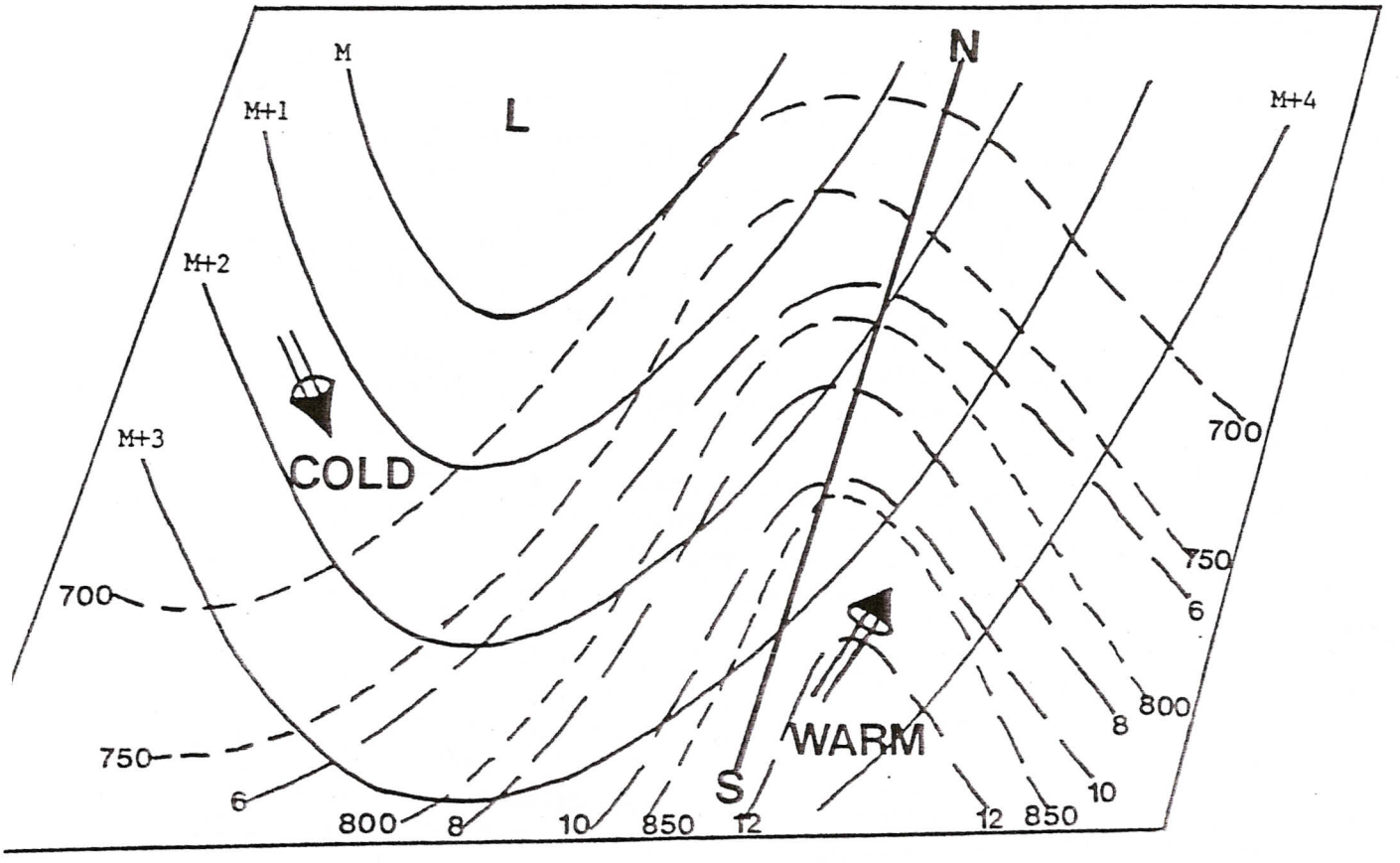


Figure 2a. Schematic depiction of 310 K isentropic surface. Solid lines are Montgomery streamfunction ($10^1$ J $kg^{-1}$), short dashed lines are isobars (mb) and long dashed lines are isohumes (gm $kg^{-1}$). Cross section shown in Fig. 2b is taken along bold, solid north-south oriented line.

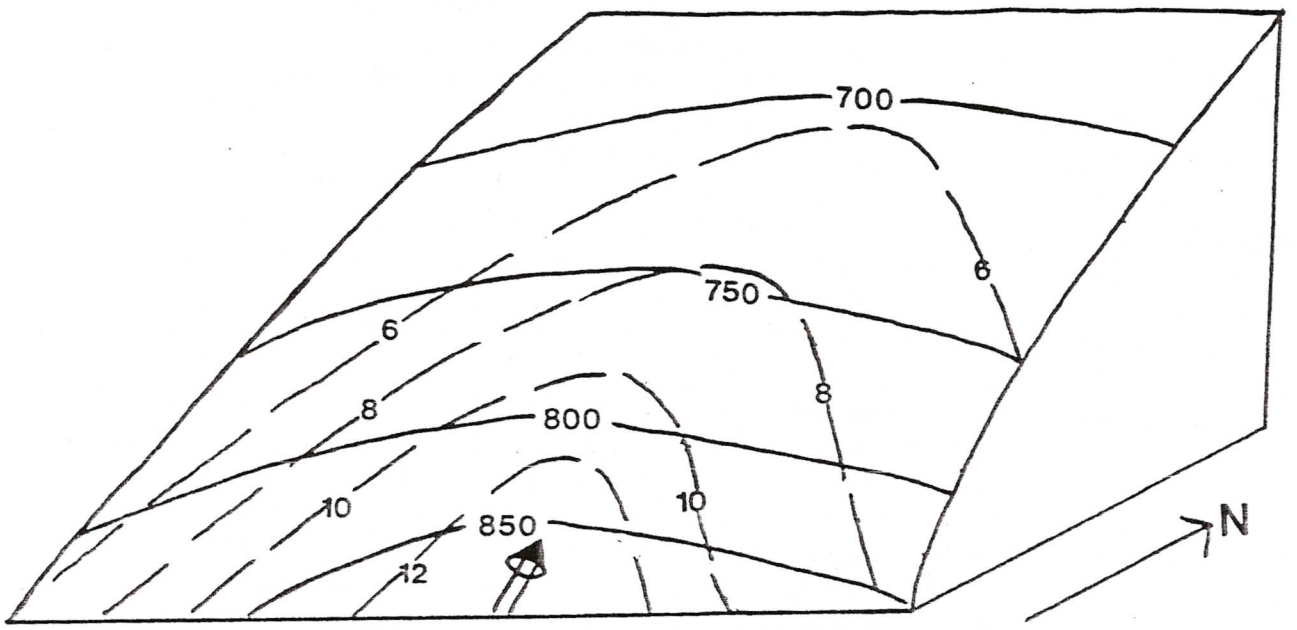


Figure 2b. Schematic depiction of isentropic surface along north-south line shown in Fig. 2a, east of short wave trough. Solid lines are isobars (mb), dashed lines are isohumes (gm $kg^{-1}$) and open arrow indicates the direction of flow along the isentropic surface.

taking place. To the east of the trough the flow is from higher pressure and mixing ratio values to lower pressure and mixing ratio values — indicating that the air is rising and advecting moist air northward. Figure 2b schematically depicts the isentropic topography along the north-south line in Fig 2a. One can see how the air rises along the isentropic hill cutting across the quasi-horizontal pressure surfaces as it heads north. The vertical motion and moisture transport is three-dimensional in this view.

(4) Frontal discontinuities are virtually nonexistent on isentropic surfaces, since frontal zones tend to run parallel to the isentropic surfaces (Bleck, 1973). This property of isentropic surfaces makes them extremely useful in diagnosing kinematic and dynamic variables, especially in baroclinic zones. Since the isentropic surfaces run parallel to the frontal zone, the variations of basic quantities (e.g., wind, moisture, temperature) take place more gradually along them; i.e., over larger scales (see Fig. 3). Constant pressure surfaces literally cut through frontal zones causing quantities associated with a frontal zone to change more radically over subsynoptic spatial scales. An interesting result of this property of isentropic surfaces is that derived quantities (e.g., vorticity, divergence) tend to display weaker gradients and be oriented quite differently than on corresponding constant pressure charts. Figure 4 schematically depicts a cross section of a frontal zone and representative isentropes in its vicinity. Note that the isentropic surfaces are sloped down towards the warm air and are compacted in the vertical within the frontal zone. The slope of the isentropic surface is a function of the thermal gradient, while the vertical compaction indicates high static stability. A constant pressure surface slopes down towards the cold air and exhibits far less slope, as noted earlier. One must always remember, that although the isentropic chart is two-dimensional, it represents a vertically tilted three-dimensional surface. This tends to make people uncomfortable since constant pressure maps are quasi-horizontal depictions or slices of the atmosphere. Novices tend to ask, "but what level am I looking at?", to which we must reply, "one isentropic level–but several pressure levels". It is a bit like studying a foreign language—if you try to translate everything to English you are in trouble. You have to try to *think* in the foreign language and not revert back to English. Similarly one should try *not* to understand isentropic analysis within a constant pressure framework, but should attempt to *think* in an isentropic perspective. This may take some time. Don't be disappointed when it all looks strange at first.

(5) The vertical separation between consecutive isentropic surfaces is a measure of the static stability. This can be represented in two ways. One method is by simply viewing a cross section and noting regions of strong (weak) stability wherever isentropic surfaces are close together (far apart). This is useful in locating upper level frontal zones, inversions, and vertical changes in stability. In many ways this is much better than using standard stability indices which are parcel-related or only computed using certain levels of the atmosphere. A second method of using this advantage is through horizontal plots of the distance between two consecutive isentropic surfaces separated by 10 K or 15 K.

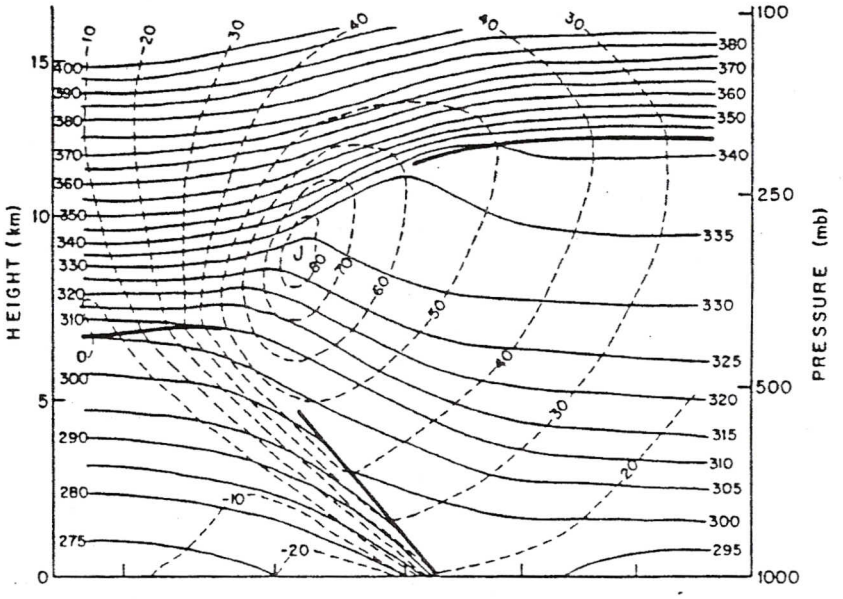


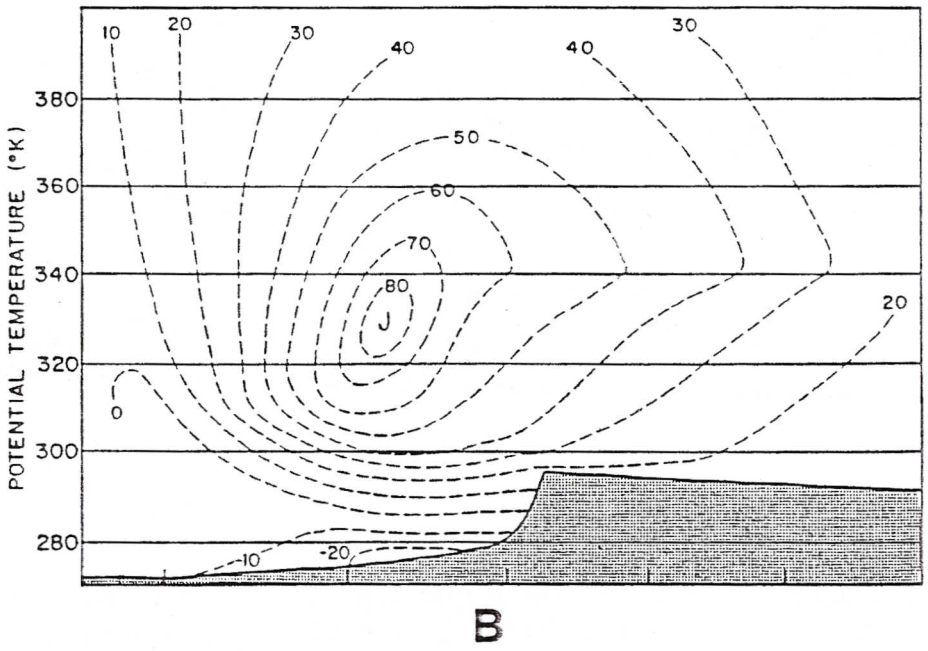


Figure 3a-b. Typical vertical cross section diagrams. The top diagram (a) shows isentropes (solid lines, °K) and isotachs of geostrophic wind component normal to the cross section (dashed lines, m $s^{-1}$). Heavy lines indicate the cold front and the tropopause. J refers to the axis of the jet stream. The bottom diagram (b) is the same cross section as in (a) but redrawn with potential temperature as a vertical coordinate. Shaded area is below the ground. (Wallace and Hobbs, 1977)

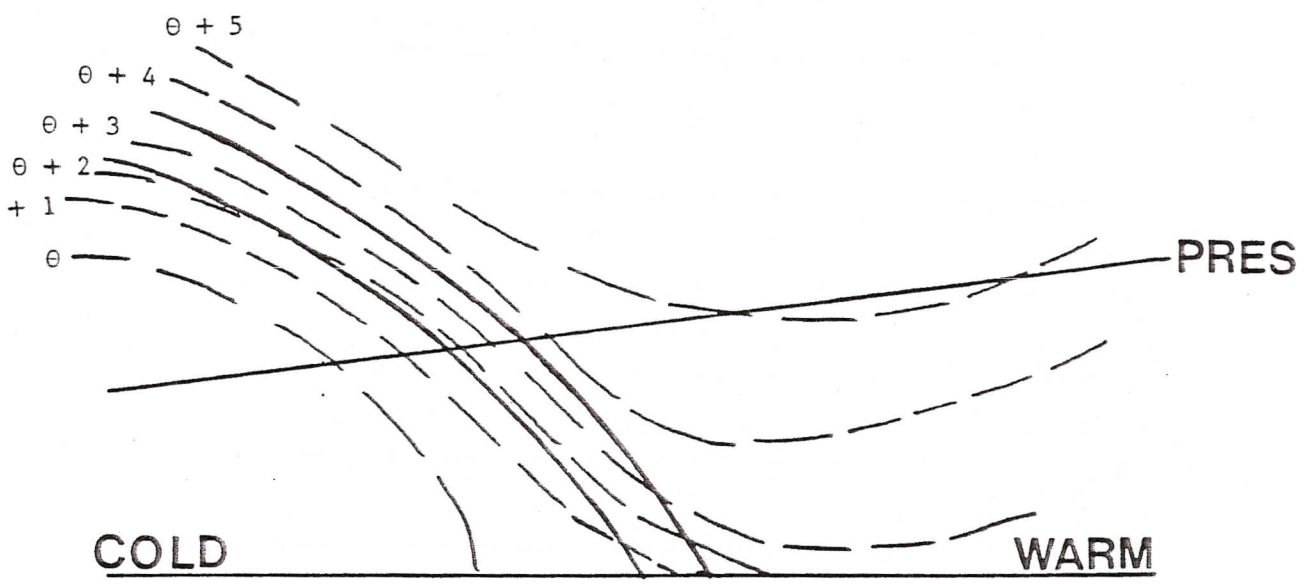


Figure 4. Schematic depiction of isentropic surfaces (dashed lines) and representative pressure surface (solid line) in the vicinity of a cold frontal zone (bold, curved lines).

Also noteworthy is the fact that static stability, $\partial P/\partial \theta$, is related via the continuity equation in isentropic coordinates (see 14) to divergence/convergence taking place in the layer. Divergence in the layer *increases* the static stability while convergence in the layer *reduces* the static stability. An important fact to think about is that divergence/convergence is *not* related to vertical motion in an isentropic framework, unlike in pressure coordinates where vertical motion is related to the vertical profile of the divergence. Divergence/convergence in a layer affects the static stability by changing the amount of mass between consecutive isentropic surfaces.

(6) The slope of an isentropic surface in the vertical is directly related to the thermal wind. This result will be discussed more rigorously in Section 3.C.1; however, this statement should not be surprising. We are all familiar with the fact that in pressure coordinates the thermal wind is proportional to the gradient of the thickness or mean temperature of the layer in question. A vertically sloping isentropic surface is indicative of a strong thermal contrast which is represented on the isentropic surface as a tight packing of isobars or isotherms. Thus, where isentropic surfaces tilt up or down significantly one can diagnose a frontal zone and a commensurate change in the wind speed with height.

In a cross-section analysis, *even in the absence of wind data,* one could diagnose regions of strong or weak wind shear. In a quasi-barotropic atmosphere the isentropic surfaces would be quasi-horizontal, indicative of weak thermal winds.

(7) Parcel trajectories may be computed on isentropic surfaces using either implicit (Danielsen, 1961) or explicit (Petersen and Uccellini, 1979) methods. These trajectories and their Lagrangian change fields have been shown by the above researchers and others to be faithful to and highly correlated with the four-dimensional flow associated with mid-latitude synoptic and even subsynoptic scale motions.

Although this result is more useful to the research community in their post analysis of storm systems it also has applications in the operational environment. Even 12-hourly isentropic data sets can be used to generate the recent history of air parcels and their 12-hour change fields to help diagnose present cloud and precipitation fields. Danielsen's and this author's work with vertical motion fields derived from changes in pressure along parcel trajectories reveal excellent correlation to cloud patterns and precipitation. Since Lagrangian omega fields are calculated over time, typically 12 hours, and are plotted at the trajectory midpoint, they are more representative of long periods of lifting/descent than instantaneous vertical motions generated by other methods.

### D. Disadvantages of Isentropic Analysis

As useful as isentropic analysis can be to the meteorologist, like any tool it has its drawbacks. However, knowing the following pitfalls will allow one to become a more intelligent user and therefore a better meteorologist. So, lest the author be accused of painting too rosy a picture--here is the other side of the story.

Experience has shown the following drawbacks to the use of isentropic analysis:

(1) Isentropic surfaces become ill-defined in regions where the lapse rate is neutral-superadiabatic; i.e., $\partial\theta/\partial Z < 0$. In the neutral case, the isentropic surface is vertical (see the portion of the 305 K surface labeled N in Fig. 5) while in the superadiabatic case it is folded (see the 300 K surface in Fig. 5). In the latter case the folded surface is said to be multi-valued with respect to pressure. This is a serious problem because a vertical coordinate should change monotonically with height. Obviously in these cases it doesn't. These type of troublesome lapse rates are often seen in the desert southwest of the U.S. (e.g, El Paso, TX; Midland, TX) especially in the 0000 GMT soundings in low levels.

One method of dealing with this problem is to eliminate the neutral and superadiabatic lapse rates before processing by checking for them in each sounding and readjusting the temperature profile to make the lapse rates slightly less than neutral. This is done by warming the top of the layer and cooling the bottom of the layer, usually by a modest amount. After this "correction" isentropic data can be generated from the constant pressure data.

(2) In near-neutral lapse rate regions there is poor vertical resolution of the atmosphere. As noted earlier the vertical difference between two isentropic surfaces is greater in less stable regions than in stable ones (see Fig. 6). Since frontal zones are baroclinic, in stable regions of the atmosphere isentropes tend to be compacted in the vertical and slope substantially in the vertical. So in these regions (as well as in upper level fronts associated with jet streaks) there is favorable vertical and horizontal resolution.

(3) The continuity of isentropic analysis is disrupted significantly by the presence of diabatic processes (Namias, 1940). This problem tends to show up mostly in the presence of (a) radiation, (b) evaporation and condensation, and (c) convection. An example of radiative effects is given in Fig. 7.

Due to cooling of the air nearest the earth's surface overnight the 300 K isentropic surface is found at progressively higher levels (A → B → C) with time. Without taking radiative cooling into account, a forecaster might attribute this decrease in pressure on the isentropic surface to advection.

Other variables will be affected by the diabatic effect as well. Since moisture typically decreases with elevation as the isentropic surface rises, the mixing ratio observed in the vicinity of this station will decrease with time. Similarly wind speed may increase and the direction veer as the surface rises (especially in the planetary boundary layer). Again, the unsuspecting observer would attribute these changes erroneously to some advective or developmental affect.

The opposite would be true during the diurnal heating cycle during which the pressure would increase, moisture increase, speed decrease, and wind direction back with time on the 300 K surface. This is a good reason for trying to avoid using isentropic surfaces too close to or within the planetary boundary layer.

If an isentropic surface is known to lie within a region of latent heating or evaporative cooling significant changes can occur as well. When latent heat is liberated the potential temperature of the substantial surface say 300 K, is raised to

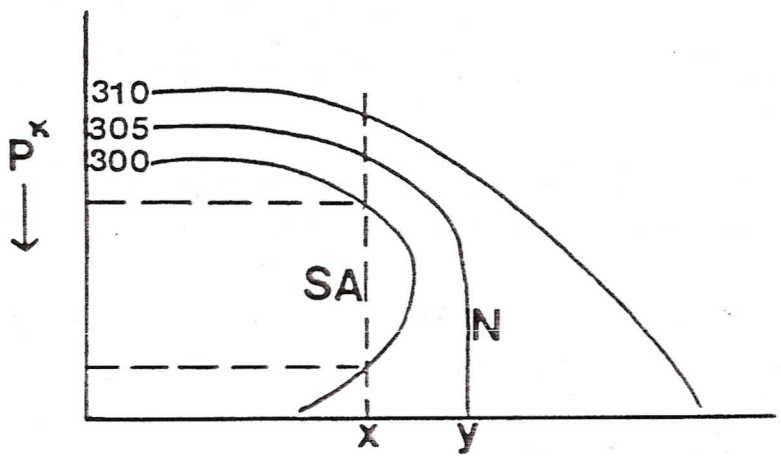


Figure 5. Cross section showing how isentropic surfaces appear in the vicinity of regions with superadiabatic (SA) and neutral (N) lapse rates.

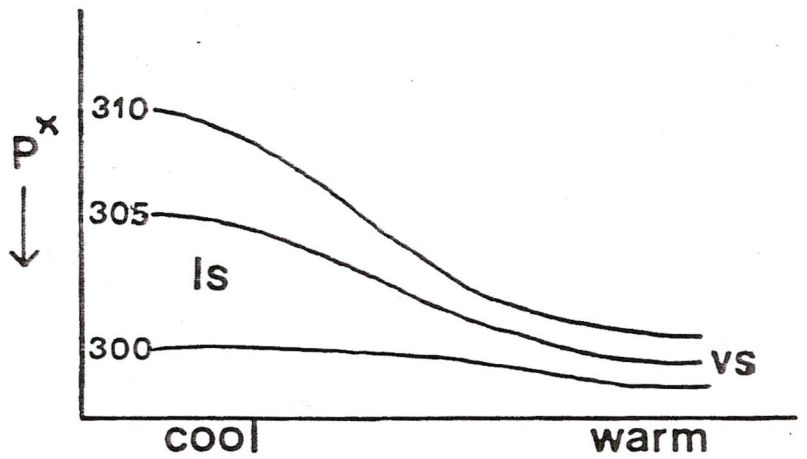


Figure 6. Cross section showing how the vertical resolution of an area may vary within a very stable (VS) and less stable (LS) region.

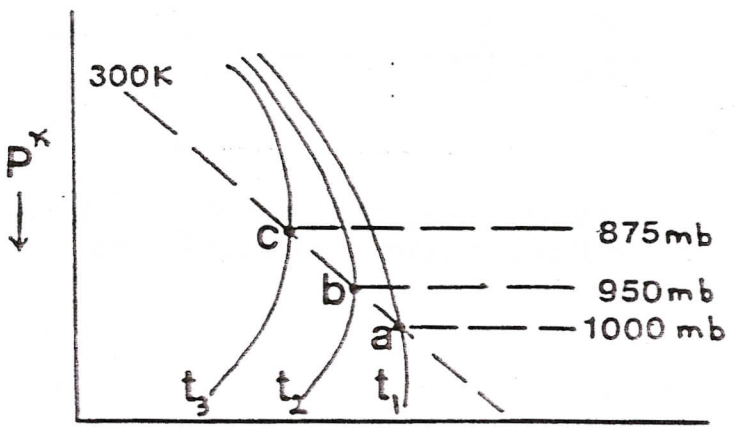


Figure 7. Soundings for progressively later time periods into the night (t1, t2, t3) illustrating how radiational influences may change the pressure level at which a given isentropic surface is found (Namias, 1940).

say, 304 K. Therefore, the 300 K isentropic surface will be found at a lower level where the mixing ratio and wind may be quite different, leading to possible erroneous interpretation by the analyst.

Similarly, when precipitation falls through an isentropic sheet which is not saturated, evaporative cooling will take place as the mixing ratio increases. As Namias (1940) notes, this lowers the potential temperature of the substantial surface from, say 300 K to, say 296 K, and therefore raises the isentropic surface. Now it is possible, if this evaporative cooling took place beneath a warm frontal inversion, that this process will raise the isentropic surface to a position within the frontal zone. In this case mixing ratio values will likely increase while the wind veers and strengthens with height. If this process was occurring beneath a cold frontal surface, the winds would likely back and strengthen with height. These scenarios vary with the strength and depth of the frontal zone.

Convection is disruptive to the continuity of isentropic surfaces mostly because it can effectively sustain the transport of moisture to higher levels. Namias (1940) notes that these vertical currents transport moisture to higher levels and replenish the moisture being precipitated out with cold frontal squall lines or even air mass type convective systems. However, he also mentions that the case of widespread convection can be quite different. The vertical transport of moisture from widespread convection can actually change the moisture pattern aloft. Such would be the case, for instance, in a Mesoscale Convective Complex (MCC) environment when convective scale feedback alters the synoptic scale flow and moisture significantly. So on a limited scale, within a squall line, the disruption of the moisture continuity on an isentropic surface is minimized as convection transports moisture vertically within the moist tongue to replenish moisture lost through precipitation. However, widespread convection can definitely contaminate the moisture continuity over larger scales of motion, rendering the analysis less useful. It is important to note that wintertime convection in unstable continental arctic/polar air masses is usually quite shallow and has very limited influence on isentropic surfaces in the free atmosphere.

(4) Isentropic surfaces tend to intersect the ground at steep angles causing analyses near where they intersect the ground to be suspect. One must be careful about over-interpreting analyses made near where the isentropic surface intersects the earth. One would do best to choose isentropic levels which never reach the ground. However, to depict moist/dry tongues associated with synoptic scale systems one tries to go as low as possible without hitting the ground. So there are trade-offs; as usual, there are no quick-fixes!

(5) Choosing the "proper" isentropic surfaces is not trivial. Generally, as in constant pressure analyses, one would like to use at least two or three isentropic surfaces to analyze. However, unlike constant pressure analyses, one has to choose different isentropic levels depending upon the time of year. Namias (1940) suggests the following *low level* isentropic surface for each season:

| Season | Low Level Potential Temperature |
|---|---|
| Winter | 290-295 K |
| Spring | 295-300 K |
| Summer | 310-315 K |
| Fall | 300-305 K |

The abrupt increase from spring to summer values is due to the normal rapid increase of free air temperature as summer convection sets in.

From experience the author has found that rather than guessing at what levels to use, one should create an isentropic cross section through the area of interest, preferably with winds and mixing ratio displayed. It is then relatively easy to choose the "right" isentropic levels in areas of jet streaks, moist tongues, etc. The lowest isentropic surface should be about 100—150 mb above the earth's surface. This ensures that it is low enough to diagnose low-level moisture and isentropic lift, while staying out of the planetary boundary layer or intersecting the earth's surface. If it is not easy or convenient to create an isentropic cross section, there is yet another technique to help choose the low-level isentropic surface. Use an 850 mb chart to locate a moist tongue and axis of southerly flow (perhaps a low-level jet). Choose an isotherm in the thermal ribbon (i.e., baroclinic zone) towards the warm side of the ribbon. Using Poisson's equation (3) or a skew-T, log P diagram, one can calculate the potential temperature knowing the temperature and the fact that you are on the 850 mb surface.

What this author *likes* about this so-called disadvantage is that it forces the meteorologist to think three-dimensionally and reason out his ideas for choosing certain isentropic levels to analyze. In the author's view this is better than using routinely generated, standard constant pressure charts simply because they are familiar or easier to take off the computer! The isentropic thinking process thereby avoids the setting in of "meteorological cancer" so often discussed in the literature (Doswell, 1986).

(6) Isentropic analyses are not generally available and require computations which can only be done in real-time by a computer. This problem has gradually been solved, especially over the last decade with the explosion of computer power. Creation of an isentropic database from standard constant pressure rawinsonde data can now be done in minutes on a minicomputer. Once the constant pressure rawinsonde data has been decoded, sorted, and arranged into direct access files on our minicomputer, we create a real-time isentropic data set in less than 5 minutes at Saint Louis University. The AFOS system now supports an isentropic analysis program (Anderson, 1984 and Little, 1985) while the VAS Data Utilization Center (VDUC) at the National Severe Storms Forecast Center (NSSFC) supports most isentropic analysis already. Wilson (1985) reports that an isentropic generation/analysis system is being used in Quebec within the Atmospheric Environment Service in Canada on a routine basis. So the computer problem is really no problem any

more. The availability is actually a function of the demand which is addressed in the next section.

(7) The "inertia" problem as described by Wilson (1985) is that most meteorologists today have been brought up on constant pressure analyses and quasi-horizontal thinking. Effort is required to change one's viewpoint. Although it should be stressed that isentropic analysis does not *replace* isobaric analysis, it is meant as a supplement to aid in diagnosis. The two viewpoints can and *should* work together. Many features seen on constant pressure charts can be located on isentropic charts, so the changeover is not as radical as it first would seem.

(8) Until recently, there was a problem using isentropic surfaces for forecasting due to the lack of numerical model forecast products in isentropic coordinates. Dr. Ralph Petersen's PC-GRIDDS software allows one to view both Nested Grid Model (NGM) and ETA model data in real time on sigma, constant pressure, and isentropic surfaces out to 48 hours. Both basic and derived fields (e.g., see Section III. D) can be viewed on a user-specified isentropic surface or computed over a layer bounded by two isentropic surfaces. In addition, isentropic cross sections can be viewed and direct/indirect circulations diagnosed using model output from 0—48 hours. PC-GRIDDS represents a tremendous leap forward in operational meteorology, allowing the meteorologist to *interpret* and *understand* model output rather than just read it. It is a surefire cure for meteorological cancer!

### E. Primitive Equations in Isentropic Coordinates

The primitive equations in isentropic coordinates are as follows:

*Momentum Equations*

$$\frac{\partial u_\theta}{\partial t} + \vec{V}_\theta \cdot \vec{\nabla}_\theta u + \frac{d\theta}{dt}\frac{\partial u}{\partial \theta} = -\frac{\partial M}{\partial x} + f v_\theta + F_x \tag{11}$$

$$\frac{\partial v_\theta}{\partial t} + \vec{V}_\theta \cdot \vec{\nabla}_\theta v + \frac{d\theta}{dt}\frac{\partial v}{\partial \theta} = -\frac{\partial M}{\partial y} - f u_\theta + F_y \tag{12}$$

*Hydrostatic Equation*

$$\frac{\partial M}{\partial \theta} = C_p \left(\frac{P}{P_o}\right)^\kappa = \frac{C_p T}{\theta} \tag{13}$$

*Mass Continuity Equation*

$$\frac{\partial}{\partial t}\left(\frac{\partial P}{\partial \theta}\right) + \vec{V}\cdot\vec{\nabla}\frac{\partial P}{\partial \theta} + \frac{d\theta}{dt}\frac{\partial}{\partial \theta}\left(\frac{\partial P}{\partial \theta}\right) = -\frac{\partial P}{\partial \theta}\vec{\nabla}\cdot\vec{V}_\theta - \frac{\partial P}{\partial \theta}\frac{\partial}{\partial \theta}\left(\frac{d\theta}{dt}\right) \tag{14}$$

*Thermodynamic Equation*

$$\frac{dQ}{dt} = C_p T_\theta \frac{d \ln \theta}{dt} \tag{15}$$

*Definition of Montgomery Stream function*

$$M = C_p T_\theta + g Z_\theta \tag{16}$$

*Poisson's Equation*

$$\theta = T\left(\frac{P_o}{P}\right)^{\kappa} \tag{17}$$

## Other Useful Diagnostic Expressions

*Geostrophic Wind Relationship*

$$\vec{V}_{geo} = \frac{\hat{k}}{f} \times \vec{\nabla}_\theta M \tag{18}$$

*Thermal Wind Relationship*

$$\vec{V}_T = \frac{\partial \vec{V}_{geo}}{\partial \theta} = \frac{R}{f}\left(\frac{P^{\kappa-1}}{P_o^{\kappa}}\right)(\hat{k} \times \vec{\nabla}_\theta P) \tag{19}$$

*Gradient Wind Relationships*

$$\hat{s}: \frac{dV}{dt} = f v_{geo} \sin\beta \tag{20}$$

$$\hat{n}: -\frac{V^2}{R} = -f v_{geo} \cos\beta + f v \tag{21}$$

*Potential Vorticity*

$$P_\theta = \frac{-g(\zeta_\theta + f)}{\frac{\partial P}{\partial \theta}} \tag{22}$$

*Description of Equations*

First, we should note that the total derivative in isentropic coordinates is written as:

$$\frac{d(\,)}{dt} = \frac{\partial(\,)}{\partial t} + u\frac{\partial(\,)}{\partial x} + v\frac{\partial(\,)}{\partial y} + \frac{d\theta}{dt}\frac{\partial(\,)}{\partial \theta} \tag{23}$$

A B C D E

where: term A is the total derivative (Lagrangian)
term B is the local derivative (Eulerian)
term C+D are the horizontal advection terms and
term E is the vertical advection term.

The expression $d\theta/dt$ represents all non-adiabatic heating/cooling (diabatic effects). It essentially represents vertical motion with respect to the isentropic surfaces. Since isentropic surfaces tilt substantially in the vertical, this "vertical motion", curiously enough, may have a horizontal component (horizontal with respect to Cartesian coordinates!). For strictly adiabatic processes term E is absent. Finally, keep in mind that the u and v wind components are measured on isentropic surfaces.

*Momentum Equations (11 and 12):* On the left-hand side (LHS) of (11) and (12) are the local time tendency of u (v) momentum, the inertial-advection term, and the vertical advection term. Notice that the latter term acts upon the vertical wind shear measured with respect to potential temperature. These three terms together are equal to the total (Lagrangian) time tendency of u (v) momentum. On the right-hand side (RHS) of (11) and (12) there is the gradient of the Montgomery streamfunction in the X (Y) direction, the Coriolis term, and the friction term. The Montgomery streamfunction is analogous to height on a constant pressure surface and serves to define the geostrophic flow on an isentropic surface.

*Hydrostatic Equation (13):* This is the equation used to compute M on the isentropic surfaces. In pressure coordinates one integrates the hydrostatic equation $\partial P/\partial Z = -\rho g$ to obtain the hypsometric equation used to obtain heights on pressure surfaces. To do this it is necessary to integrate up from the earth's surface using the temperature profile obtained by the rawinsonde. Similarly, here, one obtains M by integrating (13) with respect to $\theta$. Thus, the Montgomery streamfunction consists of a thermal term ($C_pT$ = enthalpy) and a geopotential energy term ($gZ$) which are *not* independent but related through the hydrostatic equation.

*Mass Continuity Equation (14):* This equation describes the change in mass between two isentropic surfaces, as measured by $\Delta P$, as a function of several processes. One can also think of this expression as a static stability tendency equation since $\partial P/\partial\theta$ is the static stability. On the LHS there are the local time tendency and horizontal and vertical advection of stability terms. Together they form the total derivative of static stability which would be useful if one were following parcels as in trajectory calculations.

On the RHS there are the divergence and diabatic terms. The divergence term changes stability in the following manner: divergence (convergence) in the layer ($\Delta P$) causes the isentropic surfaces to compact (separate) in the vertical thereby causing the stability of the column to increase (decrease). This shrinking/stretching of the column between two isentropic surfaces in response to divergence/convergence in the layer maintains mass continuity.

The diabatic term looks complex but can be described easily in physical terms. Note that it is *not* just diabatic heating that is measured but its change in the vertical. Thus, if the diabatic heating/cooling was uniform in the layer this term would be zero. However, let us say that there was diabatic cooling in lower levels due to evaporation and diabatic heating in upper levels due to latent heating. Then, as seen in Fig. 8, the static stability would increase with time. Essentially what happens is that in the presence of latent heating the 310 K surface is warmed to 314 K, meaning that the 310 K surface becomes redefined at a *higher* pressure. At the same time the 305 K surface is being cooled to 301 K, redefining the 305 K surface to a *lower* pressure. The net result is to increase the stability as the two surfaces approach each other in the vertical. Other examples of this nature could be shown depicting diurnal stability increases/decreases in the presence of solar heating and terrestrial cooling processes.

*Thermodynamic Equation (15):* As Wilson (1985) notes, all adiabatic advection and vertical motion is accounted for in the horizontal momentum equations through M. The thermodynamic equation in isentropic coordinates states that diabatic *heating* ($dQ/dt > 0$) causes isentropic surfaces to propagate through the atmosphere in a direction *toward* lower potential temperature values. The explanation for this is that adding heat to a parcel will increase its potential temperature ($d\ln\theta/dt > 0$). Alternately, the surface in the presence of diabatic heating will become "redefined" at a lower level of the atmosphere. Conversely, in regions of diabatic cooling isentropic surfaces propagate upwards towards higher potential temperature levels.

*Montgomery Stream function (16):* This expression states that the streamfunction on an isentropic surface is the sum of the enthalpy, $C_pT$, and the geopotential at that level. Again, these terms are related to each other through the hydrostatic equation (13).

*Poisson's Equation (17):* This equation is the founding expression for isentropic coordinates. It enables one to compare parcels of air by computing the temperature they would have if they were brought up (down) to 1000 mb--a base state level.

*Geostrophic Wind Relationship (18):* This expression relates the geostrophic wind to the pattern of Montgomery streamfunction. The relationship is similar to that on a constant pressure surface--the geostrophic wind blows parallel to the Montgomery streamfunction with lower values to the left of the wind (in the northern hemisphere). The geostrophic wind is also proportional to the gradient of Montgomery streamfunction and inversely proportional to the Coriolis parameter, f. One can create a geostrophic wind scale, similar to those used on constant pressure surfaces, which helps the analyst isopleth lines of constant M on an isentropic surface. Examples are given in Figs. 9-10 for two different polar stereographic scales (1:15 million and 1:10 million). To use them, place one point of a compass on one point on the Y axis at the latitude in question and the other point to the right on the isotach value you want. The distance measured between the points is the distance two

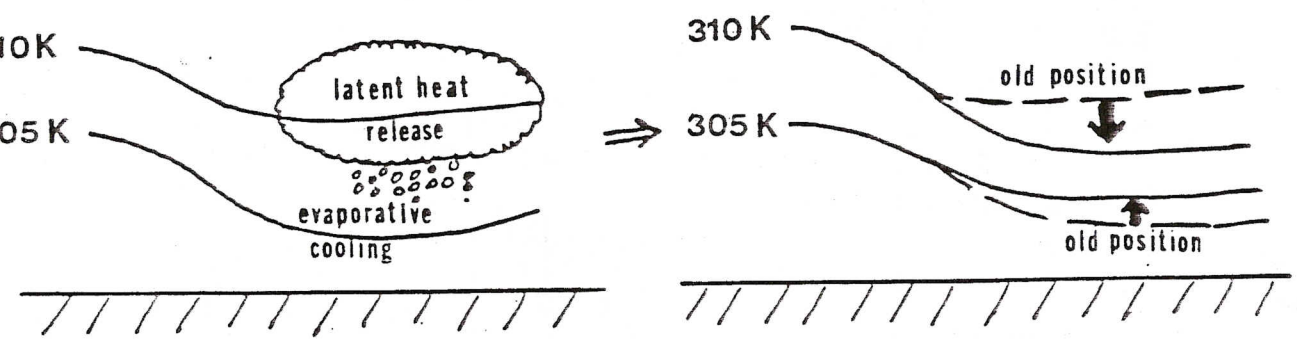


Figure 8. Schematic diagram depicting the stability changes that can take place in the presence of diabatic heating/cooling.

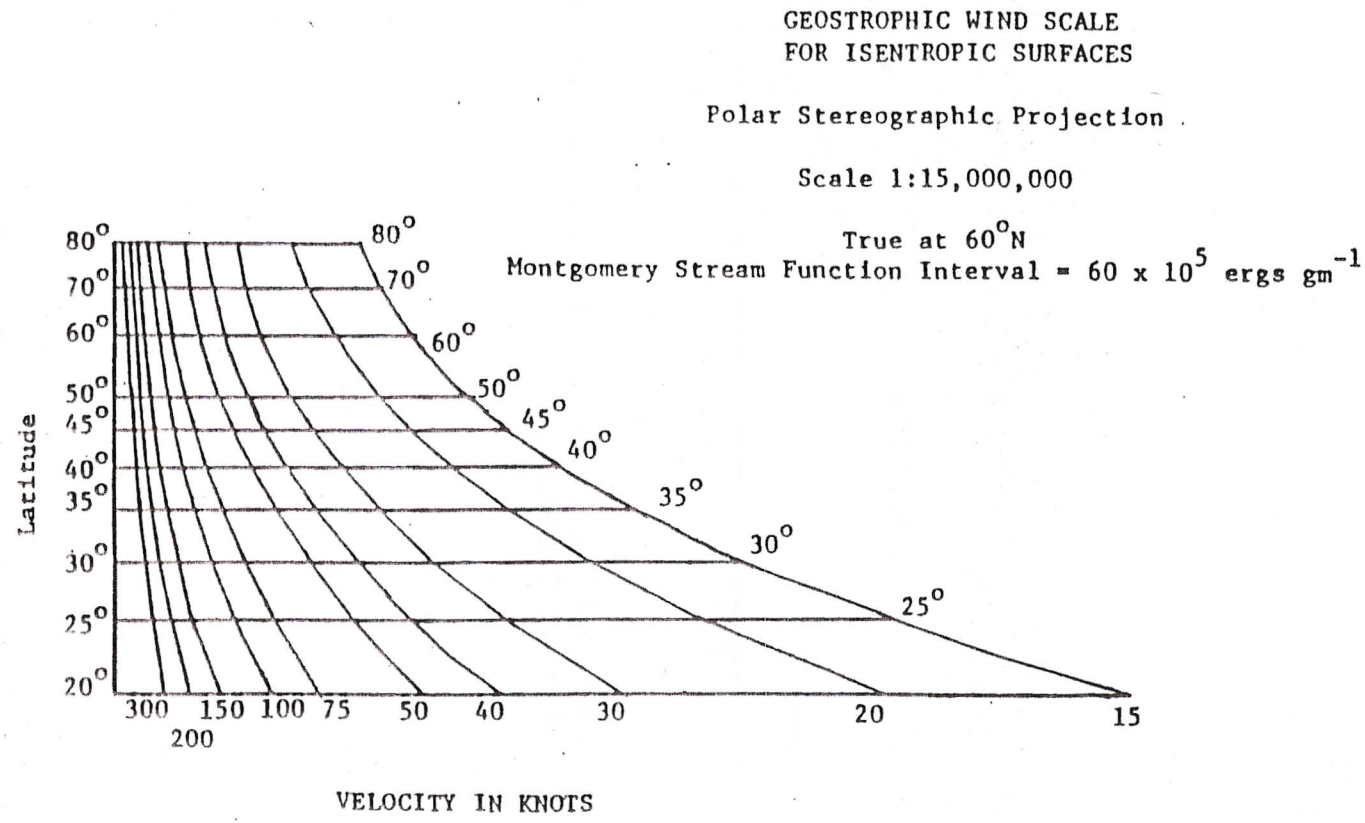


Figure 9. Geostrophic wind scale for an isentropic surface on a polar stereographic map projection with a 1:15 million map scale.

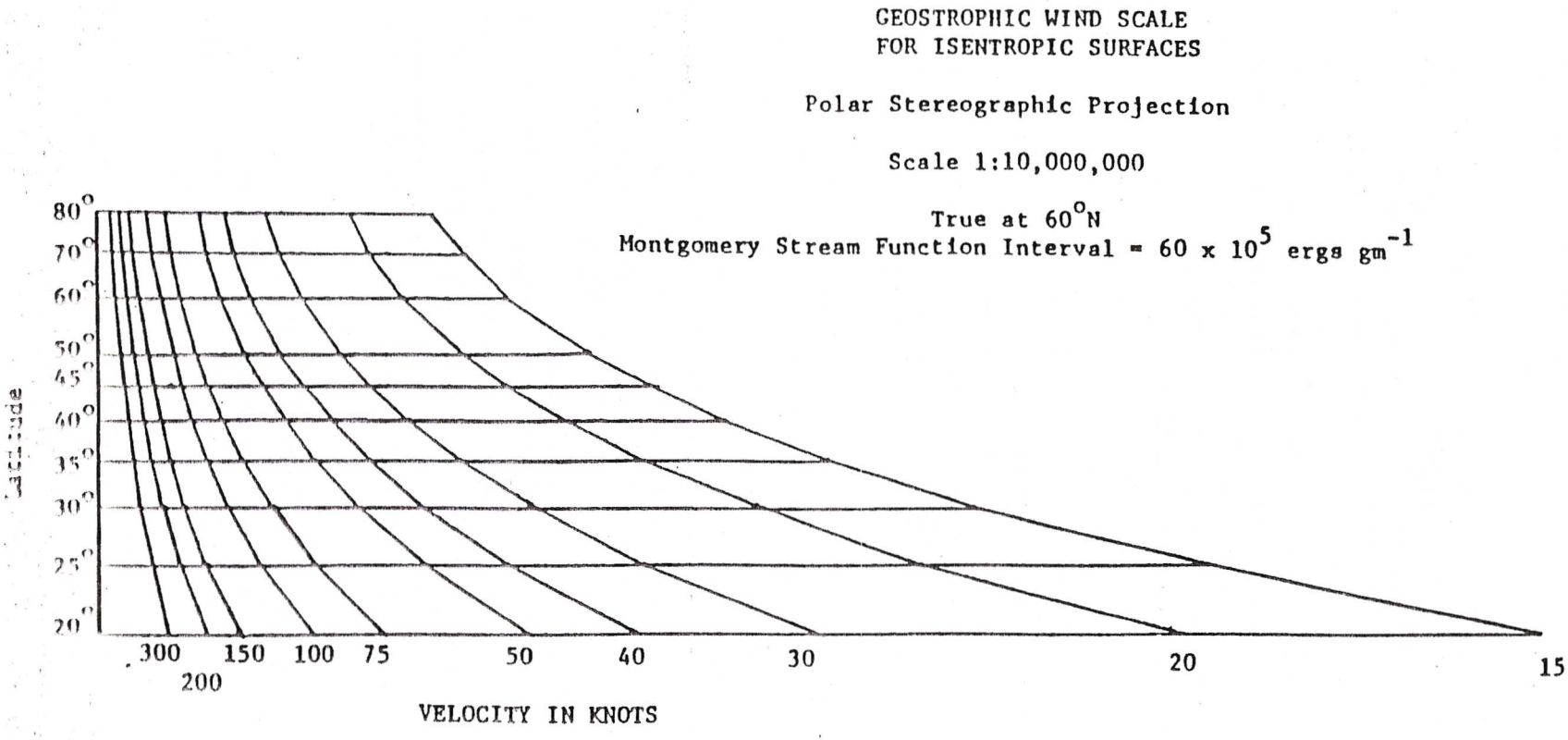


Figure 10. Geostrophic wind scale for an isentropic surface on a polar stereographic map projection with a 1:10 million map scale.

M lines should be apart (if drawn at intervals of 60 x $10^1$ J/kg) to support the given wind speed.

*Thermal Wind Relationship (19):* The thermal wind (the vertical shear of the geostrophic wind) in isentropic coordinates is proportional to the mean pressure gradient in the layer. Since isobars on an isentropic surface are equivalent to isotherms, the thermal wind is also proportional to the mean temperature gradient in the layer as is the case with pressure coordinates. The strength of the thermal wind is related to the vertical tilt of the isentropic surfaces, which is related to the pressure gradient recorded on them. The thermal wind "blows" parallel to the mean isobars in the layer with low pressure (cold temperatures) on the left and high pressure (warm temperatures) on the right looking downwind. This diagnostic relationship is very useful in interpreting cross-sectional analyses and will be discussed in greater detail in Section 3.C.1.

*Gradient Wind Relationships (20-21):* The gradient wind equations are useful for studying accelerated and curved flow. Equation (20) shows that acceleration (deceleration) takes place when the wind blows across the isopleths of Montgomery streamfunction towards lower (higher) values, $\beta > 0$ ($\beta < 0$). For geostrophic flow $\beta = 0$ and there is no acceleration. Equation (21) describes curved flow as it includes the centrifugal force (term 1). For $\beta = 0$ it reduces to the standard gradient wind equation.

*Potential Vorticity (22):* Potential vorticity is defined as the ratio of the absolute vorticity, represented as $\zeta + f$, and the static stability in the column bounded by two isentropic surfaces. Under adiabatic, frictionless flow, potential vorticity is conserved, making it a useful "tag" for parcels. Reiter (1972) discusses how conservation of potential vorticity can be used to trace air parcels out of the stratosphere into the troposphere along tropopause "folds." Much of Danielsen's work referenced earlier used this conservation principle. Holton (1979, p. 87-92) uses conservation of potential vorticity to describe lee side cyclogenesis. Under conservation of potential vorticity, if a layer bounded by two isentropic surfaces shrinks (stretches) in the vertical the absolute vorticity of the column must decrease (increase) in response. After an isentropic layer has crossed the Rocky Mountains, for example, it generally increases in depth as the lowest level follows the topography while the uppermost level remains relatively fixed, leading to increased vorticity to the lee of the mountains.

### F. Constructing an Isentropic Data Set from Rawinsonde Data

The isentropic analysis program that creates isentropic station data from rawinsonde data came originally from a research program written for Danielsen's work in the 1960's. The versions of this program used at Saint Louis University (SLU) and by the Atmospheric Environment Service in Canada are nearly the same. The total computation time to run the program on the University minicomputer is on the order of 5 minutes. Standard and significant level rawinsonde data are needed. In the SLU version, wind data at constant height intervals (PPBB group) are used to

interpolate winds to significant levels (TTBB group). This creates a complete sounding of pressure, height, temperature, dew-point, wind direction, and wind speed for processing. The user can select the interval between isentropic levels in the troposphere and stratosphere.

The actual procedures for the computation and interpolation of isentropic data are described in Duquet (1964) and in Wilson et al. (1980). Montgomery streamfunction values are computed by integrating (13) from the surface upward. Interpolated of all other variables except wind is done assuming linearity with respect to $P^{\kappa}$ where $\kappa = R/C_p = 0.286$. Winds are interpolated linearly with respect to height; direction and speed are interpolated separately. Duquet (1964) notes that the latter method of interpolation tends to smooth the wind hodograph. For each sounding the following variables are computed at each isentropic level:

(1) Montgomery streamfunction (M) in units of $10^1$ J/kg.

(2) Pressure (P) in millibars.

(3) Virtual Temperature ($T_v$) in degrees C.

(4) Height (Z) in gpm. The height is determined by integrating the hypsometric equation from the ground up.

(5) Actual specific humidity (q) in gm/kg. This is obtained by computing $e_s$ (the saturation vapor pressure) from the Clausius-Clapeyron equation using the interpolated *dew point* temperature and then finding q from the relation:

$$q = \frac{.622\, e}{P - .378\, e} \tag{24}$$

(6) Saturation specific humidity ($q_s$) in gm/kg. This is found as in (24) except using the interpolated *virtual temperature*.

(7) Relative humidity in percent computed as the ratio of $e/e_s$ or $q/q_s$.

(8) Wind speed and direction in degrees and m $s^{-1}$.

(9) Stability, upper and lower, measured as the distance in mb to the adjacent higher and lower isentropic levels.

(10) Wind shear at a given level is determined from the winds and streamfunctions at the levels immediately above and below the isentropic surface. Directions are given in degrees. Speed shears are multiplied by appropriate constants and displayed in millibars per degree latitude. These unusual units are useful to the analyst since they relate the vertical wind shear to the isobaric gradient on an isentropic surface as discussed earlier in (19).

With respect to the Montgomery streamfunction it should be noted that when stated in units of $10^1$ J/kg, a difference of *one* in the last digit corresponds to a height difference of *1 meter*. Therefore, a difference of 60 x $10^1$ J/kg, which is a typical contour interval for M, corresponds to 60 meters in height on a constant pressure surface.

As noted earlier in the SLU version of the Duquet program, neutral-superadiabatic lapse rates will result in multiple pressure levels for one isentropic

surface. At Saint Louis University we follow a method described by Haltiner and Williams (1980) to check each sounding for adiabatic or superadiabatic lapse rates, adjusting these layers to create slightly stable lapse rates. This is accomplished by cooling the bottom of the layer and warming the top of the layer to stabilize it while conserving the total energy. After all layers are adjusted the sounding is examined again to stablize layers which may have been destabilized by the above procedures.

## III. ISENTROPIC ANALYSIS TECHNIQUES

In this section we will explore various analysis procedures for both vertical and "horizontal" plots of isentropic data. Emphasis will be placed on practical applications to everyday forecast problems.

There are basically three different charts used in isentropic analysis: the psi chart, the sigma chart, and the isentropic cross section. The psi chart is named after $\psi$, which typically represents a streamfunction--in this case the Montgomery streamfunction. In this set of notes we have used M instead of $\psi$. The sigma chart is so named because static stability ($\partial P/\partial\theta$) is often represented as $\sigma$. It should be noted that several researchers/analysts prefer to plot all their isentropic surface data on one map rather than split it up into two charts. This is a user-selectable feature and therefore is left to the reader. For completeness we will show several station models so that the reader may compare the various options.

### A. Psi Charts

On the psi chart the following variables are plotted: Montgomery streamfunction, wind direction and speed, mixing ratio, and relative humidity. The M value can be plotted in cgs or mks units. A typical value is 30,600 x $10^5$ ergs/gm or equivalently 30,600 x $10^1$ Joules/kg. Either way, the leading digit is usually not plotted--the 3 or 2 preceding it is understood. A typical station model plot is shown in Fig. 11.

Contour intervals will vary according to the season but typical values for warm/cold seasons are as follows:

| Variable | Contour Interval | |
|---|---|---|
| Montgomery Stream Function | 30/60 x $10^1$ | J/kg |
| Pressure | 25/50 | mb |
| Wind Speed | 10/20 | m $s^{-1}$ |
| Actual Specific Humidity | 2/1 | gm/kg |
| Relative Humidity | 50/70/90 | % |

As on any chart a maximum of three types of isopleths is suggested, preferably using a color scheme along with solid, dashed, or dotted lines. The "starting value" of the Montgomery streamfunction is a function of the level. It is usually best to start at an even number; e.g. 31,000 or 29,800 x $10^1$ J/kg, whenever possible and, of course, to be consistent from day to day on the same surface. The Montgomery streamfunction field helps to define the flow of the geostrophic wind and also to identify short/long wave activity much as on a constant pressure chart.

Isobars also should be started at some even number like 600 or 700 mb. They help to define cold and warm tongues on the isentropic surface. Strong gradients of pressure also can be used to locate frontal zones as seen in Fig. 12. Anderson

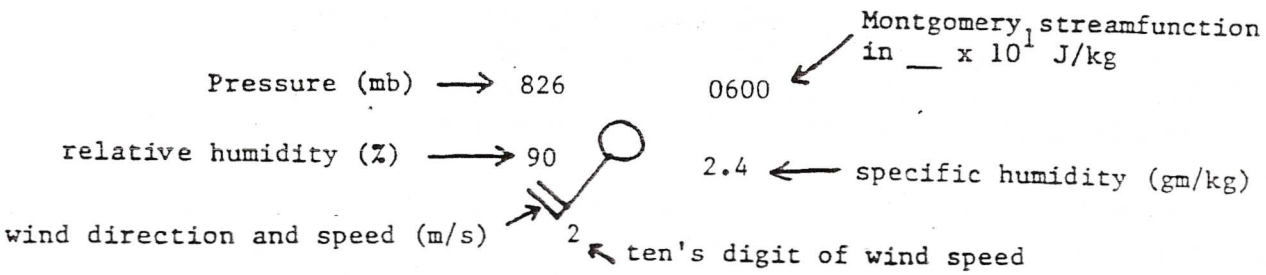


Figure 11. Station model plot for psi charts.

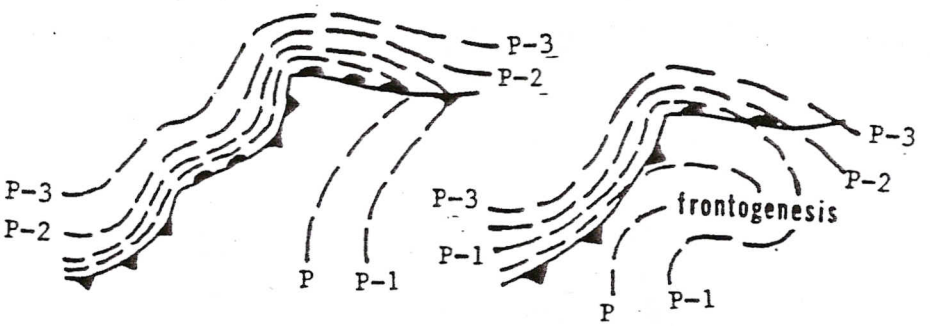


Figure 12. Isobaric topography in the vicinity of fronts (a) and isobaric topography associated with frontogenesis in the warm sector (b) (Namias, 1940).

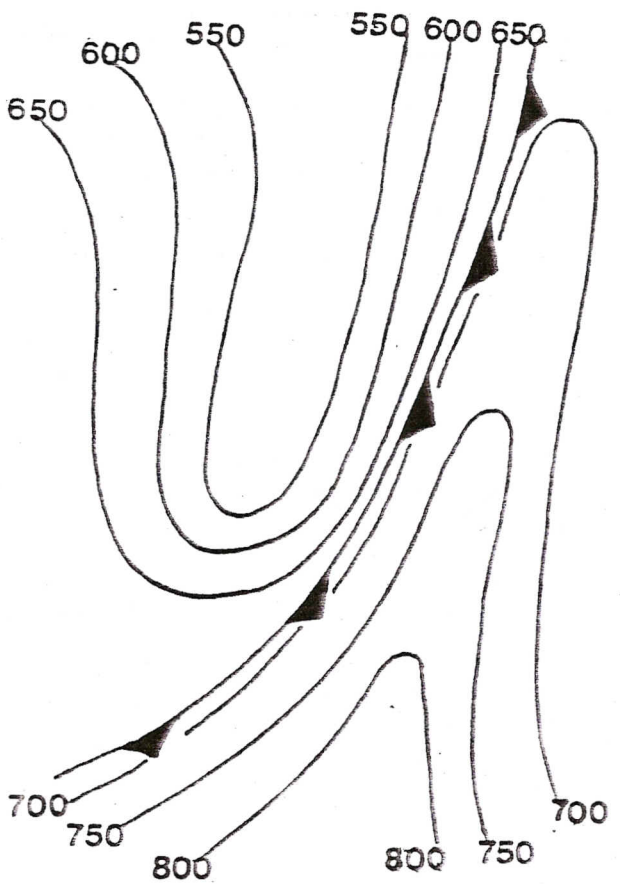


Figure 13a. Isentropic pressure pattern in the vicinity of a strong, mature cold front (Anderson, 1984).

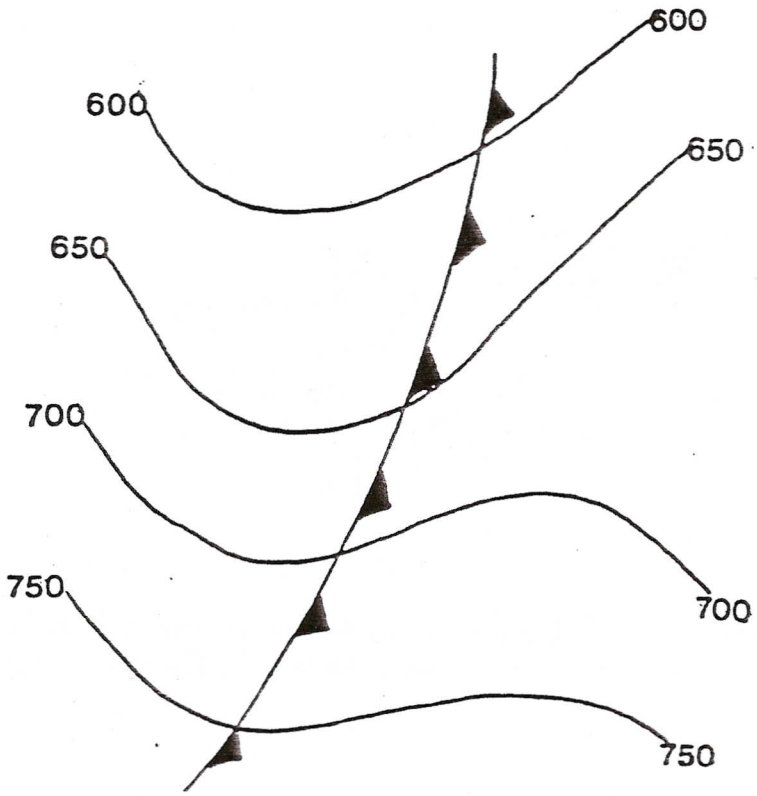


Figure 13b. Isentropic pressure pattern in the vicinity of a frontolysizing cold front (Anderson, 1984).

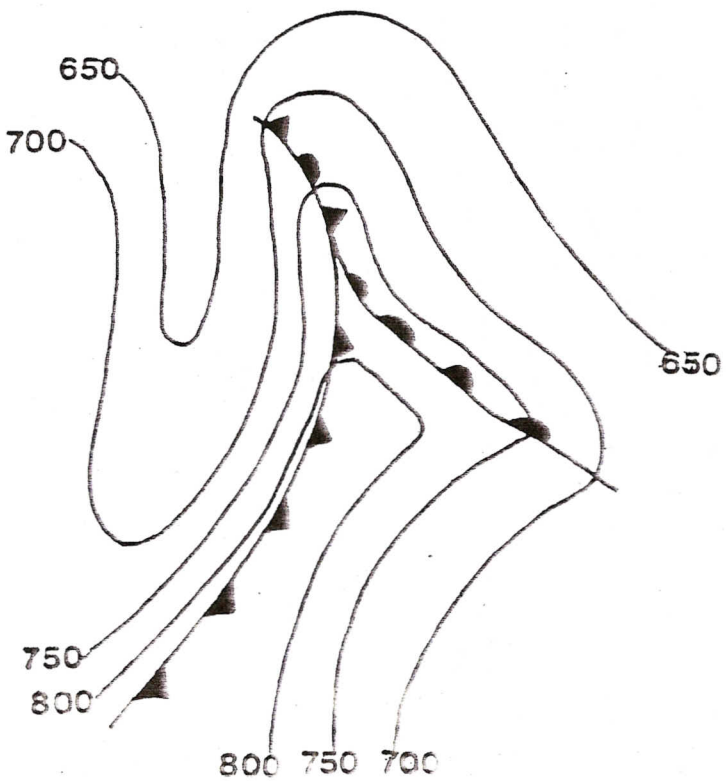


Figure 13c. Isentropic pressure pattern in the vicinity of an occluding frontal system (Anderson, 1984).

(1984) has described various isobar patterns in the vicinity of frontal systems. Figure 13a shows a pressure pattern in the vicinity of a strong mature cold front. The cold front is placed at the leading edge of the pressure gradient with the warm (high pressure) thermal ridge extending in a narrow tongue ahead of the front. Isobars are usually found to cross a frontal system undergoing frontolysis (Fig. 13b). The lack of structure in the pressure field is indicative of a weakening thermal gradient and decaying frontal zone. In the case of an occluding system warm tongues tend to be diagnosed along the warm front and occlusion portions of the cyclone with a cold (low pressure) trough extending southward behind the cold/occluded fronts (Fig. 13c). Also, as discussed earlier, the cross-isobar component of the wind can be used qualitatively to estimate the upslope/downslope adiabatic vertical motion. Isobars are good as reference values, especially for someone just beginning isentropic analysis and remind the analyst of the three-dimensional nature of this "horizontal" surface.

Mixing ratio isopleths (isohumes) are, of course, essential for depicting moist/dry tongues and their advection. Figure 14 depicts an idealized isohume pattern associated with an occluding system. It should be noted that in winter it is not uncommon to receive substantial precipitation out of clouds in which the specific humidity is less than 1 gm/kg (Byers, 1938). Therefore, the isohume contour internal is seasonally dependent and level-dependent as specific humidity values often decrease rapidly with height. A typical isentropic upslope pattern is depicted in Fig. 15 with a south-southwesterly flow on this isentropic surface air being lifted as it transports moisture northward.

With two isentropic levels analyzed one can often diagnose regions where convective instability is being increased as dry air aloft is advected over moist air below. Such a situation is shown in Fig. 16. Notice how low level moist air is currently being overlain by upper level dry air thereby increasing the convective instability. In other cases it may be possible to predict this pattern based on advection patterns at the two levels.

Relative humidity is helpful to estimate how close some areas are to saturation so that the analyst may be careful in interpretation. To avoid map clutter one may isopleth the 50, 70, 90% values or merely shade in green values exceeding 70%.

Isotachs may be drawn as well to help diagnose jet streaks at low, middle, or high levels. Keep in mind that the jet streak depicted on an isentropic chart is being drawn in its three-dimensional detail so one is not only seeing its length and width, but its depth. One intangible benefit of such an analysis is that it reinforces the view of the atmosphere as a continuous fluid. Such an appreciation is difficult to obtain with constant pressure analyses, which are two-dimensional and quasi-horizontal.

### B. Sigma Charts

The sigma chart is primarily a stability chart. The variables typically plotted on it are pressure, thermal wind, the number of millibars needed to reach the $\theta + 5$ K isentropic surface, and the number of millibars needed to reach the $\theta - 5$ K isentropic surface. In this station model we have assumed that the 5 K interval was chosen

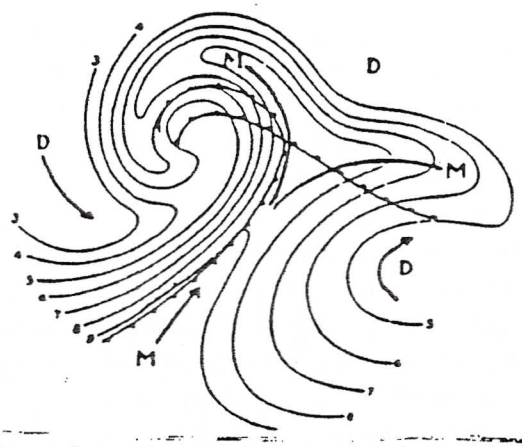


Figure 14. Fronts indicated at the surface and schematic flow pattern around an occluded cyclone as shown by the moisture lines in an isentropic surface in mid-air (Namias, 1940).

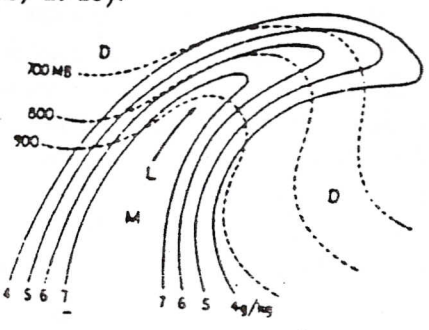


Figure 15. Illustrating probable upslope motion of a moist current as deduced from the relation of the moisture lines to the isobars on an isentropic surface (Namias, 1940).

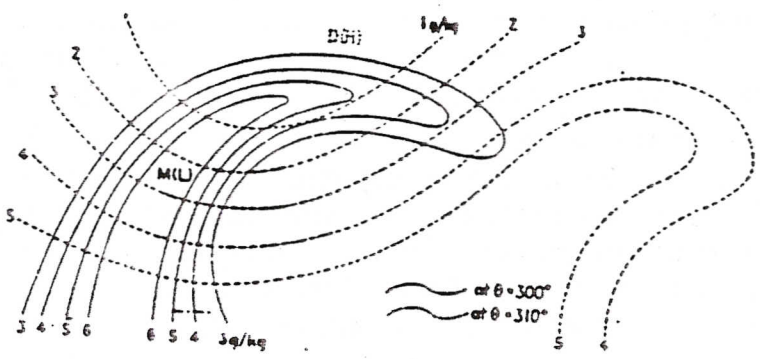


Figure 16. Flow pattern at different isentropic surfaces which leads to increasing convective instability. Solid (dashed) lines are isohumes at low (upper) level (Namias, 1940).

as an option when creating the data set. However, this number depends on the interval chosen, which is up to the researcher/analyst. The plotting model varies among researchers but looks essentially as shown in Fig. 17.

Some people plot the total of the two LHS numbers in the bottom right corner, thus indicating the stability over a 10 K interval. These numbers indicate the static stability ($\partial P/\partial \theta$) which on a cross section would show up as the distance in millibars between two adjacent isentropic surfaces. The greater the distance between two adjacent isentropic surfaces, the less stable the layer. Small distances between isentropic surfaces indicates great stability. In the stratosphere, for instance, the static stability is usually around 10 K per 50 mb or less, while tropospheric values are generally around 10 K per 100-200 mb! By isoplething the total static stability (the sum of the LHS numbers) we can obtain an excellent diagnosis of the instability.

Typical contour intervals will once again vary with the season but are typically as follows:

| Variable | Contour Interval |
|---|---|
| Pressure | 25/50 mb |
| Static Stability | 10/20 mb |

Although it might be better to analyze for the total static stability (lower $\Delta P$ + upper $\Delta P$) it is good to see the breakdown of the two layers to see where the greater instability is located.

The plotted thermal wind is computed for the layer surrounding the actual isentropic level in question. If one were analyzing the 300 K surface, the thermal wind would be valid for the 295-305 K layer (if a 5 K interval was chosen). One can use the thermal wind directions to help draw the isobars since, according to (19), the thermal wind in a layer "blows" parallel to the mean isobars of the layer. Similarly, the gradient of the isobars can be qualitatively checked by noting the speed of the thermal wind. Strong (weak) thermal winds are associated with large (small) isobaric gradients on isentropic surfaces. One word of warning—these wind shears are based on the actual wind—not the geostrophic wind. So the degree to which this actual wind shear "obeys" the pressure gradient depends on the degree to which the actual wind "obeys" the geostrophic wind. It is possible for ageostrophic wind components; e.g., those in the vicinity of convective systems or jet streaks, to produce wind shears which are out of balance with the expected geostrophic shear. In any event, forecasters, especially those in aviation, should find these wind shear calculations informative for the diagnosis/prediction of turbulence. Other forecasters may use the wind shear to measure the significance of a frontal boundary or elevated inversion.

For completeness, we also show two other plotting models which essentially combine the features of the psi and sigma charts. Wilson (1985) uses the plotting model shown in Fig. 18. He uses one variable that has not been discussed yet—the saturation pressure or lifted condensation pressure. Essentially this is the level to which the parcel must be lifted to achieve saturation. It gives a quick assessment of

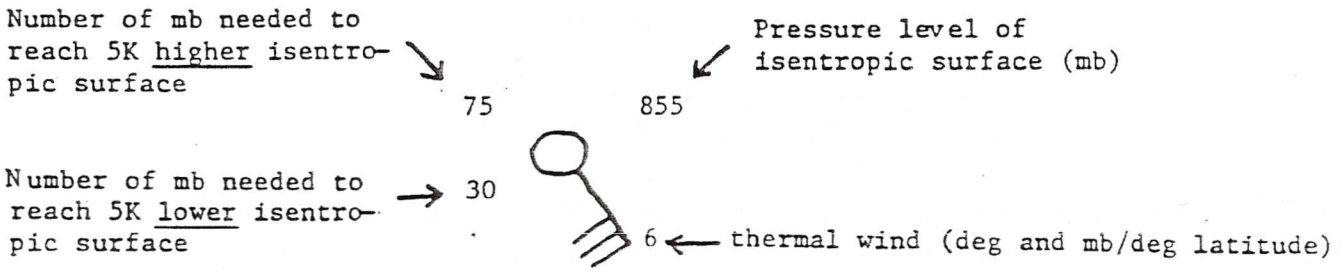


Figure 17. Station model plot for sigma charts.

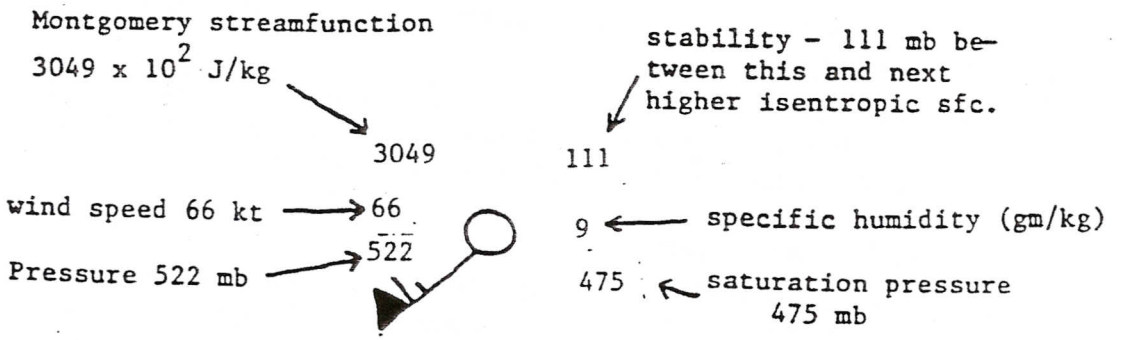


Figure 18. Wilson (1985) station model plot.

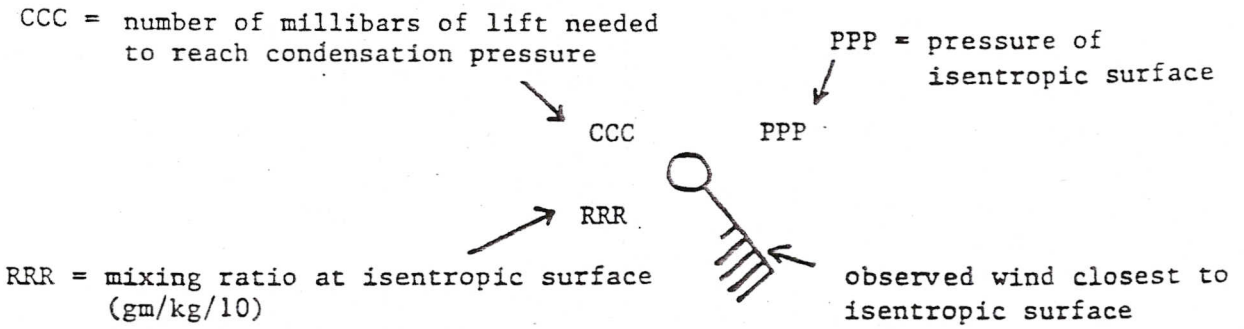


Figure 19. Plotting model used by ISENT (NWS Southern Region isentropic plotting program used on AFOS), Little (1985).

how close the atmosphere is to saturation at a station. More will be said of this later. Other variables are as described earlier.

Little (1985) describes a program for AFOS called ISENT which plots isentropic data in the form shown in Fig. 19.

As with any analysis scheme you should pick the station model(s) that suit your needs. The author usually tries to avoid analyzing more than three variables per map—preferably only two for easier viewing and presentation.

### C. Cross Section Analysis Techniques

We now will turn our attention to vertical "slices" through the atmosphere--cross sections. They usually are the first step in choosing the "horizontal" isentropic surfaces to analyze. One typically chooses the surfaces which are embedded in an interesting feature; e.g., baroclinic zones, jet streaks, or moist tongues. Generally, in addition to the isentropes, it is also interesting to display mixing ratio (or specific humidity) and/or winds on the cross section. The mixing ratio profiles are useful in gauging the depth of the moist layer and possible areas of convective instability (dry air over moist air). The wind profile is useful at depicting the vertical extent of jet streaks or wind maxima but also has an interesting relationship to the tilt of the isentropic surfaces. This is the subject of the next section.

#### 1. Thermal Wind Relationship in Isentropic Coordinates

An isentropic cross section is generally chosen to be *normal* to a jet streak or wind maximum and therefore *across* a baroclinic zone (i.e., frontal zone). This allows one to depict the vertical and horizontal dimensions of the jet streak and attendant baroclinic zone. Mixing ratio profiles are also quite variable and interesting in this area, too. Since the baroclinic zone is, by definition, a region of strong thermal contrast, one would expect to see a great tilt of the isentropic surface from high in the cold air to low in the warm air. From thermal wind consideration this requires strong vertical wind shear through these zones.

From our earlier discussion of the thermal wind you may recall that it "blows" parallel to the mean isobars in the layer or normal to the pressure gradient such that low (cold) pressure is to the left of the thermal wind looking downstream. In a cross section depiction we are graphically representing only a *component* of the total isobaric gradient. There is no guarantee that the chosen cross section is exactly parallel to the isobaric gradient associated with the jet streak. Therefore, we plot on the cross section only the *wind components* normal to the plane of the cross section. Wind components *into* the plane of the cross section are generally designated as positive while those wind components *out of* the plane of the cross section are designated as negative. It is these normal wind components which have a relationship to the pressure gradients depicted in the cross section.

To obtain the normal wind components it is necessary to know the angle between the plane of the cross section and true north-south. However, rawinsonde stations do not generally all lie on a straight line. So what is done? In the SLU cross section program we compute a least squares regression line for the stations chosen. The position of the stations is then chosen on this regression line

perpendicular to the original station location as seen in Fig. 20. One must intelligently choose stations which are approximately on a line because the regression line computation is "dumb"; i.e., even a series of stations along a curve will be placed on a *line*. Let the user beware!

Figure 21 is a schematic example of how we can relate vertical wind shear to the tilt of isentropic surfaces in a cross section. Notice how the upper isentropic surface slopes down from the cold air (pt. A) to the warmer air (pt. B). Therefore, the gradient of pressure in the plane of this cross section points from A to B. Since the thermal wind points into or out of the cross section with cold air to the left (looking downwind), the thermal wind will point into the page in this case. The net result is that we expect the wind components into the page to *increase* with height in this area of the cross section. This means that for this N-S cross section westerly winds will increase with height. We can now state three general rules (assuming north is to the left and south is to the right):

(1) When isentropic surfaces slope *down*, the thermal wind is positive; i.e., wind components *into* the plane of the cross section increase with height.

(2) When isentropic surfaces slope *up*, the thermal wind is negative; i.e., wind components *out of* the plane of the cross section increase with height.

(3) When isentropic surfaces are horizontal (quasi-barotropic), the thermal wind is approximately zero and the normal wind component does not change with height.

On a typical cross section one plots the potential temperature, specific humidity and normal wind components as shown in Fig. 22.

In the troposphere it is useful to draw isentropes at 2-4 K intervals, but as one nears the stratosphere it is best to double the interval to at least 4-8 K as the stability is very strong. Since water vapor decreases quickly with height a good contour interval for specific humidity is 1-2 gm/kg. Finally, isotachs can be drawn at 5 m/s intervals. Remember that values can be + or -; therefore, a zero line may need to be drawn.

**2. Isentropic Topography in the Vicinity of Upper-Level Fronts and Jet Streaks**

An averaged, idealized cross section from north to south is shown in Fig. 23. There are many interesting features in this cross-section. They include:

(A) The polar frontal jet (PFJ) and its associated polar front are seen around 40-50°N. The polar front is depicted as a sloping zone (indicating strong thermal contrast) and as a compacted isentrope zone indicating stability. Although it is shown in Fig. 23 as identifiable all the way to the surface, this is not always the case, since the isentropic surfaces lost continuity in the boundary layer. The PFJ is placed at about 350 mb, a little lower in the atmosphere than perhaps it should be. It is above the polar front where the vertically-integrated result of the thermal wind effects is greatest. Note how the isentropes slope up above the PFJ, indicating a reversal of the thermal wind in the stratosphere and a subsequent decrease in westerly momentum. Also notice how there is a gap in the

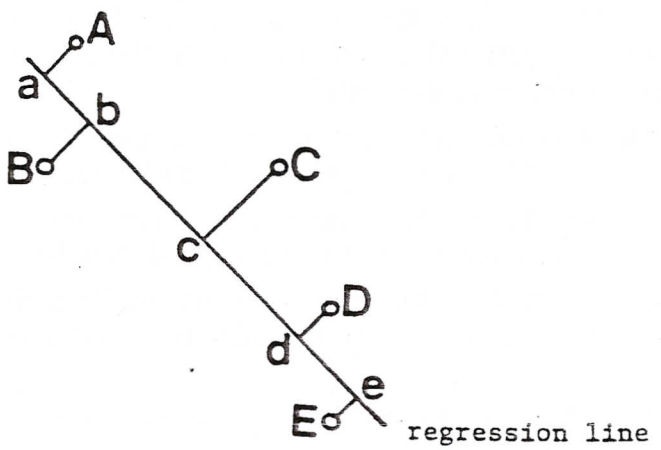


Figure 20. Schematic showing how stations are depicted with respect to the regression line and their original positions.

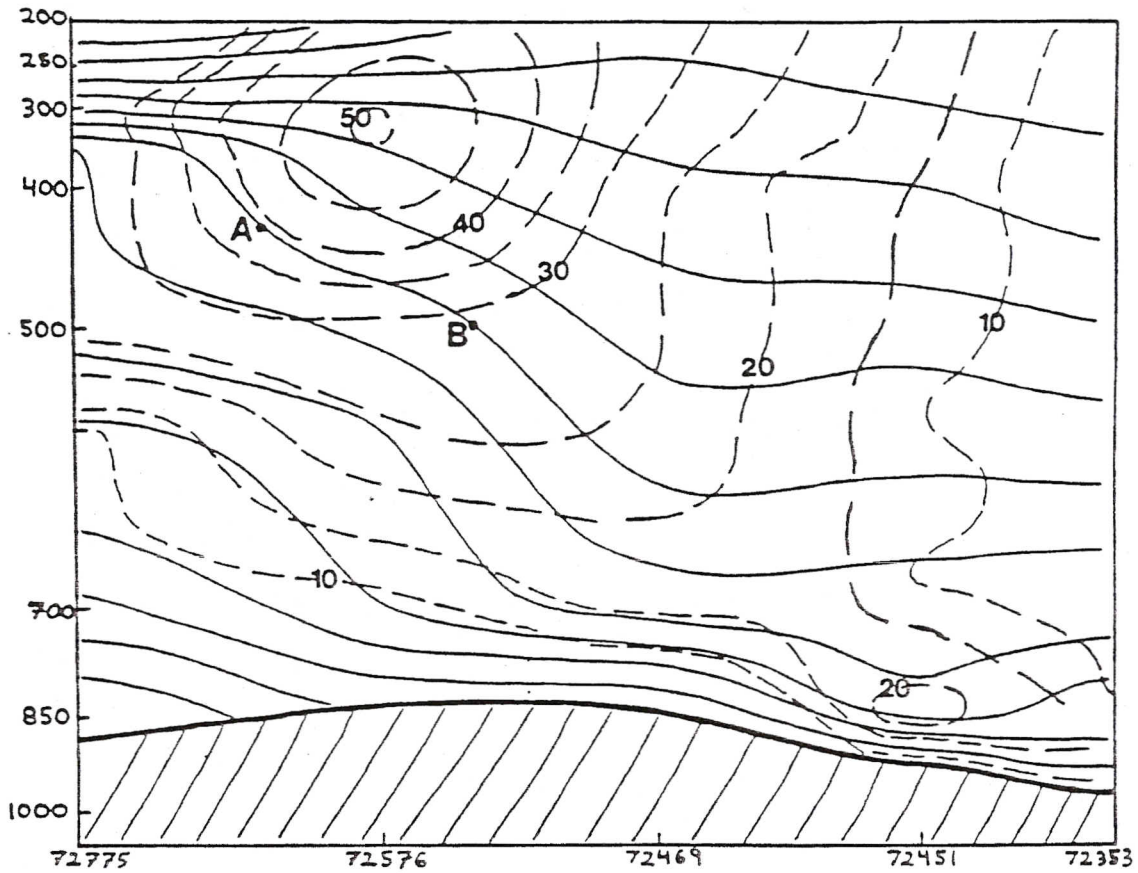


Figure 21. Cross section illustrating the relationship between sloping isentropic surfaces and the vertical wind shear. Solid lines are isentropes and dashed lines are normal wind components where + (-) indicates winds into (out of) the plane of the cross section.

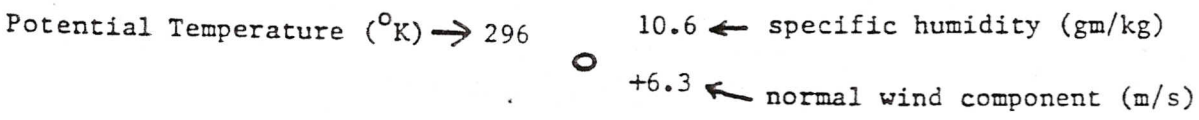


Figure 22. Cross section plotting model.

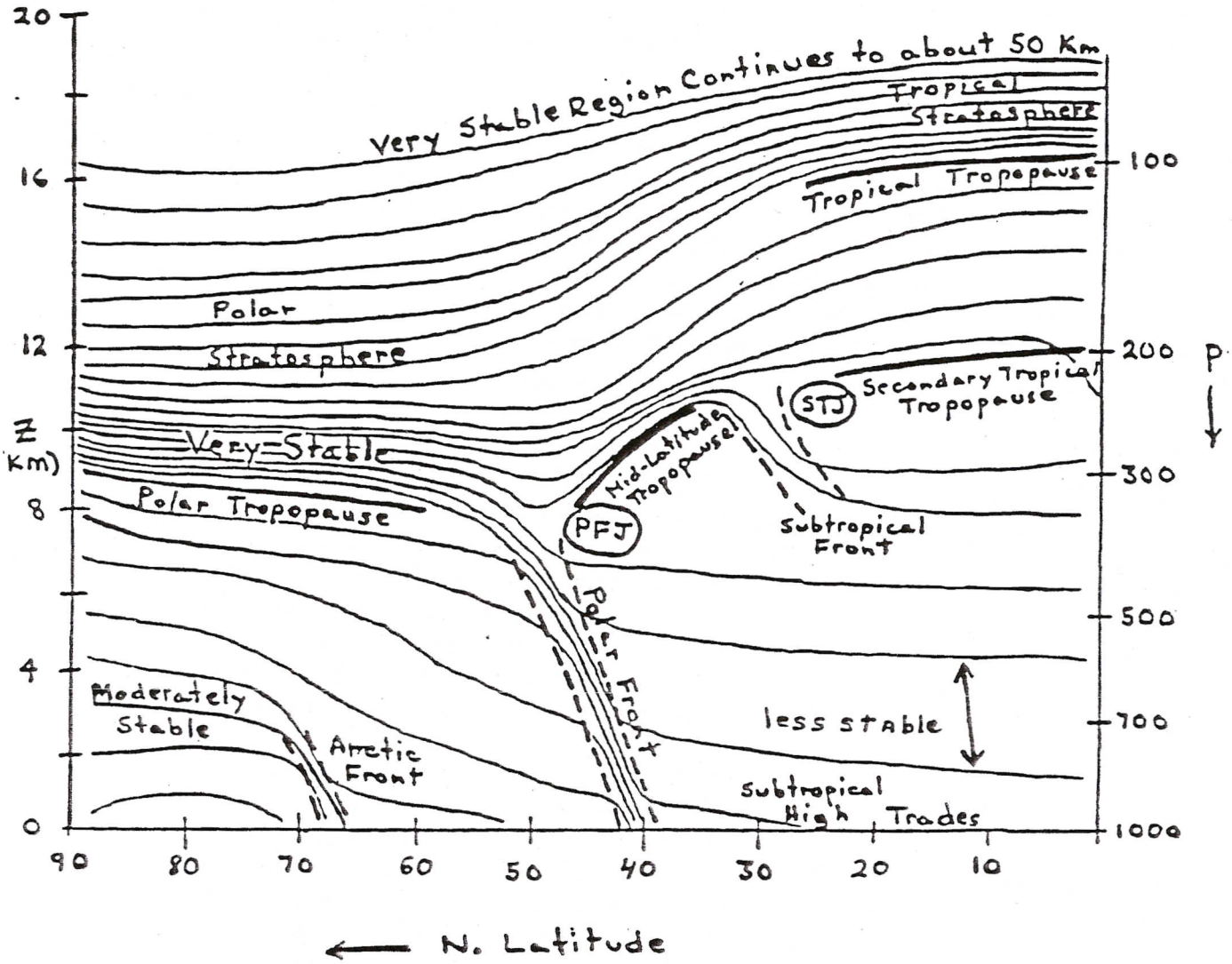


Figure 23. Idealized and averaged picture for the annual mean or the Spring and Autumn seasons. In summer the tropopause lifts at middle and high latitudes, the tropospheric gradients and the Arctic front weaken or vanish, and the associated jet streams weaken or vanish. The subtropical jet (STJ) stream in particular weakens and the subtropical highs shift poleward. In winter the polar frontal jet (PFJ) stream often merges with the STJ stream especially over the continents; the gradients in the troposphere are stronger then and the stability is greater, but nowhere near as stable as the stratosphere. The sloping isentropes imply that the westerlies increase with height in the troposphere, and decrease with height to become easterlies in the stratosphere, except at very high latitudes. There is again a strong seasonal variation in the stratosphere, with westerlies at high latitudes moving southward to middle latitudes and strengthening in winter.

tropopause in the vicinity of the PFJ. In fact the polar front appears as an extension of the strongly stable air of the stratosphere. In this region there is considerable stratospheric-tropospheric air exchange. This shows that the tropopause is not quite the "lid" or impermeable layer it was once thought to be. We will return to this concept later.

(B) The air in the troposphere is much less stable than the stratospheric air. This is seen by comparing the vertical distances between isentropes in both regions. The air in the troposphere is *not* unstable generally but *relatively less stable* —the farther apart the isentropes the less stable the lapse rate. Potential temperature lapse rates of 10 K/100 mb are not uncommon, whereas in the stratosphere lapse rates are generally about 10 K/50 mb or more.

(C) The arctic front shows up as a shallow, few kilometer deep layer of stable air with strong vertical tilt. This is a good example of how one can gauge the depth of systems and perhaps, as in this case, determine whether a system in low levels is vertically coupled to the upper air flow.

(D) The subtropical jet (STJ) is shown to be associated with a weak upper tropospheric front. This is not unexpected since the STJ is not explained through thermal wind arguments as is the PFJ. It comes about as a result of air flowing north in the upper branch of the Hadley cell circulation attempting to conserve its angular momentum. As it flows north its angular velocity increases in response to a shorter distance to the earth's axis of turning. The STJ can be even stronger than the PFJ, with speeds of up to 260 knots observed over southern Japan (Palmen and Newton, 1969). Palmen and Newton (1969) also observed that the STJ is characterized by great steadiness in both wind direction and geographic location, and tends to have an anticyclonic curvature. The STJ tends to be associated with a "break" between the mid-latitude tropopause at around 250 mb (noticeably higher than the PFJ) and the tropical tropopause typically found at 100 mb. Often on jet charts or 200 mb charts it is difficult to determine if a jet streak is part of the PFJ or STJ. A cross section of winds will help diagnose these two jet streams. However, in the winter it is not uncommon for the two jet systems to merge as the PFJ moves southward with the polar front.

(E) The tropopause, especially in middle and higher latitudes, is easy to locate, except near significant jet streaks where the tropopause "breaks" occur. The tropopause appears as a zone where the vertical lapse rate of potential temperature increases by about an order of magnitude.

### D. Useful Diagnostic Variables Computed from Isentropic Data

Once an isentropic data set has been generated from rawinsonde data it is relatively straightforward to interpolate the station data to a grid on a map projection (e.g., lambert conformal, polar stereographic). This can be done using one of the more popular objective analysis schemes (e.g., Barnes, 1973). Details of this procedure will not be discussed in this paper. For an excellent treatment of this subject see Koch et al. (1983). Once grids of u, v, P, q, M are obtained for a particular isentropic surface numerous diagnostic variables may be computed. In this section

we will briefly discuss some of these variables and how they might be used in diagnostic analysis.

**1) Static Stability:** This variable can be expressed as $\Delta P$ = P (upper $\theta$ surface) - P (lower $\theta$ surface) which is always <0, although some people like to define it in the opposite sense so that it is always > 0. In any event, it is a relative measure of instability which *does not* take moisture into account. Horizontal plots of this variable on an isentropic surface, using adjacent surfaces for the computation, are "quick and dirty" estimates of stability and stability change. Units are millibars.

**2) Moisture Advection/Convergence:** Moisture advection is expressed mathematically as $-\vec{V}\cdot\vec{\nabla}q$. Values > 0 (or < 0) indicate increasing (or decreasing) moisture locally. Local increases or decreases of moisture; e.g., through evaporation or condensation, are neglected. Essentially it evaluates quantitatively what one can estimate qualitatively by superimposing the flow (streamlines or Montgomery streamfunction) over the isohumes. Units are generally gm/kg-hr x $10^{-1}$. (Multiplying by 10 inflates the values to bring out important features.)

To take this one step further, one can compute moisture convergence on isentropic surfaces expressed as $-\vec{\nabla}\cdot q\vec{V}=-\vec{V}\cdot\vec{\nabla}q-q\vec{\nabla}\cdot\vec{V}$. As you can see, it includes the advection of moisture *and* the effect of divergence/convergence on the moisture field. In an isentropic framework this variable measures not only the advection of moisture but also the destabilization (or stabilization) that takes place with convergence (or divergence). Thus, positive values indicate positive moisture advection and/or destabilization due to convergence. This is often useful in forecasting convection. Negative values indicate drying out due to negative moisture advection and/or stabilization associated with divergence. Units are gm/kg-hr x $10^{-1}$.

**3) Adiabatic Vertical Motion:** This variable can be expressed as:

$$\omega_{adiabatic} \approx (\vec{V}-\vec{C})\cdot\vec{\nabla}_\theta P$$

where, as noted earlier, $\vec{C}$ is the speed of the system (cyclone or anticyclone). System (or storm) relative vertical motions tend to be better correlated to satellite imagery than those obtained by assuming $\vec{C}$ = 0. Non-zero values of $\vec{C}$ account for the fact, that the isentropic surface is moving horizontally. Saucier (1455) cautions, that, "Isentropic motion is considered motion in which the potential temperature of an air parcel is conserved (i.e., $d\theta/dt$ = 0) and the particle remains on its isentropic surface; it should not be understood as motion necessarily parallel to isentropic surfaces, since the surfaces usually are displaced also."

Figure 24a-b illustrates how the motion of a short wave trough may contribute to the vertical motion on an isentropic surface. Note, that at time $t_o$, the 300 K isentropic surface at station A is located at 900 mb. The plan view of the isentropic surface (Fig. 24a) reveals airflow from high to low pressure, implying upward vertical motion. However, over the next 12 hours the trough "lifts" and becomes negatively tilted, so that the 300 K surface is now at 1000 mb at station A (Fig. 24b). Thus, over the 12 hour period the 300 K surface moved from 900 mb to 1000 mb, thereby,

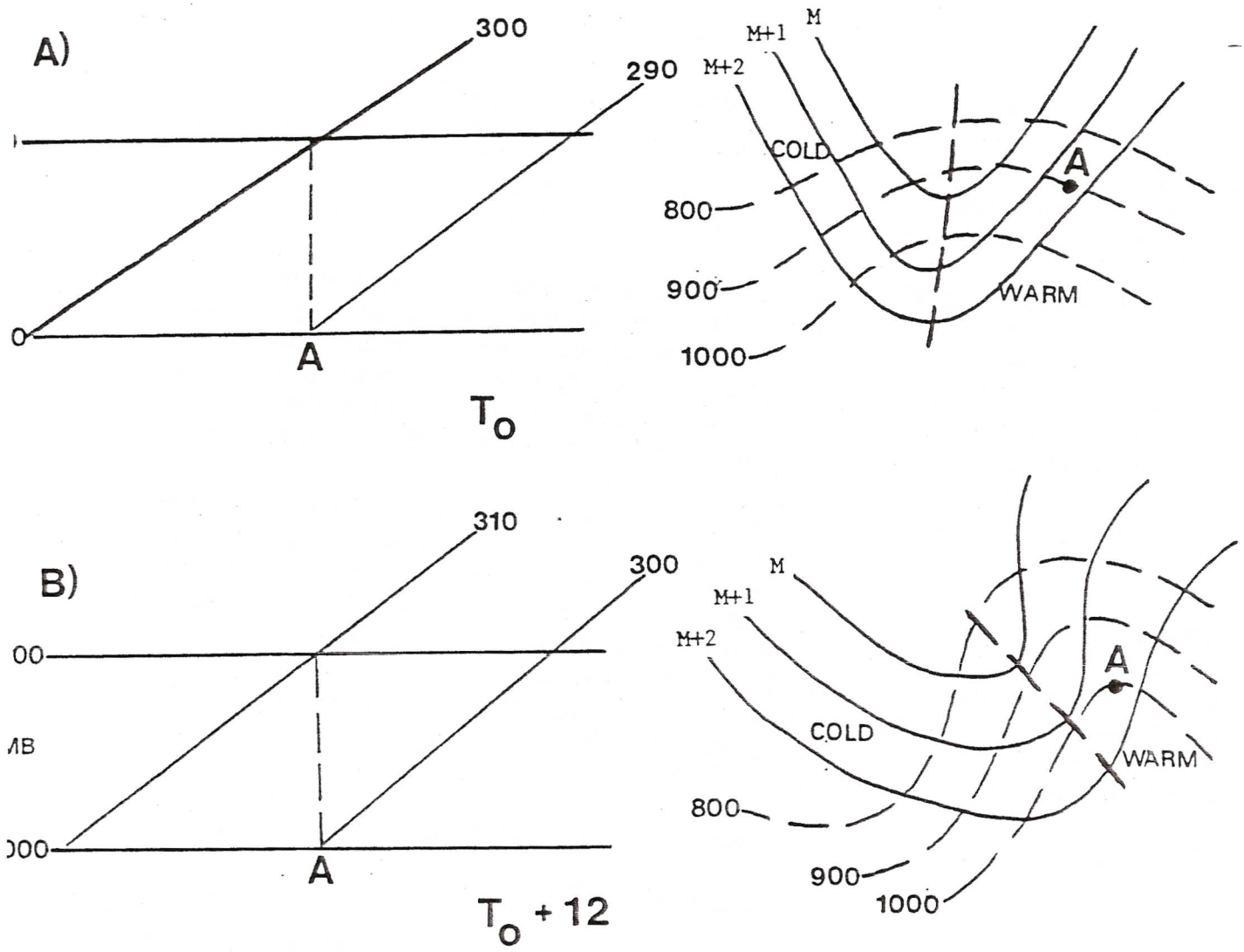


Figure 24a-b. Schematic illustration depicting how movement of system affects vertical motion on an isentropic surface. (a) At time $t_o$ cross section of isentropes at point A. Below, plan view of short wave trough; solid lines are Montgomery streamfunction and dashed lines are isobars (mb) on 300 K isentropic surface. (b) Same as (a), except for time $t_o$ + 12 hours.

contributing to the *downward* vertical motion. This effect on system motion on the vertical motion field is accounted for by using system-relative flow, instead of ground-relative flow.

Negative (positive) values imply upward (downward) motion on an isentropic surface. This expression is a reasonable approximation to (7) since, as described by Homan and Uccellini (1987), the local pressure tendency term will always act against the diabatic term in (7). The remaining term shown above is thus a good approximation to vertical motion, especially at the synoptic scale. It is essentially measuring what you would qualitatively estimate from the cross-isobar component of the streamlines or Montgomery streamfunction. Units are generally μbars/s to be consistent with standard measures of vertical motion.

**4) Static Stability Tendency:** This variable is taken from the continuity equation (14) discussed earlier. Assuming no diabatic effects we can write (14) as:

$$\frac{\partial}{\partial t}\left(\frac{\partial P}{\partial \theta}\right) = -\vec{V}\cdot\vec{\nabla}\left(\frac{\partial P}{\partial \theta}\right) - \frac{\partial P}{\partial \theta}\left(\vec{\nabla}\cdot\vec{V}\right) \qquad (25)$$

Since $\partial P/\partial\theta$ is always $< 0$ (for $\theta$ to be a valid coordinate!) it flips the sign of the tendency term. If either the advection *or* the divergence term is *negative* they contribute to *destabilization*. Likewise, *positive* values indicate a tendency towards *stabilization*. The advection term simply moves existing patterns of static stability about, while the divergence term can create or destroy static stability. Divergence in the layer acts to *increase* stability (+ sign) while convergence acts to *decrease* stability (- sign). To compute these terms one uses $\partial P/\partial\theta$ centered on the isentropic surface whose u and v wind components are used. Units can be written as mb/K-s x $10^{-5}$.

**5) Absolute Vorticity:** Absolute vorticity can be computed as:

$$\eta_\theta = \zeta_\theta + f = \frac{\partial v_\theta}{\partial x} - \frac{\partial u_\theta}{\partial y} + f \qquad (26)$$

using u and v wind components on an isentropic surface. Absolute vorticity is one of the most basic variables used for analysis in synoptic meteorology. Vorticity is useful in diagnosing short waves and their intensity, the same as on isobaric surfaces. It is especially helpful in depicting strong horizontal shear zones associated with westerly jets with little curvature. Units are x $10^{-5}$ $s^{-1}$.

**6) Potential Vorticity:** This variable is written as shown in (22):

$$P_\theta = \frac{-g(\zeta_\theta + f)}{\dfrac{\partial P}{\partial \theta}}$$

Potential vorticity is useful as a tracer for atmospheric flow under adiabatic, frictionless conditions. It can be especially useful, when interpolated to cross sections, to diagnose the intrusion of stratospheric air which generally has potential vorticity values about one order of magnitude greater than tropospheric values (Reiter, 1972). When air extruding into the troposphere along the polar front experiences

convergence, it increases its cyclonic spin in an effort to conserve its potential vorticity. Staley (1960) notes that the potential vorticity of a parcel is changed only by diabatic heating and/or friction.

Potential vorticity is measured in PVU, potential vorticity units, where 1 PVU is equal to $10^{-6}$ $m^2$-K/s-kg. Some older papers define potential vorticity without g on the RHS and use cgs units. Potential vorticity defined in the latter manner has the units $10^{-6}$ K/mb-s. For the record, 1 PVU is equivalent to 10 x $10^{-6}$K/mb-s. Stratospheric values of potential vorticity are generally > 1.5 PVU.

7) **Condensation Pressure:** This variable was first suggested by Byers (1938) to help better represent moisture on isentropic surfaces. It is simply defined as the pressure to which unsaturated air must be raised dry-adiabatically in order to reach saturation; i.e., the condensation level. It is typically expressed in millibars. The key advantage of condensation pressure over specific humidity is that condensation pressure better represents moisture differences at low values of q. This can be seen best in Fig. 25, which presents condensation pressures vs. specific humidity for various potential temperatures. Note that along each isentropic surface the slope ( $\partial P/\partial q$ )$_\theta$ is greatest at low values of q. Byers (1938) notes that on an isentropic surface a specific humidity between 1 and 0.5 gm/kg is poorly represented, while condensation pressure isobars make it stand out about as much as a 5-10 gm/kg difference. This is important, especially in winter when low specific humidity values are often associated with significant precipitation and clouds. Simple algorithms are available to compute the condensation pressures for unsaturated air. In practice, one can think of condensation pressures on an isentropic surface as being equivalent to dew points on a constant pressure surface.

Anderson (1984) notes that condensation pressure isobars can be useful in identifying frontal positions. A moist tongue, represented as a ridge of condensation pressure is usually present along or slightly ahead of a strong, mature cold front (Fig. 26a). As a cyclone occludes the moist tongue will typically branch into two tongues—one turning cyclonically to the northwest and the other anticyclonically to the northeast. The occlusion is usually found in the vicinity of the branching (Fig. 26b). Anderson (1984) notes that the precipitation is often heaviest in this area.

8) **Condensation Ratio:** Byers (1938) defines this variable as the ratio of the condensation pressure (Po) and the actual pressure (P) of a point on an isentropic surface. It is a measure of nearness to condensation and is dimensionless. Condensation ratio can then replace relative humidity on the psi chart.

Byers (1938) points out that nearness to condensation can also be estimated by the distance between an isobar (P) and an isobar of condensation pressure (Po) having the same value. If the prevailing flow is expected to move a Po isobar over a P isobar of the same value, saturation and precipitation can be expected.

9) **Condensation Difference:** Anderson (1984) notes that the condensation ratio is not easy to analyze. He suggests computing the condensation difference by subtracting the value of the condensation pressure from the corresponding pressure value on an isentropic surface. The smaller the value of the condensation difference the closer the parcel to saturation. Due to smoothing and round-off errors, a

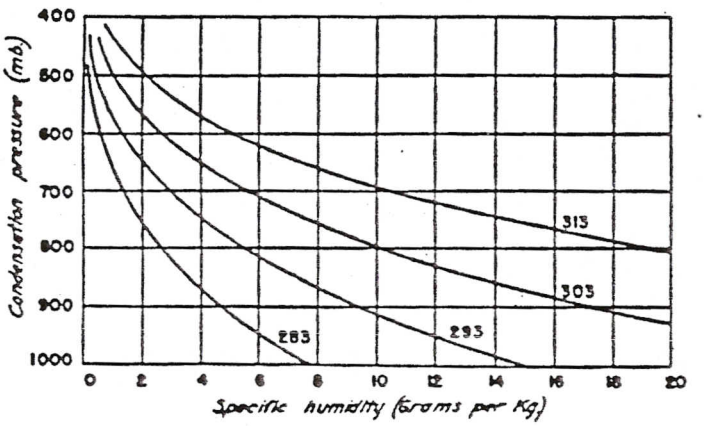


Figure 25. Condensation pressure (mb) vs. specific humidity for 283, 293, 303, and 313 K isentropic surfaces. Note the great slopes for low specific humidities (Byers, 1938).

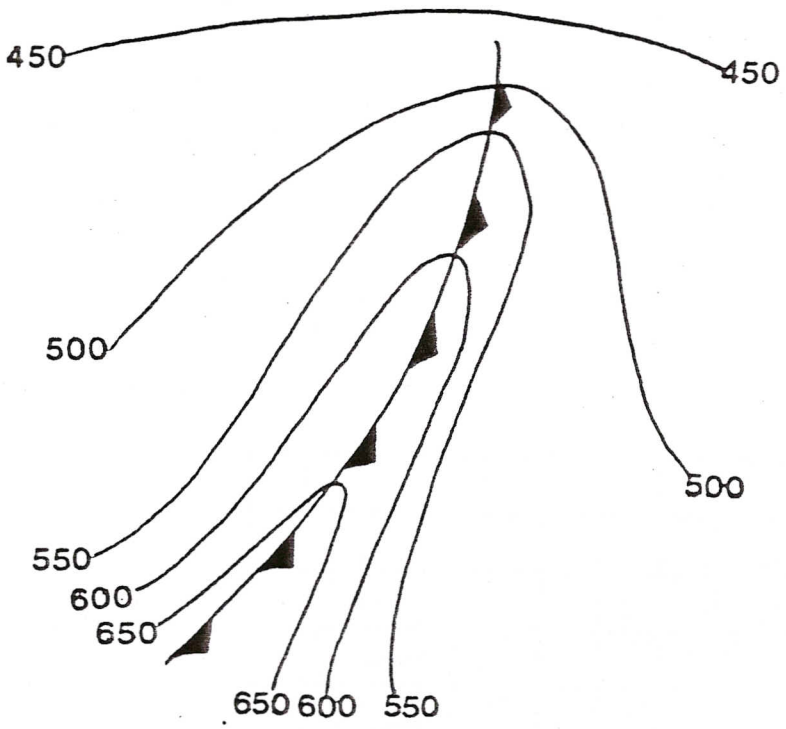


Figure 26a. Isentropic condensation pressure pattern over a mature, strong cold front (Anderson, 1984).

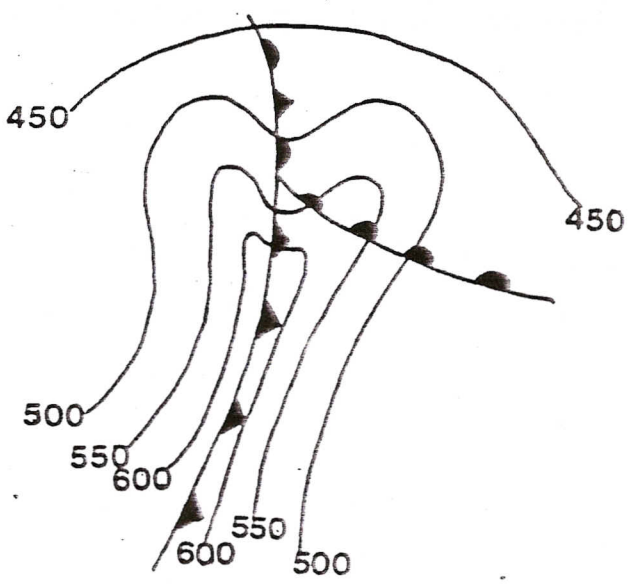


Figure 26b. Isentropic condensation pressure pattern over an occluding frontal system (Anderson, 1984).

difference of less than 20 mb represents saturation. For summer over the western U. S. he found values < 100 mb to be useful indications of near-saturation. Essentially, condensation difference on an isentropic surface is equivalent to dewpoint depression on a constant pressure surface.

Edson (1966) discusses the use of the "condensation pressure spread" for cloud forecasting. Figure 27 is his diagram illustrating the relationship of this variable to cloud cover for various pressure levels.

10) **Streamlines:** On the McIDAS system and the isentropic program designed by Anderson (1984), a streamline analysis is available for display, usually to overlay with one other variable. Streamlines, it should be remembered are based on the actual wind and display the instantaneous field of motion. They can be overlaid with the Montgomery streamfunction to depict regions of ageostrophic flow . They also are excellent for depicting regions of convergence/divergence which, in an isentropic framework, are associated with destabilization/stabilization. However, they do not display any speed information. So, although streamlines crossing isobars, for instance, generally imply vertical motion, one cannot get a quantitative measure of vertical motion from such a field.

Anderson (1984) states that streamlines will tend to converge in the vicinity of frontal boundaries (Fig. 28a), especially in regions of frontogenesis. When streamlines flow across a front as depicted in Fig. 28b the front is weak and in the process of frontolysis.

System-relative (S-R) streamlines can be obtained by subtracting the system u and v speed components from each grid points' u and v wind components. S-R streamlines, when overlain with the pressure field on the isentropic surface, reveal the cross-isobar flow with respect to the system and helps one to better visualize the S-R vertical motion field.

11) **Moisture Stability Flux:** Ralph Petersen of the Development Division of NMC and the author of PC-GRIDDS, devised the parameter called the Moisture Stability Flux (MSF). It is defined as:

$$MSF = -\nabla \cdot \left[ \left( \bar{q}\, \Delta P \right) \vec{V} \right] = -\vec{V} \cdot \nabla \left( \bar{q} \Delta P \right) - \left( \bar{q} \Delta P \right) \nabla \cdot \vec{V} \qquad (27)$$

$$\qquad\qquad\qquad\qquad\qquad\qquad\qquad\qquad\qquad\qquad \mathbf{A} \qquad\qquad \mathbf{B}$$

where $\bar{q}$ is the average mixing ration in the layer from $\theta$ to $\theta + \Delta\theta$, $\Delta P$ is the distance in millibars between the two isentropic surfaces (a measure of the static stability) and $\vec{V}$ is the wind. Term **A** is the advection of the moisture and static stability. Term **B** is the convergence field acting on the moisture/static stability field. Basically, MSF values > 0 indicate that the layer is becoming more moist and less statically stable due to advection and/or convergence. MSF can be useful in the prestorm environment to evaluate the large scale support for deep convection. Units are generally gm - Pa / kg - hr.

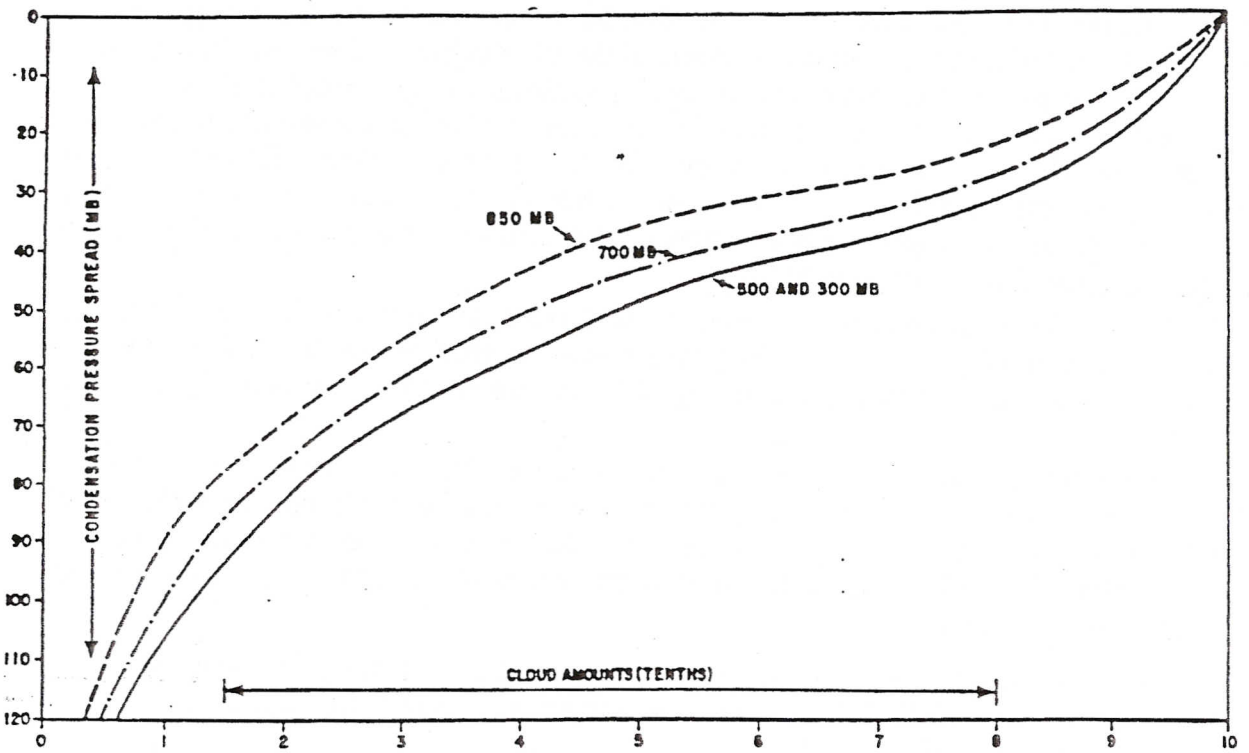


Figure 27. Condensation-pressure spread to cloud-conversion table (Edson, 1966).

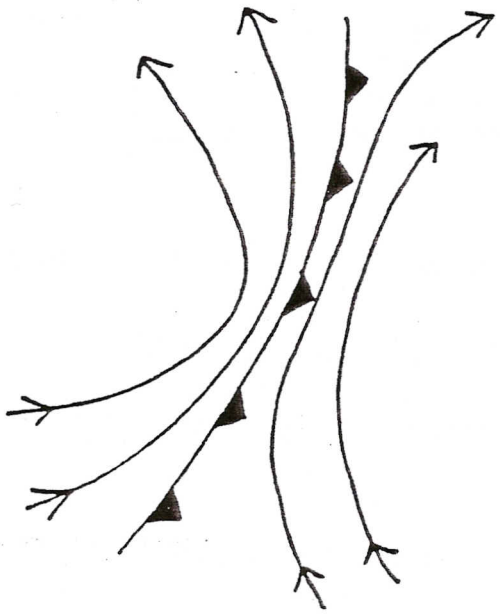

Figure 28a. Isentropic streamlines in the vicinity of a strengthening cold front (Anderson, 1984).

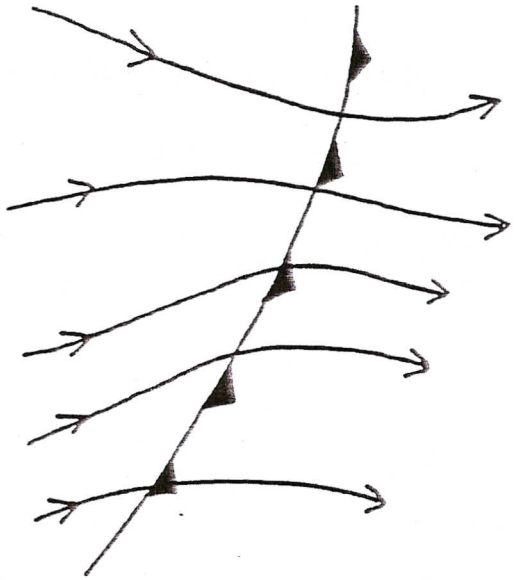

Figure 28b. Isentropic streamlines in the vicinity of a weakening cold front (Anderson, 1984).

## IV. SPECIALIZED APPLICATIONS OF ISENTROPIC ANALYSES TO DIAGNOSTIC/FORECAST PROBLEMS.

There have been numerous applications of isentropic analysis techniques to the study of extratropical systems and, more recently, to mesoscale systems. In this section we will briefly describe some of these applications, referring the reader to the original papers for a more in-depth treatment of each approach.

### A. Isentropic Trajectories

There are two basic approaches to computing trajectories on an isentropic surface (Dutton, 1976):

1. If the equations of motion are solved on a grid with fine resolution, then trajectories can be computed for any parcel by geometrical methods.
   This is known as the explicit method.
2. If a sufficient number of conservation properties of an air parcel can be identified, then we can observe their values in a parcel at one time and then find the parcel's new location at a later time by finding where the same combination of values of these variables occurs.
   This is known as the implicit approach.

#### 1. Implicit Approach

Danielsen (1961) outlined the implicit approach of computing isentropic trajectories which is based on a total energy equation.

We begin with the two dimensional inviscid equations of motion in isentropic coordinates:

$$\frac{d\bar{V}}{dt} = -\bar{\nabla}M - f\hat{k}\times\bar{V} \tag{28}$$

Dotting (28) with $\bar{V}$ yields:

$$\frac{d}{dt}\left(\frac{V^2}{2}\right) = -\bar{V}\cdot\bar{\nabla}M \tag{29}$$

Next, we write the total derivative of M assuming adiabatic conditions

$$\frac{dM}{dt} = \frac{\partial M}{\partial t} + \bar{V}\cdot\bar{\nabla}M \tag{30}$$

Solving for the advection term in (30) and substituting into (29) results in:

$$\frac{d}{dt}\left(M - \frac{V^2}{2}\right) = \frac{\partial M}{\partial t} \tag{31}$$

This is an energy relationship which can be applied to a parcel trajectory by integrating (31) over time, resulting in:

$$M_f - M_i + 1/2(V_f^2 - V_i^2) = \int_{t_1}^{t_2} \frac{\partial M}{\partial t} dt \tag{32}$$

The RHS term of (32) can be approximated at the initial (i), midpoint (m) and final (f) points of the trajectory and weighting the midpoint, i.e.,

$$\int_{t_1}^{t_2} \frac{\partial M}{\partial t} dt = \frac{\Delta M_i + 2\Delta M_m + \Delta M_f}{4} \tag{33}$$

resulting in a finite difference form of the integrated energy relationship:

$$M_f - M_i + 1/2(V_f^2 - V_i^2) = \frac{\Delta M_i + 2\Delta M_m + \Delta M_f}{4} \tag{34}$$

This relationship *and* a distance formula written as:

$$D = \frac{V_i + V_f}{2} \Delta t \tag{35}$$

can be used to construct a trajectory. Essentially, the energy relationship (34) and the distance formula (35) must be solved simultaneously by choosing a point on an initial isentropic surface at a certain time, and then exploring the downstream area on the same isentropic level X hours later (usually 12) which balances both equations. This can be done graphically but is quite laborious, even though Danielsen's early work was done this way (Danielsen, 1966). Later on this process was adapted to a computer as described by Danielsen and Bleck (1967) and Haagenson and Shapiro (1979).

Figure 29a displays the initial time period on the 328 K isentropic surface used in a study by Danielsen and Reiter (1960) for trajectory calculations. The isentropic trajectory is plotted in Fig. 29b to display the same surface 12 hours later over the central U. S. Notice how a trajectory, initially located on the anticyclonic side of the jet streak, turns towards higher values of M and descends from approximately 370 mb to 460 mb while slowing down enroute. Its path agrees well with the "digging" trough into the central U. S.

### 2. Explicit Approach

Petersen and Uccellini (1979) note that there are some problems with the implicit approach. The simultaneous solution of (34) and (35) for *anticyclonic* trajectories does not always converge to a unique solution. Secondly, the estimation of the local derivative term (RHS term of (34)) is only fair, at best, for the 12-hour time interval imposed by operational data availability. The basic technique applied to (34) and (35) makes it difficult to account for varying accelerations that take place along the trajectory. The explicit technique of constructing isentropic trajectories provides a better alternative that is easier to code up for a computer.

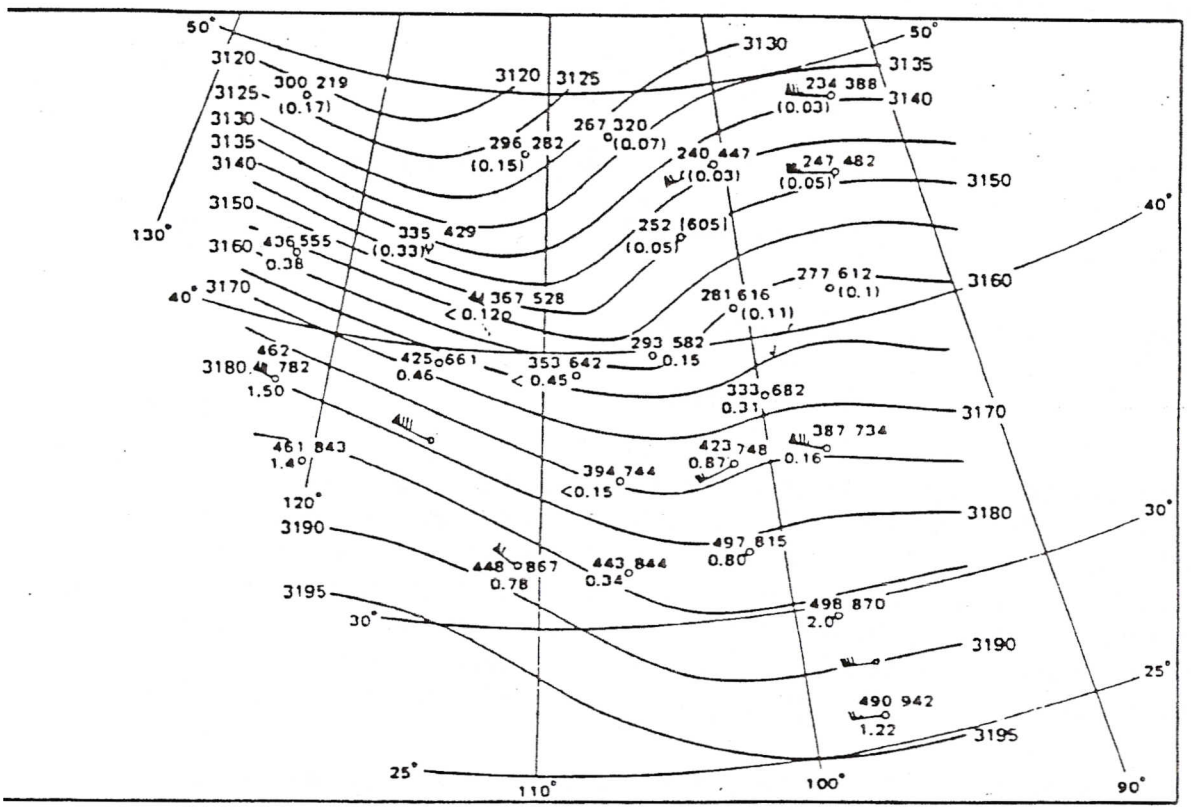


Figure 29a. Isentropic surface, $\theta$=45°C, 0300 GMT 8 January 1953. Numerical values to the left of each station indicate pressure (mb) and specific humidity (gm/kg); to the right are the last three digits of the Montgomery streamfunction (M). Isolines of M are labeled in units of $10^6$ $m^2$ $s^{-2}$ (Danielsen and Reiter, 1960).

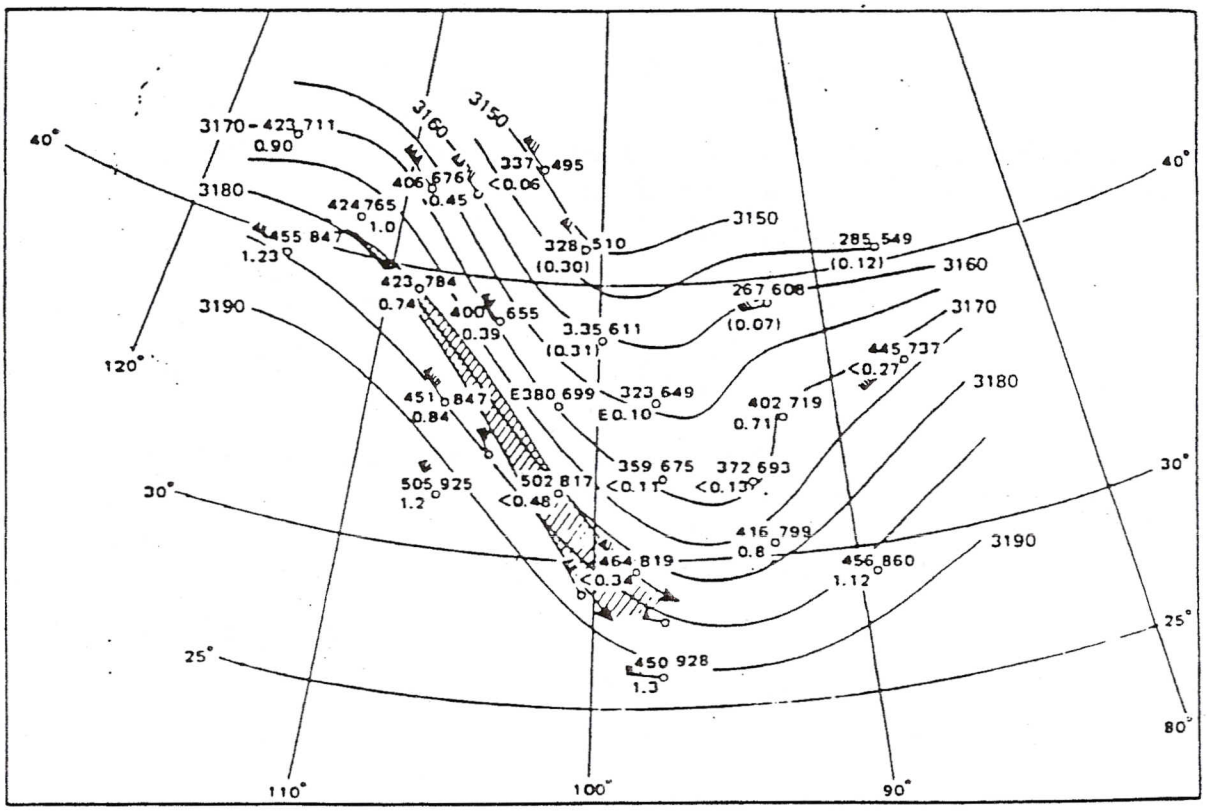


Figure 29b. Isentropic surface, θ=45°C, 1500 GMT 8 January 1953. Trajectories are shown for the time period 0300-1500 GMT on that day. The spread between the two trajectories allows for inaccuracies in wind reports (Danielsen and Reiter, 1960).

To begin with, one needs to have gridded values of u and v wind components for the initial time period and M values for both the initial and final time periods. Next, we compute the accelerations in x and y space from the inviscid equations of motion in isentropic coordinates; i.e.,

$$\frac{\Delta u}{\Delta t} = -\frac{\Delta M}{\Delta x} + fv \tag{36}$$

$$\frac{\Delta v}{\Delta t} = -\frac{\Delta M}{\Delta y} - fu \tag{37}$$

using standard finite difference techniques to compute the M derivatives. Then we compute the new u and v velocities for the parcels with:

$$u^1 = u^o + \frac{\Delta u}{\Delta t}\Delta t \tag{38}$$

$$v^1 = v^o + \frac{\Delta v}{\Delta t}\Delta t \tag{39}$$

which are "starter" formulas used for the first time increment, $\Delta t$. Superscripts refer to the time step. For other than the first time step we use,

$$u^{t+1} = u^t + \Delta t\left[\frac{3}{2}\frac{\Delta u^t}{\Delta t} - \frac{1}{2}\frac{\Delta u^{t-1}}{\Delta t}\right] \tag{40}$$

$$v^{t+1} = v^t + \Delta t\left[\frac{3}{2}\frac{\Delta v^t}{\Delta t} - \frac{1}{2}\frac{\Delta v^{t-1}}{\Delta t}\right] \tag{41}$$

Finally, we compute the new position of the parcel with:

$$x^{t+1} = x^t + 1/2\Delta t(u^{t+1} + u^t) \tag{42}$$

$$y^{t+1} = y^t + 1/2\Delta t(v^{t+1} + v^t) \tag{43}$$

A time step of 15-30 minutes is typically used. An M field is needed for each time step. This is done by linearly interpolating in time between the two M fields. Also, for each iteration in time one needs M derivatives in x and y space interpolated to the parcel location. One typically computes these derivatives at grid points and interpolates them to the parcel location. It is important that the interpolation scheme be accurate. Petersen and Uccellini (1979) used an overlapping polynomial technique which they describe in their paper.

The application of this explicit technique is very straightforward and yields trajectories which are nearly energy-conservative. If one has gridded fields of u, v, P, q and M for *both* time periods, it is possible to compute change fields following the parcel as well as keep track of the parcel's relative humidity. This enables you to quantitatively determine how long to "trust" the parcel trajectory, perhaps even

terminating it upon saturation.

Figures 30a-b show the isentropic charts and trajectories derived from the explicit approach from a study by Petersen and Uccellini (1979). Note how well these trajectories follow the flow.

**3. Trajectory-Derived Variables**

Once a trajectory has been calculated, it can be informative to produce change fields based on the trajectory's initial and final points. Changes in enthalpy, internal energy, potential energy, kinetic energy, pressure, and potential vorticity can be computed by using these variables' values at the end points of the parcel and plotting the "delta" value at the parcel's spatial midpoint. If enough calculations are done in this way, one can then analyze this Lagrangian-derived, irregular set of data. Much information concerning the thermodynamics and dynamics of the atmosphere can be learned in this way.

Consider the following information from an isentropic trajectory:

| $\theta$ = 305 K 12 Hour Changes | | | |
|---|---|---|---|
| M Initial = $30500 \times 10^1$ | J/kg | M Final = $30560 \times 10^1$ | J/kg |
| P Initial = 250 | mb | P Final = 500 | mb |
| V Initial = 50 | m $s^{-1}$ | V Final = 30 | m $s^{-1}$ |

From this information we can calculate the following "delta" values:

| | | |
|---|---|---|
| $\Delta$ Enthalpy = | $+ 45 \times 10^3$ | J/kg |
| since $\Delta$ T = | + 45 | K |
| $\Delta$ Internal Energy = | $+ 32.25 \times 10^3$ | J/kg |
| $\Delta$ Potential Energy = | $- 45.38 \times 10^3$ | J/kg |
| since $\Delta$ M = | $+0.6 \times 10^3$ | J/kg |
| $\Delta$ Kinetic Energy = | $-0.8 \times 10^3$ | J/kg |
| $\omega = \Delta P/\Delta t$ = | + 5.79 | $\mu$bars/s |

At a glance we can see that this parcel warmed 45 K as it descended 250 mb adiabatically, thereby increasing its enthalpy and internal energy while decreasing its potential and kinetic energies as it "crossed over" to higher M values. Note that the kinetic energy change is about an order of magnitude less than the other changes. The descent rate of + 5.79 $\mu$bars $s^{-1}$ is substantial for the synoptic scale.

Figure 31 shows isentropic trajectories for the 12 h period 00-12 UTC, 14 December 1987 on the 300 K surface. At the spatial midpoint of each trajectory is plotted the Lagrangian vertical motion in $\mu$bars $s^{-1}$. Note the negative values in

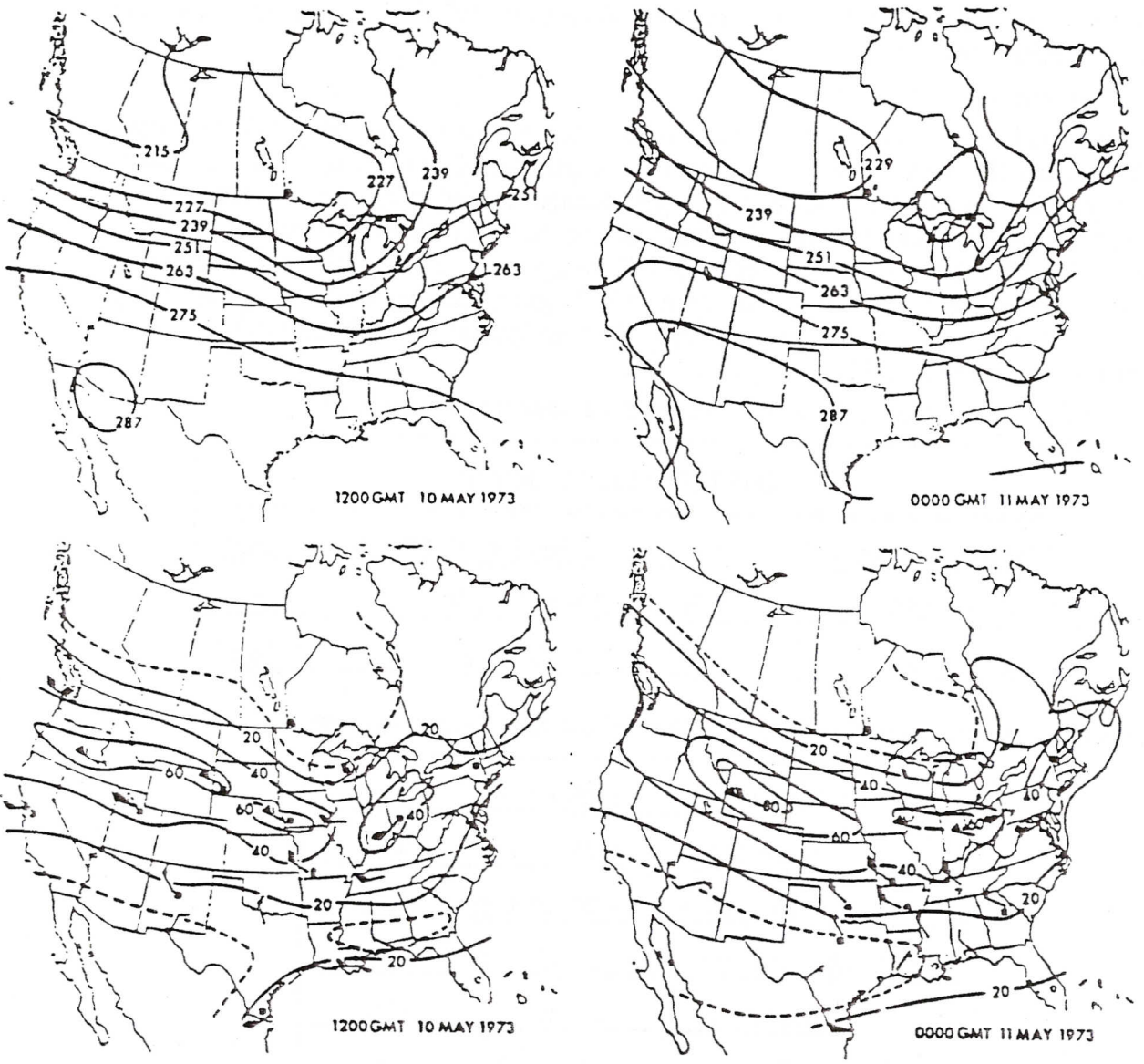


Figure 30a. 330 K isentropic surface for 1200 GMT 10 May and 0000 GMT 11 May 1973. At the top, the $\psi$ analysis (275=3.275 x $10^5$ $m^2$ $s^{-2}$). At the bottom, the isotach analysis (m $s^{-1}$). Wind barbs represent selected station wind reports rounded to the nearest 5 m $s^{-1}$; solid barb = 50 m $s^{-1}$, long barb = 10 m $s^{-1}$, short barb = 5 m $s^{-1}$. The number at the station is the actual last digit of the wind report (Petersen and Uccellini, 1979).

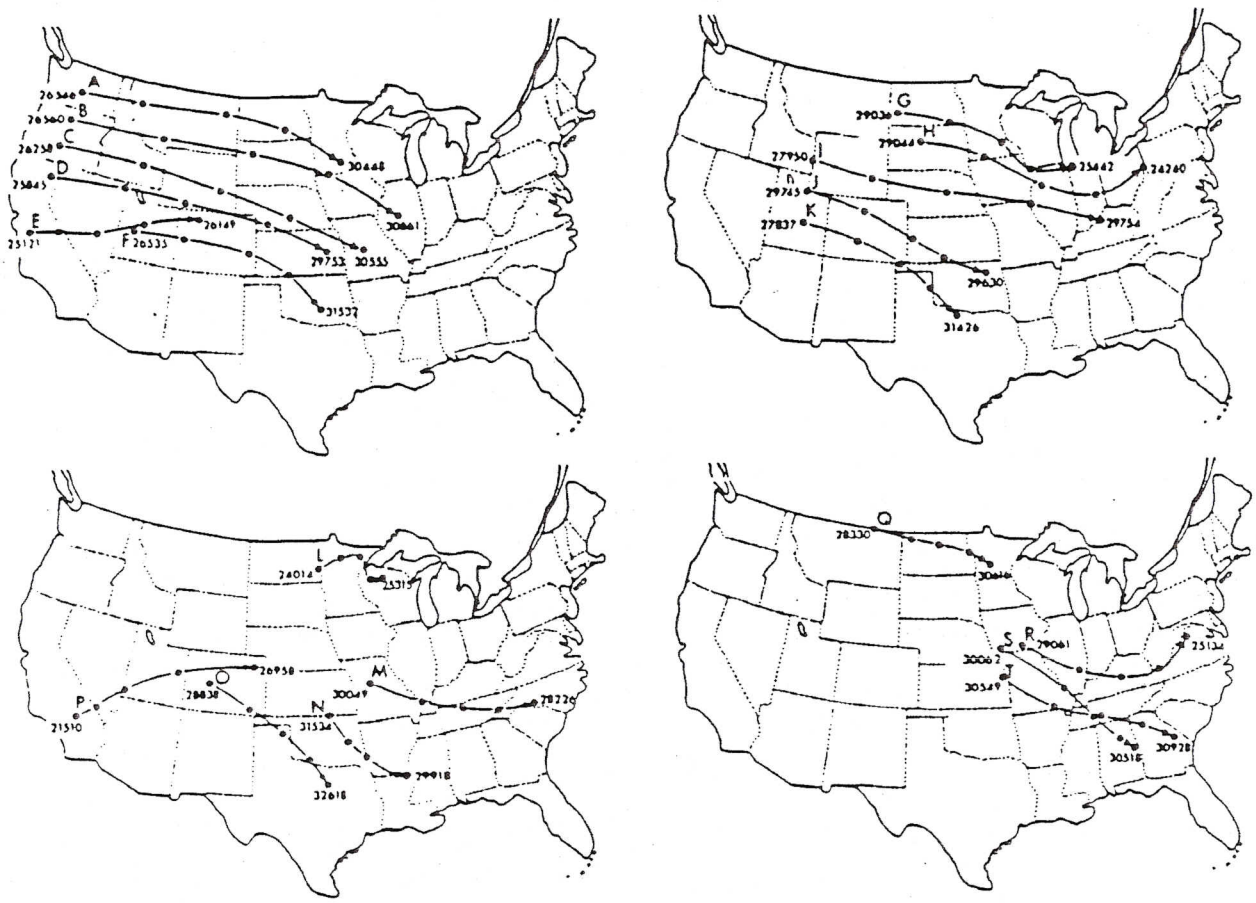

Figure 30b. Trajectories computed for 1200 GMT 10 May through 0000 GMT 11 May 1973 on the 330 K isentropic surface using discrete model technique. Positions at 3 hour intervals are indicated by the solid black dot. The initial and final wind direction and speed are indicated (31426 = 314°, 26 m $s^{-1}$) (Petersen and Uccellini, 1979).

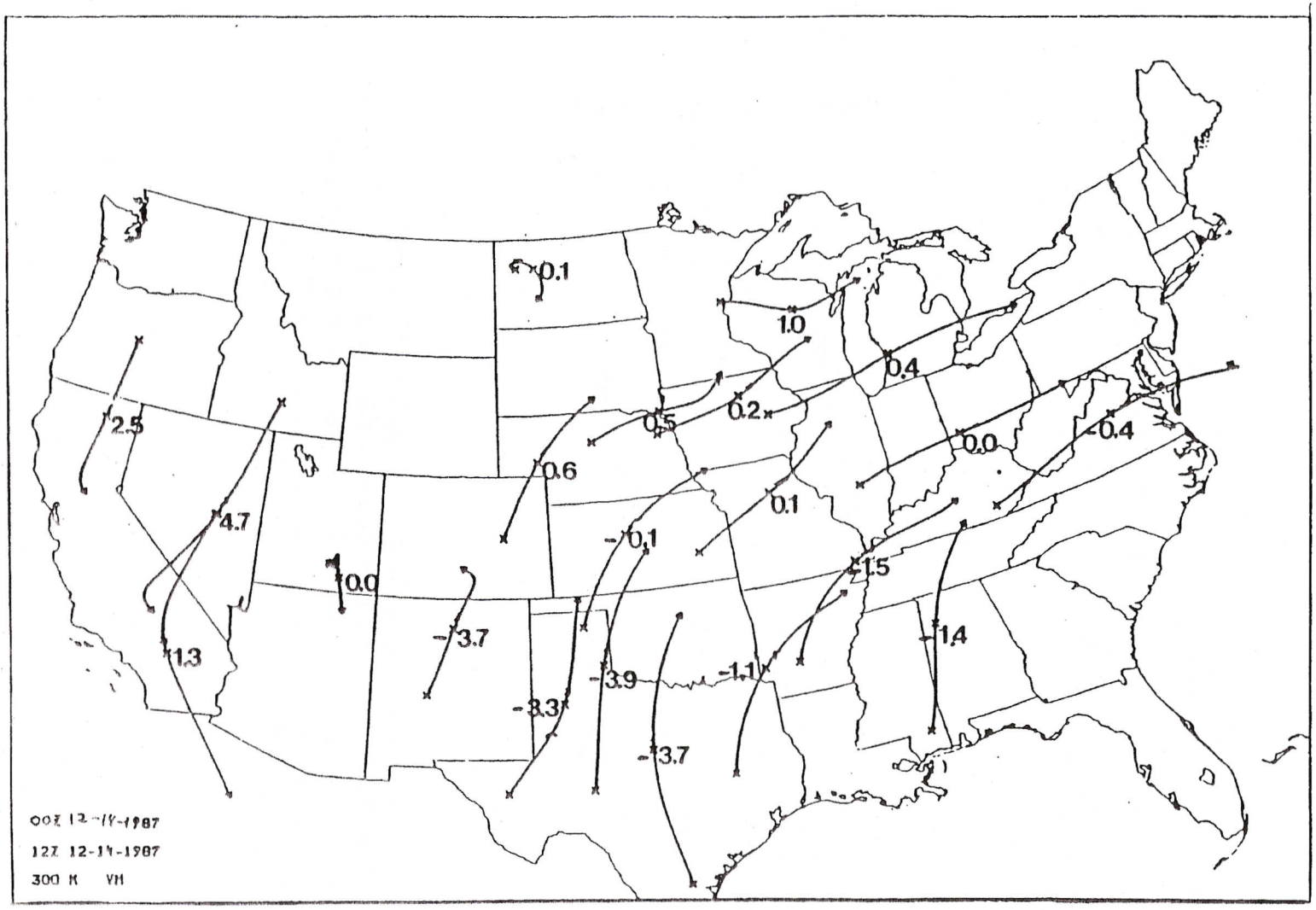


Figure 31. Twelve hour isentropic trajectories computed using the explicit method for the period 0000 - 1200 UTC 14 December 1987, for the 300 K surface. Numbers plotted at the spatial midpoint of each trajectory are the Lagrangian vertical motion in $\mu$bars $s^{-1}$. During this time period heavy snow was falling in eastern New Mexico and northwestern Texas.

New Mexico and Texas indicating upward vertical motion. Over this time considerable snow was falling this area.

### B. Potential Vorticity and Tropopause Folding

It is difficult to do justice to this topic in this paper. The goal of this section is to simply acquaint the reader with some of the past and present work with respect to the topic of stratospheric extrusions or tropopause "folds". For an excellent review of this topic the reader is urged to read Keyser and Shapiro (1986).

As routine upper air soundings became available and the vertical temperature structure of the atmosphere began to be diagnosed, the concept of a tropopause "lid" capping the troposphere became entrenched in meteorological terminology. This natural inversion above the "weather sphere" appeared to preclude any vertical transport of mass between the troposphere and stratosphere. Secondly, as Reiter (1972) notes, "isobaric thinking" led to the acceptance of a jet axis as representing a discontinuity of absolute and potential vorticity. This made it difficult to envision how air masses could cross the jet axis under conservation of either of those two quantities. Therefore, the jet axis was thought to be a barrier to lateral exchange processes.

However, from the mid 1950's to this day much research documentation has shown a substantial mass exchange between the stratosphere and troposphere along tropopause "folds" or "breaks" (see Reed, 1955; Staley, 1960; Danielsen, 1968; Reiter, 1972, 1975; Shapiro, 1980; Uccellini et al. 1985). Several of these authors used stratospheric tracers of ozone, radioactivity, and potential vorticity to document airflow into the troposphere. Air descending from the stratosphere is also characteristically "bone dry" (i.e., RH $<10\%$).

Figures 32a-f display a synoptic situation during which a tropopause fold formed. The top three panels (Fig. 32a,c,e) show the rapid deepening of a a mid-tropospheric wave over the central U. S. from 0300 GMT 13 December to 0300 GMT 15 December 1953. Note the intensification of the thermal gradient attendant with the developing jet streak at 500 mb. By the end of the period a hyperbaroclinic zone is established along the east coast, with wind speeds exceeding 150 knots. Cross sections taken perpendicular to the jet (Fig. 32b,d,f) diagnose the development of the tropopause fold. The strong static stability and negative wind shear help to define the stratospheric air. The tropopause is lowest where the air is coldest in the mid-troposphere. Stratospheric air sinks over the first 24-hour period and then finally extrudes into the troposphere by the last time period (Fig. 32f). The stable baroclinic zone associated with the strong frontal zone is defined by both highly compacted isentropic surfaces and strong vertical wind shear. The vertical shear of the geostrophic wind is nearly zero in those areas outside the frontal zone where the isentropic surfaces are quasi-horizontal.

Uccellini et al. (1985) have documented a tropopause fold that took place during the President's Day Cyclone of 18-19 February 1979. From a forecaster's viewpoint, what is most interesting about their study is how they correlate a fold in the tropopause to subsequent explosive cyclogenesis for this east coast storm. Key diagrams from their study are shown in Fig. 33a-d. In the last diagram one can

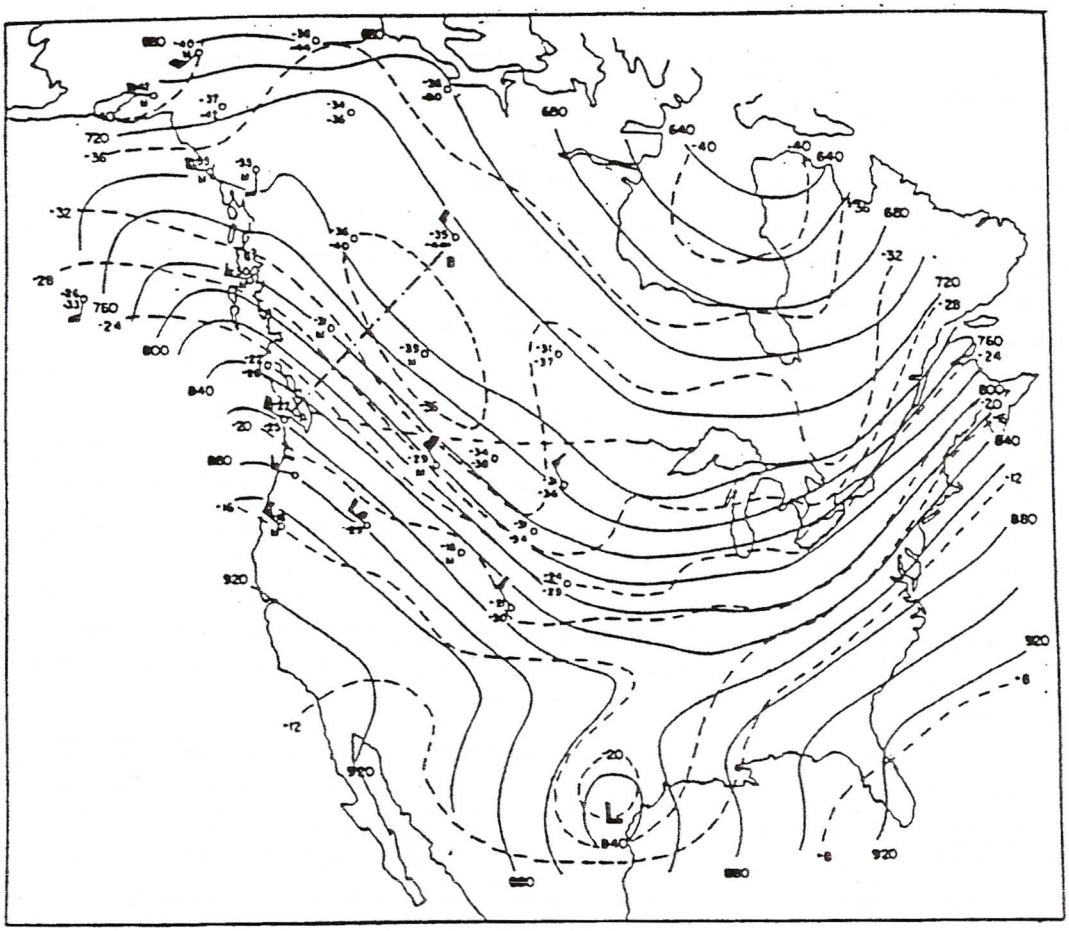

Figure 32a. 500 mb surface for 0300 GMT 13 December 1953. The chart shows contours (thin solid lines) and isotherms (thin dashed lines). Observed temperatures and dew points (°C) and winds are added in critical areas (Reed, 1955).

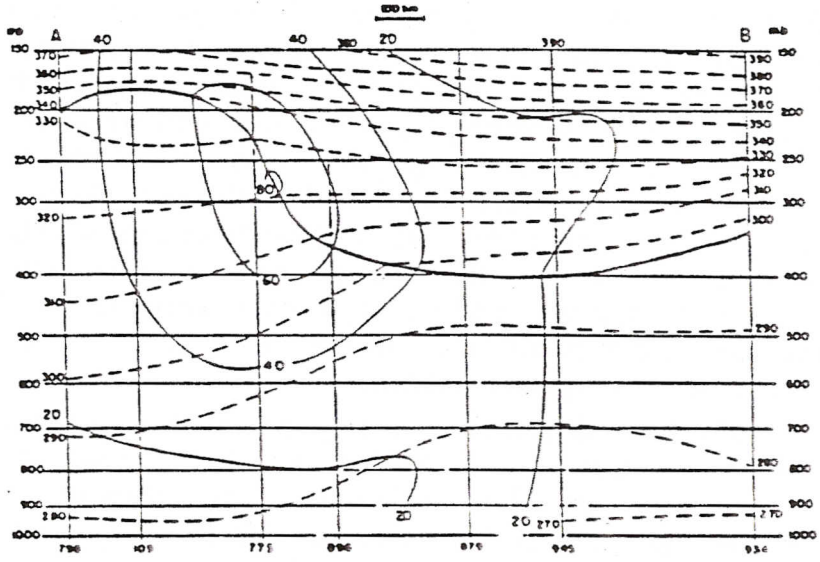

Figure 32b. Cross section along line A-B in Figure 32a. Thin solid lines give geostrophic wind speed (m s$^{-1}$) normal to the section, dashed lines are isentropes. The thick solid line represents the tropopause (Reed, 1955).

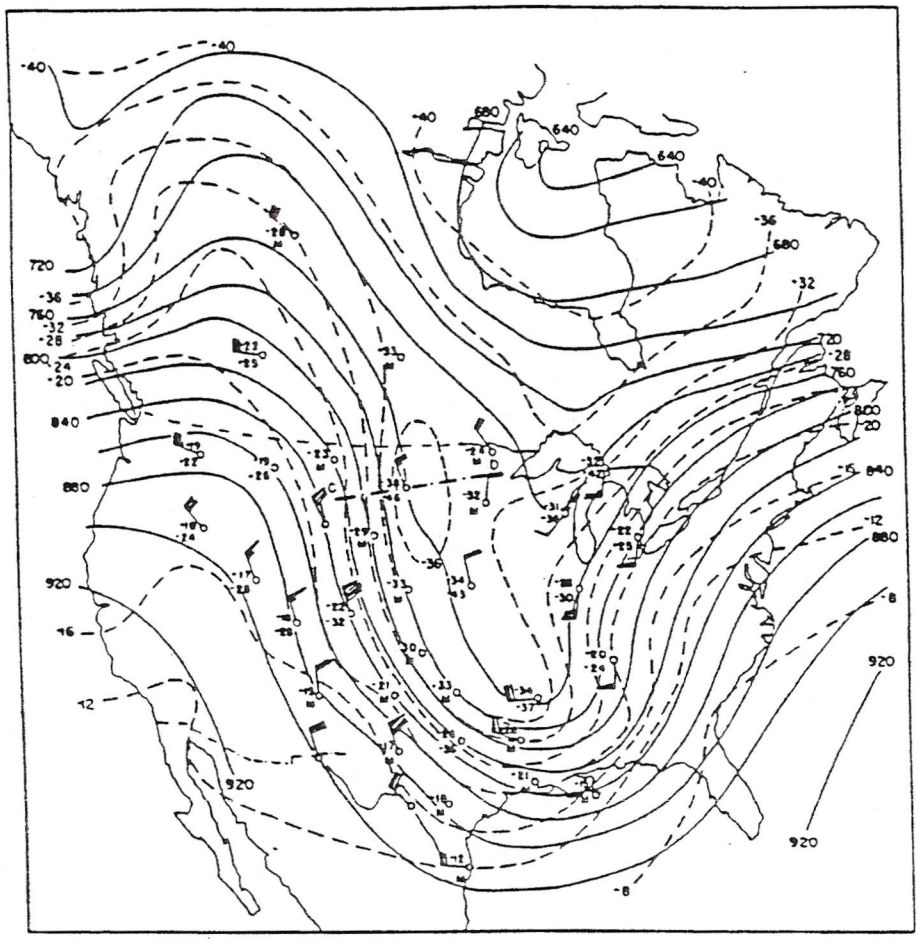

Figure 32c. 500 mb surface for 0300 GMT 14 December 1953. Notation same as in Figure 32a (Reed, 1955).

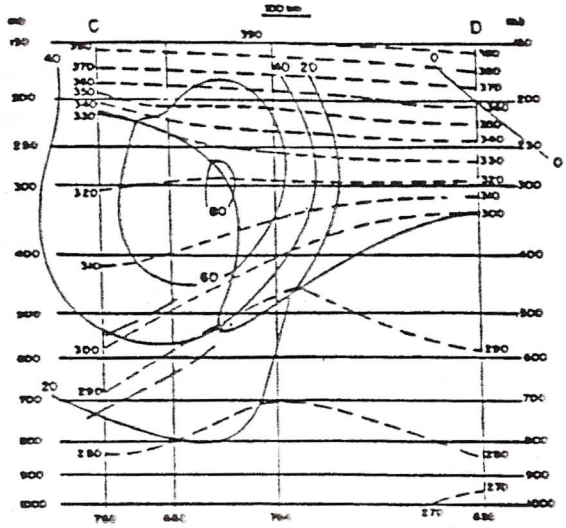


Figure 32d. Cross section along line C-D in Figure 32c. Heavy dashed lines represent boundaries of stable air; otherwise notation same as in Figure 32b (Reed, 1955).

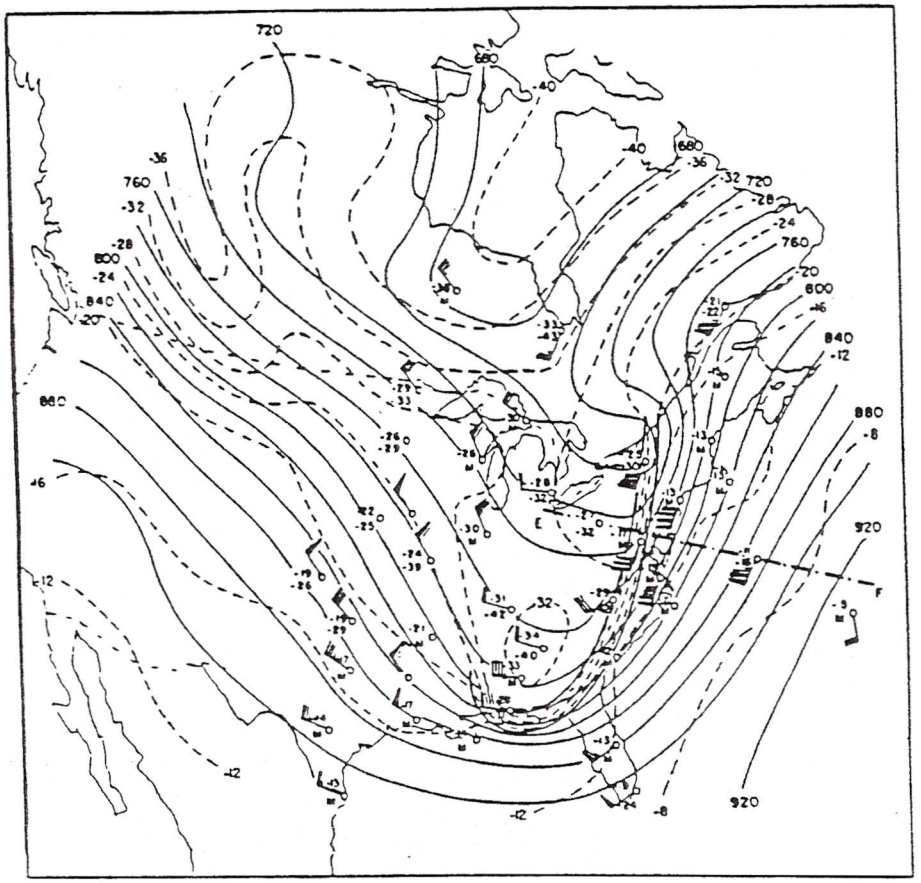


Figure 32e. 500 mb surface for 0300 GMT 15 December 1953. Heavy solid lines represent boundaries of frontal zone (Reed, 1955).

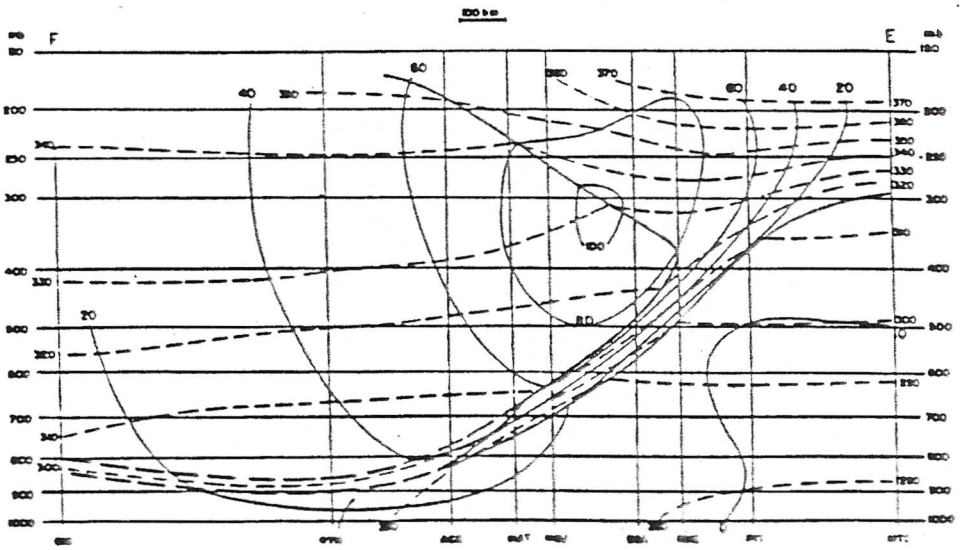


Figure 32f. Cross section along line E-F in Figure 32e. Notation same as in Figure 32b and 32d (Reed, 1955).

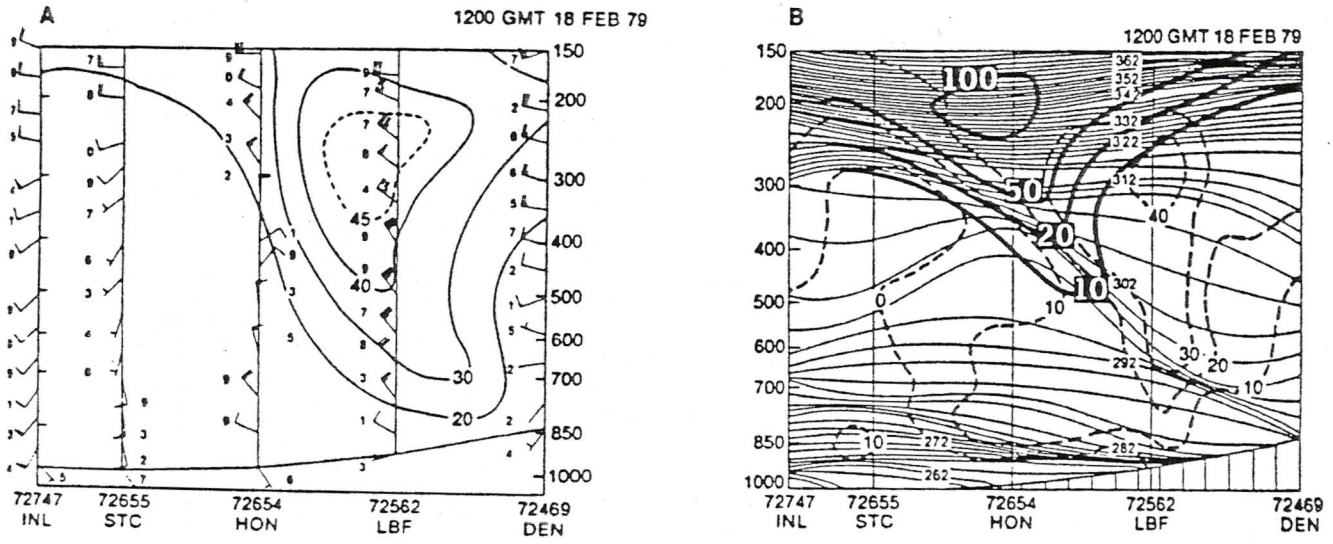


Figure 33a-b. Vertical cross section from International Falls, MN (INL) to Denver, CO (DEN) for 1200 GMT 18 February 1979. The left panel (A) is an isotach analysis for total wind speed (m $s^{-1}$); wind barbs plotted with last digit of wind observation. The right panel (B) shows isentropes (solid, K); geostrophic wind (dashed, m $s^{-1}$) computed from the horizontal thermal gradient in the plane of the cross section; potential vorticity, $-(\zeta + f)/(\partial\theta/\partial P)$, heavy solid, where 10 = 10 x $10^{-6}$ K $mb^{-1}$ $s^{-1}$. Potential vorticity analysis is only shown for upper portion of frontal zone and stratosphere (Uccellini, *et al.*, 1985).

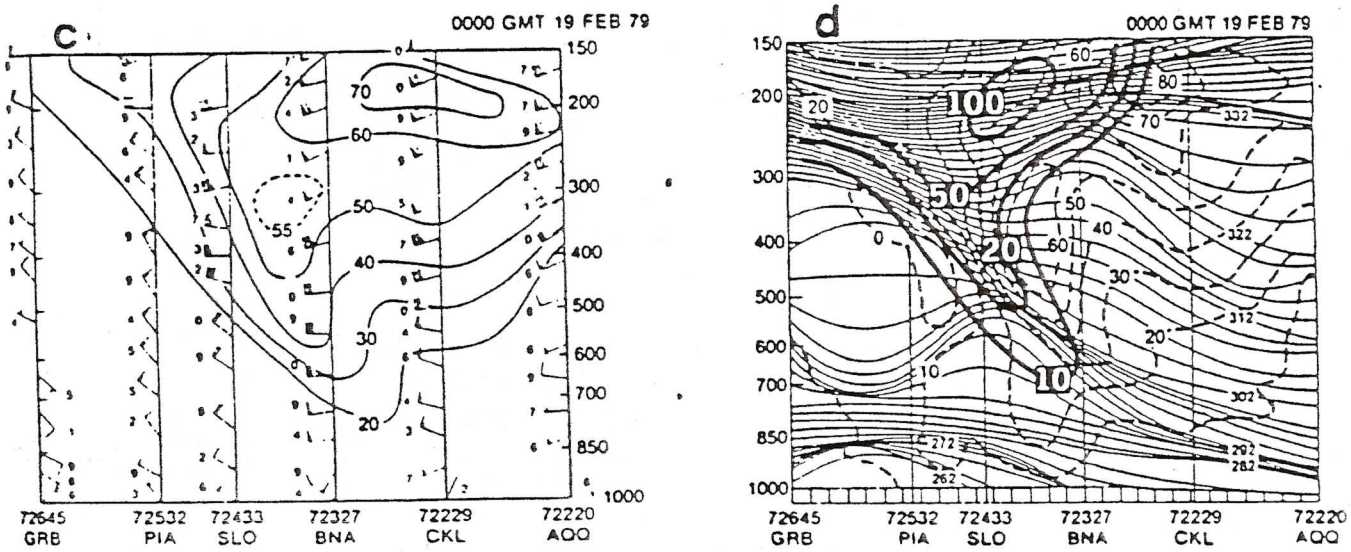


Figure 33c-d. Vertical cross sections from Green Bay, WI (GRB) to Apalachicola, FL (AQQ) for 0000 GMT 19 February 1979. Depictions same as in Figure 33a-b (Uccellini, *et al.*, 1985).

identify a stratospheric extrusion from the stable baroclinic zone descending from Peoria, Illinois (PIA) to Appalachicola, Florida (AQQ) and the high potential vorticity values along the frontal zone. Uccellini et al. (1985) show that stratospheric air descended along this zone at least 12 hours *preceding* cyclogenesis. It moved down to 800 mb toward the east coast to an area upstream of where rapid cyclogenesis occurred. There, it experienced adiabatic mass convergence and in an effort to quasi-conserve potential vorticity vertically stretched and increased its absolute vorticity. Their work is further substantiated by ozone measurements from the Total Ozone Mapping Spectrometer (TOMS) flown aboard the Nimbus 7 satellite. TOMS measures the vertical ozone distribution in the stratosphere. A maximum in ozone concentration is positively correlated with a relatively thick stratosphere and a thin troposphere. They have shown significant positive increases in TOMS ozone measurements in the vicinity of these tropopause folds. Shapiro et al. (1982) have used the TOMS in a similar application to show how ozone maps from TOMS can locate jet streaks at tropopause levels and gauge their intensity from the intensity of the gradient of the ozone distribution. This could be a useful technique for locating jet streak activity over data sparse regions and approximating their magnitudes.

Utilizing isentropic cross sections with mixing ratio, normal wind components and potential vorticity in the operational setting may provide clues to timing the intensity and onset of significant winter storms. The author's experience is that tropopause folds are more typical with the stronger systems (central pressure <990 mb) during the cold season. The practical application of this technique is yet to be proven—but the potential exists and the data can be computed in real-time.

Hirschberg and Fritsch (1991a-b) describe the characteristics of a tropopause undulation which is associated with the development of extratropical cyclones in midlatitudes. A tropopause undulation is *not* the same as a tropopause fold, but is associated with a deep layer of stratospheric air descending to levels greater than 400 mb. Figure 34a-d from Hirschberg and Fritsch (1991a) reveals the main features of a tropopause undulation. At 200 mb, it is seen as a relative warm core of air (Fig. 34a) with a strong thermal gradient and warm air advection downstream. The west-east cross section shown in Fig. 34b reveals strong warm air advection over a deep layer in upper-levels to the east of the trough. The tropopause undulation is also characterized by high static stability and anomalously high potential vorticity (Fig. 34c-d). A tropopause undulation is on a larger scale than a tropopause fold. Significant surface pressure falls and mid-level vorticity spin up typically take place downstream of the tropopause undulation. The reader is urged to read Hirschberg and Fritsch (1991a-b) for more details concerning the relationship of tropopause undulations and cyclogenesis.

### C. Slantwise Convection

The traditional Norwegian frontal model displays an organized, narrow line of showers associated with the cold front and a broad shield of relatively light precipitation ahead of the warm front. However, forecasters often see mesoscale bands of heavy, convective precipitation ahead of surface warm fronts or in the vicinity of occluded fronts. Typically, these bands of heavy precipitation are oriented approximately along the thermal wind (e.g., 1000-500 mb layer) and have a half-width

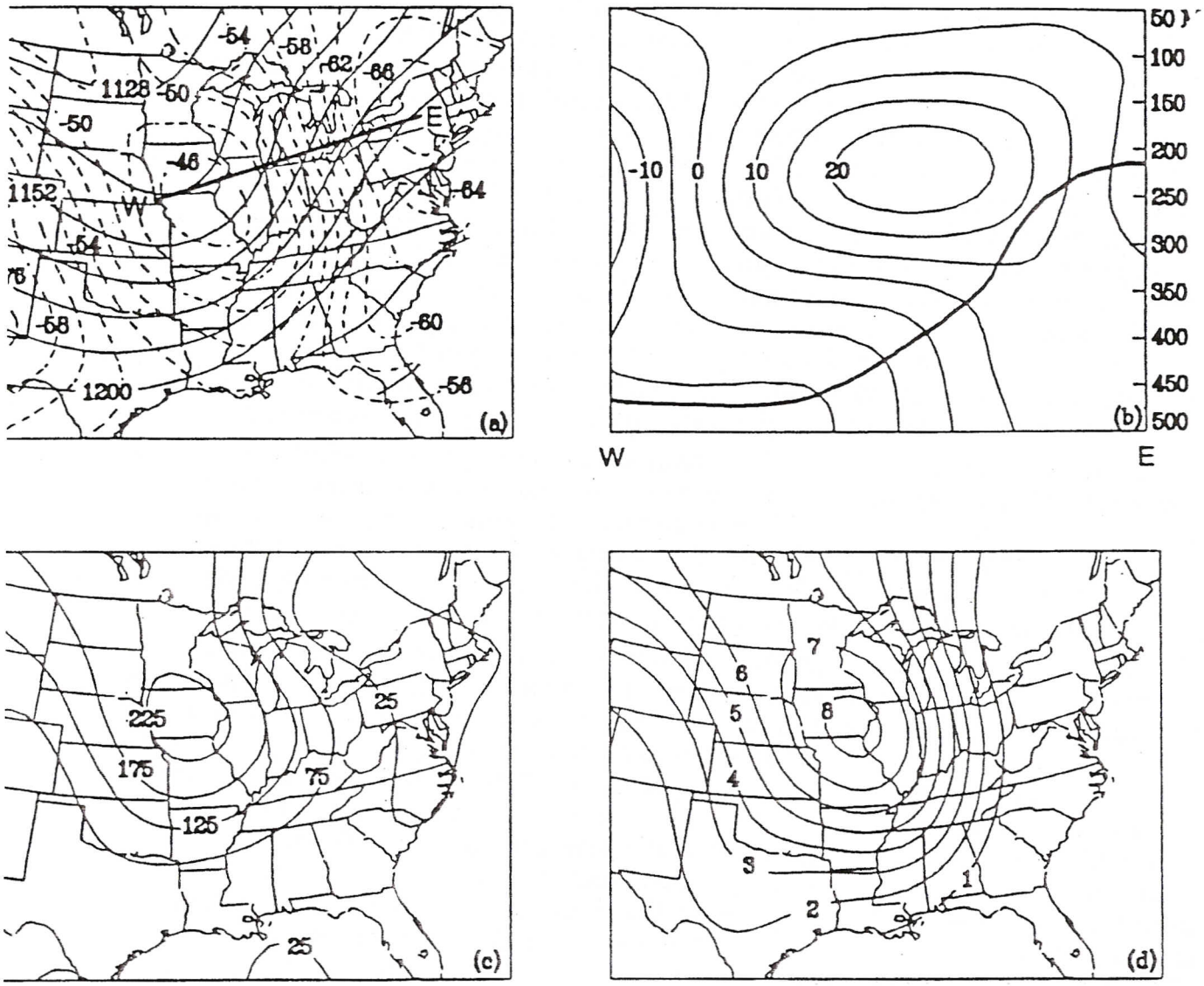


Figure 34a-d. Characteristics of tropopause undulations: (a) 200-mb heights (solid, dm) and temperature (dashed, °C). (b) West-east cross section of temperature advection (solid, $10^{-1}$ K $h^{-1}$) and tropopause (heavy solid line). Section taken between W and E in (a). (c) 300 mb static stability ($10^{-3}$ K $mb^{-1}$). (d) 250 mb isentropic potential vorticity ($10^{-6}$ $m^2$ $s^{-1}$ K $kg^{-1}$). (Hirschberg and Fritsch, 1991a).

(lateral distance from the point of maximum precipitation to the point receiving half this amount) on the order of 100 km. Sometimes these mesoscale bands of precipitation can be explained by local topographic effects or by secondary vertical circulations induced by mesoscale frontogenetical zones. However, recently it has been suggested that they may be the result of "slantwise" convection forming in regions of moist symmetric instability. Thus, a complete understanding of moist symmetric instability and its diagnosis using standard rawinsonde data is important to the operational forecaster. As noted by Lussky (1989), "slantwise convection is essentially the manifestation of symmetric instability which exists along a slantwise (both horizontal and vertical) path." Since slantwise parcel motions are required for slantwise convection, the criteria for symmetric instability involve both an assessment of vertical and horizontal stability. As we shall soon see it is possible to have *slantwise* convection in an otherwise vertically stable atmosphere.

Symmetric instability is actually due to a combination of vertical (buoyancy vs. gravitational) and horizontal (inertial vs. centrifugal) forces. Often the atmosphere supports slantwise convection even though it is weakly *stable* in both the vertical and horizontal. Thus, the atmosphere is unstable only for certain slantwise motion. To assess symmetric instability one needs to force the parcel both vertically and horizontally. Much of the early work on symmetric instability comes from Emanuel (1983,1985) and Bennetts and Hoskins (1979).

**1. Inertial Instability**

First we will investigate accelerations that act upon the parcel when it becomes displaced from its geostrophically balanced flow. We set up a vertical cross-sectional normal to a unidirectional, geostrophically balanced base-state flow, i.e.,

$$\bar{v}_g = + \frac{1}{\bar{\rho} f} \frac{\partial \bar{P}}{\partial x} \tag{44}$$

or

$$\frac{\partial \bar{P}}{\partial x} = \bar{\rho} f \bar{v}_g \tag{45}$$

We define the geostrophic absolute momentum as:

$$M_g = \bar{v}_g + fx \tag{46}$$

where f is the Coriolis parameter and x is the distance in meters from the left edge of the cross section. The cross section is taken normal to the geostrophic flow. With this orientation the pressure gradient in the y direction vanishes as the y axis points in the direction of the flow. (46) defines the geostrophic absolute momentum of the environment, whereas we can define the parcel value as:

$$M = v + fx \tag{47}$$

Now,

$$\frac{du}{dt} = -\frac{1}{\rho}\frac{\partial \bar{P}}{\partial x} + fv = -f\bar{v}_g + fv \tag{48}$$

$$\frac{du}{dt} = f(v-\bar{v}_g) = f(M-M_g) \tag{49}$$

which states that when the parcel M value is < (>) $M_g$ the parcel will accelerate to the west (east), i.e., normal to the flow. It can be shown that a parcel of air tends to conserve its absolute momentum, M.

Thus, when a cross section is chosen normal to the geostrophic wind ($v_g$) and x is the horizontal distance along the cross section, one can test for parcel acceleration in the plane of the cross section by comparing the parcel M value to the environment's $M_g$ value. As will be shown later, an environment may be inertially stable with respect to purely horizontal flow but inertially unstable for certain slantwise motions.

**2. Buoyant Instability**

Basic discussions concerning convection note that the third equation of motion can be written as,

$$\frac{dw}{dt} = \frac{g}{T_{env}}\left[T_p - T_{env}\right] \tag{50}$$

where $T_{env}$ is the environmental air temperature and $T_p$ is the parcel temperature. Using Poissons's equation we can write,

$$\theta_p = T_p\left[\frac{1000}{P}\right]^{\kappa};\ \theta_{env} = T_{env}\left[\frac{1000}{P}\right]^{\kappa} \tag{51}$$

Solving for $T_p$ and $T_{env}$ in (51) and substituting into (50) results in:

$$\frac{dw}{dt} = \frac{g(\theta_p - \theta_{env})}{\theta_{env}} \tag{52}$$

For a nearly saturated environment we need to use the equivalent potential temperature ($\theta_e$) which is conserved for moist parcel ascent. For the latter case Sanders and Bosart (1985) write (52) as,

$$\frac{dw}{dt} = g\left[\frac{(\theta_{e_p} - \theta_{e_{env}})}{\theta_{e_{env}}} - (\exp Q^1 - 1)\right] \tag{53}$$

where $Q^1 = L(q_p - q_{env}) / C_pT$ is a measure of latent heat effects. Clearly if $\theta_p > \theta_{env}$ for a dry (RH < 100 %) atmosphere or if $\theta_{e_p} > \theta_{e_{env}}$ for a near-saturated atmosphere (RH > 90 %), the air parcel will accelerate vertically. As will be shown

shortly, it is possible for a region to be stable for purely vertical motions but unstable for parcels moving in a slantwise manner. Dry parcels tend to conserve their $\theta$ value while $\theta_e$ is conserved for moist or dry ascent. It should be noted that typically $\theta_e$ for the environment and $M_g$ increase upward and to the right in a given cross-sectional diagram, as described earlier. We will now examine the instability criteria for slantwise convection.

### 3. Conditional Symmetric Instability

To illustrate how one might diagnose regions of the atmosphere which may experience slantwise convection we consider Fig. 35 from Sanders and Bosart (1985).

*Parcel A* moves left:

$$M_p > M_g \text{ therefore, } \frac{du}{dt} > 0$$

$$\theta_{e_p} > \theta_{e_{env}} \text{ therefore, } \frac{dw}{dt} > 0.$$

So the parcel moves *up* and to the *east but* since the $\theta_e$ stratification is stable the parcel does eventually go back to its point of origin. The acceleration to the east is opposite to its initial displacement (to the west) and the thermal stratification is stable, so the parcel moves up and to the right and then eventually down. It will also eventually move to the west since it will have $M_p < M_g$ after a while. This parcel is stable.

*Parcel B* moves up:

$$\theta_{e_p} < \theta_{e_{env}} \text{ therefore, } \frac{dw}{dt} < 0$$

and

$$M_p < M_g \text{ therefore, } \frac{du}{dt} < 0.$$

So the parcel accelerates down and to the west. However, the horizontal acceleration does not affect the stable downward acceleration; it quickly lessens since the fluid is inertially stable. As the parcel moves west it will soon "feel" an acceleration to the east as its M will be $> M_g$. So the downward motion is opposite to its initial impulse and the inertially stable environment will eventually force parcel B back to its original position. This parcel is also stable.

*Parcel C:* slantwise displacement to left and up.

Its slope is between the M and $\theta_e$ isopleths.

Here, $\theta_{e_p} > \theta_{e_{env}}$ therefore, the parcel accelerates *up*

and $M_p < M_g$ therefore, the parcel accelerates to the *west*.

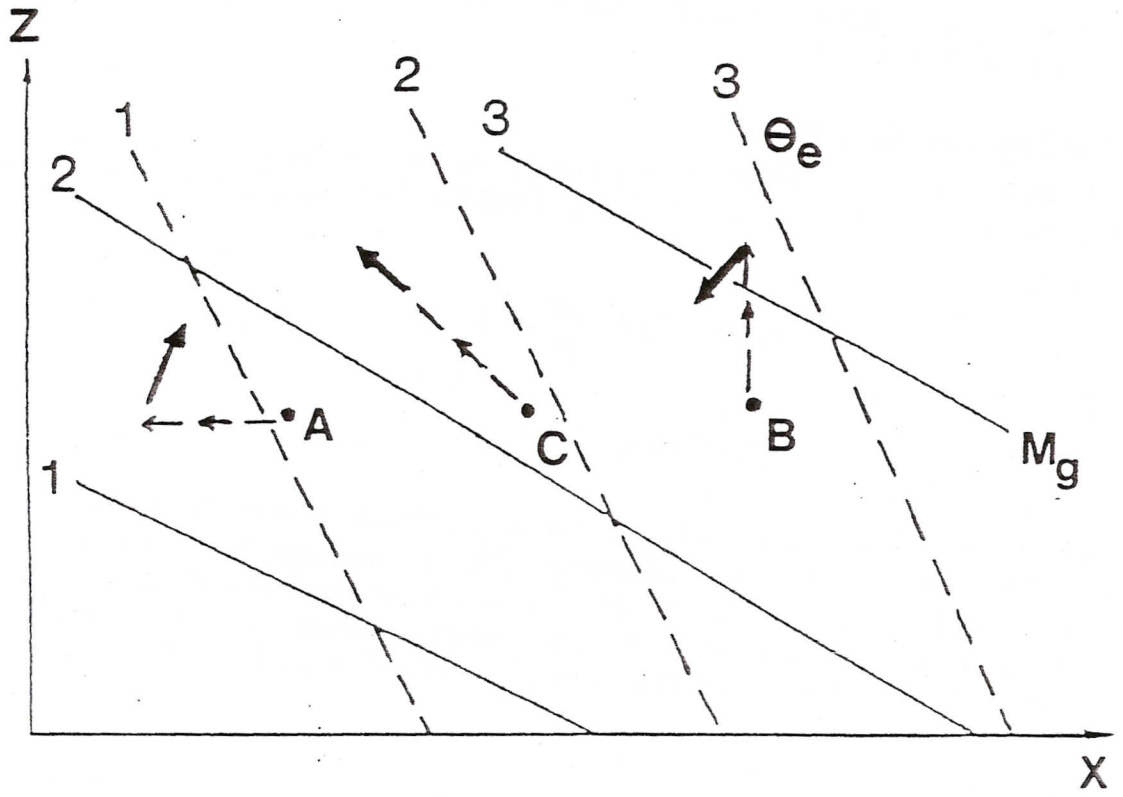


Figure 35. Schematic vertical cross section illustrating symmetric instability. Solid lines represent the absolute momentum, $M_g$, of the basic flow. Dashed lines represent equivalent potential temperature. Lettered points show sample displacements (dashed) and accelerations (arrowheads). (From Sanders and Bosart, 1985).

In this case the parcel accelerates in the same direction as its initial movement. This *slantwise* displacement is *unstable!* Therefore, slantwise convection requires the slope of the $M_g$ surfaces to be shallower (less) than the slope of the $\theta_e$ surfaces; i.e.

$$(\partial z/\partial x)_{M_g}/(\partial z/\partial x)_{\theta_e} < 1 \qquad \text{C S I} \tag{54}$$

The term symmetric instability generally refers to the condition where $M_g$ surface are shallower than $\theta$ surface (i.e., dry air parcels).

If the atmosphere is moist but unsaturated the condition expressed in (54) is a necessary but <u>not</u> sufficient condition. So if $\theta_e$ decreases upward along $M_g$ surfaces we say there is potential slantwise instability. In a saturated environment under the same conditions the atmosphere is said to have conditional symmetric instability (CSI). Thus, in a moist but unsaturated atmosphere large scale lifting may bring the air to saturation with time converting potential to conditional symmetric instability. In regions of CSI a parcel displaced in a slantwise fashion may become positively buoyant, in spite of the fact that the environment is statically and inertially stable. The term "symmetric" denotes that the perturbation does not vary along the basic current (Bluestein, 1986). Some authors prefer the term "slantwise" over "symmetric" to emphasize the type of motion necessary for this instability to be realized.

Bluestein (1986) notes that symmetric instability is favored under the following conditions:

1. high vertical wind shear
2. large anticyclonic wind shear
3. low static stability

High vertical wind shear is required as it will result in rapid increases in $M_g$ at a particular station. Thus, $M_g$ surfaces will be oriented more horizontally and tend to be shallower than adjacent $\theta$ (or $\theta_e$) surfaces. Large anticyclonic wind shear may create a region where the absolute vorticity is $< 0$ ; i.e., an inertially unstable zone (see Holton, 1979, p. 215-216). In such regions the horizontal response will be greater for a given degree of forcing. Finally, low static stability (or low convective stability, if using $\theta_e$) is required as it will result in $\theta$ (or $\theta_e$) surfaces which are tilted close to the vertical, thereby increasing the chance of having $M_g$ surfaces being more shallow than adjacent $\theta$ or $\theta_e$ surfaces.

Figures 36a-b show an example of CSI over Denver, Colorado at 0000 UTC 20 January 1991. The cross section shown in Fig. 36a was taken along a northwest-southeast line, normal to the 850-300 mb thickness over Denver, Colorado. The cross section depicts a region of CSI from 400-600 mb. As one can see, the isopleths of $\theta_e$ are more vertical than the isopleths of $M_g$ in the later region. Figure 36b shows the Doppler radar reflectivity from the Mile-High Radar at Denver, Colorado at 2300 UTC 19 January 1991. It reveals several bands of precipitation (in this case, snow) south of the radar site. One to five inches of snow fell within these narrow mesoscale bands.

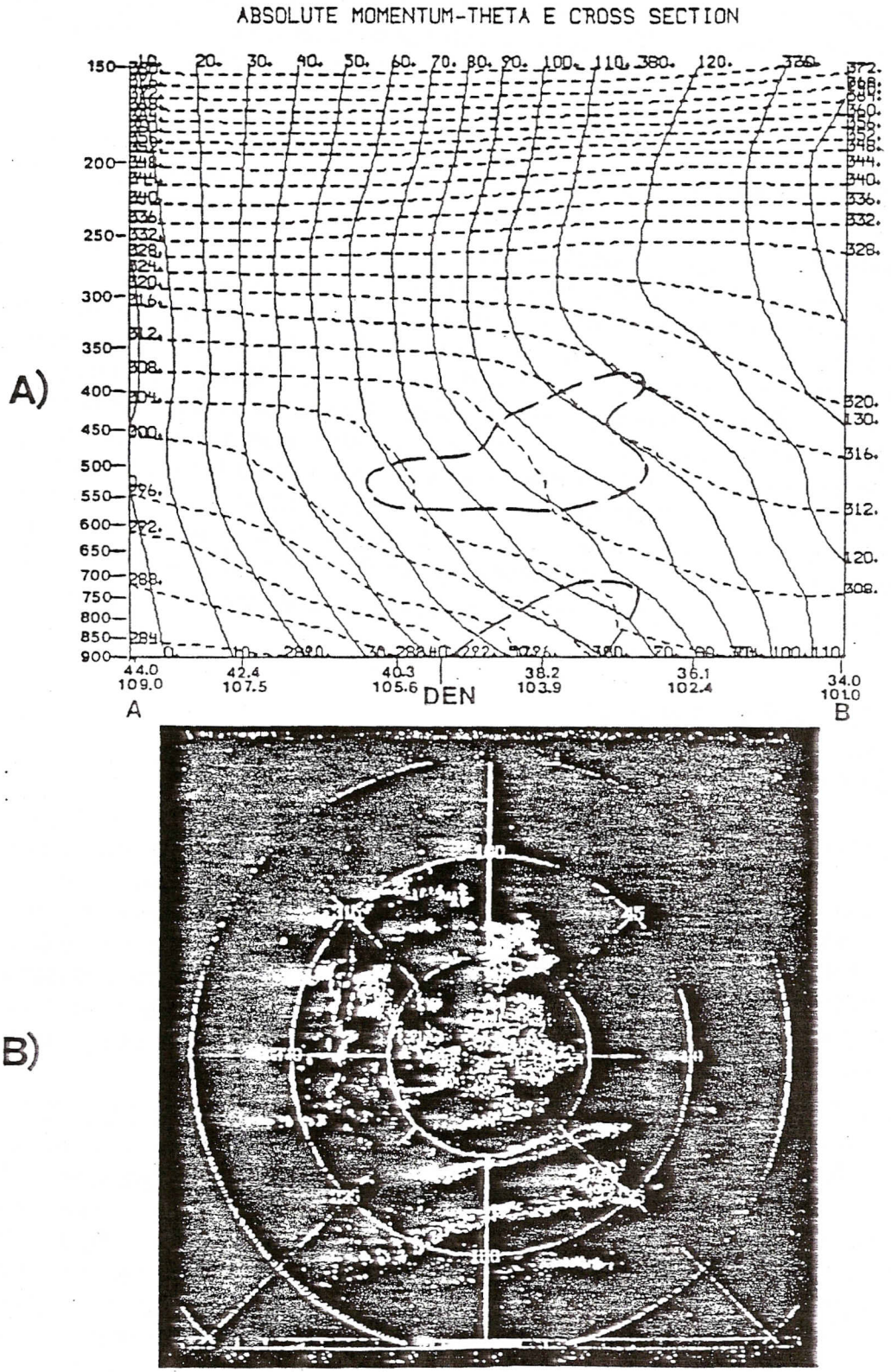


Figure 36a-b. (a) Cross section of $\theta_e$ (dashed, °K) and $M_a$ (solid, m $s^{-1}$) at 0000 UTC 20 January 1992. Region enclosed by thick dashed lines denotes CSI. DEN = Denver, Colorado. (b) Plan Position Indicator at 1.6° elevation angle from the Mile High Radar at Denver, Colorado at 2300 UTC 19 January 1992. Reflectivity in dBZ is indicated by the bar along the bottom of the fig-

It should be pointed out that in order to display $M_g$ values one needs first compute the total geostrophic wind (either on constant pressure or isentropic surfaces) on gridded surfaces in the vertical. Then, one must compute the component of $V_g$ normal to the plane of the cross section. This value is then added to the quantity fx where x is the distance in meters to the right on the horizontal axis. Generally, one chooses the x axis to be oriented normal to the thermal wind typically over a deep mid-tropospheric layer (e.g. 850-300 mb). Sanders and Bosart (1985) state that the geostrophic value must be used because $M_g$ contains a representation of the horizontal pressure gradient force through $v_g$, which is assumed to be in geostrophic balance. Reuter and Yau (1990) note that cases where the flow patterns have significant curvature are not correct to use for CSI analysis as they violate the condition of geostrophic balance assumed in the theory. Sanders (1986) does offer a method for incorporating a curvature term to account for gradient wind effects, but it is not easily amenable for operational diagnosis. It is important to note, that CSI is only defined for a convectively stable region. If there is convective instability present (i.e., $\theta_e$ decreases with height) then convective processes will dominate CSI over smaller space-time scales. For a further review of applying CSI in an operational environment, see Snook (1992).

Lussky (1989) applied an AFOS application program to diagnose CSI which uses the total wind instead of the geostrophic wind to compute M surfaces. This method is useful for operational diagnose of CSI relative to time constraints. It assumes that the total wind field contains gradient accelerations which are weak compared to the accelerations associated with CSI. This may not be a valid assumption in regions of strong ageostrophic wind vectors, e.g., in the exit/entrance regions of jet streaks and/or jet streaks with significant cyclonic/anticyclonic curvature.

## 4. Relationship of Slantwise Convection to Frontogenesis

Several researchers (e.g., Gyakum, 1987; Moore and Blakley, 1988; Sanders and Bosart, 1985; and Sanders, 1986) have noted that frontogenetical forcing in regions of CSI often work in a synergistic fashion to enhance vertical motion over mesoscale bands. As described by Holton (1979, p. 237-240) frontogenesis results in a thermally direct circulation, i.e., upward vertical motion on the warm side and downward vertical motion on the cold side. If CSI is present in a region of diagnosed frontogenesis region the intensity of the upward vertical motion is increased while the scale length is constricted. For example, in the case of a strengthening warm front the direct thermal circulation will be sloped to the north (into the cold air) where, if CSI is present, heavy precipitation bands can develop parallel to the mid-tropospheric thermal wind vector. Sanders (1986) refers to the role of CSI in this process as a catalyst and a provider of structural detail in the vertical motion and, hence precipitation pattern.

Bluestein (1986) suggests that..."mesoscale convective lines may be forced by the circulations triggered by symmetric instability along fronts." Lussky (1989) states that a diagnosis of regions where slantwise convection is possible may help forecasters by narrowing down the location of the more convective, intense and

unsteady precipitation. It may also help the forecaster be alert for the potential for heavier precipitation in those areas.

### D. Short Term Forecasting of Severe Convection Using Isentropic Analysis

Although isentropic analysis is best suited to cold season cases of cyclogenesis/frontogenesis when horizontal thermal gradients are most distinct in mid-latitudes, several authors have suggested its use in the short term forecasting of severe convection. Namias (1938) was probably the first researcher to promote using isentropic charts as an aid in thunderstorm forecasting. He emphasized the use of cross sections of potential temperature and specific humidity and "horizontal" isentropic analyses as useful charts in diagnosing and anticipating moisture patterns. He noted that, "tongues of dry and moist air may be followed from day to day by means of these charts, for it is reasonable to suppose that the major atmospheric motions are approximately adiabatic." This is especially true in the pre-convective environment before the onset of strong solar and latent heating.

More recently Wilson et al. (1980) and Moore (1985) have described analysis procedures on isentropic charts which can help forecasters diagnose severe convective threat areas on meso alpha scales of motion. Wilson et al. (1980) constructed a four panel chart consisting of:

(1) one panel with only station models as described in Fig. 18,
(2) one panel with isopleths of Montgomery streamfunction and pressure,
(3) one panel with isopleths of Montgomery streamfunction and stability, and
(4) one panel with isopleths of Montgomery streamfunction and specific humidity.

A mid-level isentropic surface is chosen to help depict upward/downward vertical motion, moist/dry tongues, moisture advection, and stability. An upper level isentropic surface is chosen to diagnose jet streaks, their strength, curvature, and proximity to the possible threat area. These two isentropic surfaces may be chosen by using climatological average values or by consulting a cross section with normal wind components and specific humidity superimposed. On the mid-level isentropic surface, a dry line can be defined as the inner moisture isopleth on the dry side of the gradient while the moist tongue is taken to be the zero moisture advection line according to the M and q analysis. On the upper level isentropic surface, jet streaks are defined according to the actual wind field and the orientation and gradient of the Montgomery streamfunction.

A depiction chart (similar to a composite chart) is prepared by placing the surface front, dry line, moist tongue, and the middle and upper-level jet streak positions on one chart. Although the authors do not mention it, one could easily add the axis (or axes) of greatest instability as well. Forecast positions of these features are placed on the chart, as well. The forecast position of the surface front is taken from forecast charts while moist tongues and dry lines are forecast using 100% of the wind speed at the lower isentropic level. Jet streak positions are subjectively forecast from prognostic charts, showing continuity and relationship to the surface front. The authors then place the maximum threat area as *west* of the mid-level dry line and *east* of the surface front, and near the mid-level jet streak. Typically the strongest convection takes place to the right (looking downstream) of the mid-level

jet streak. Greatest destabilization takes place between the mid-level moisture maximum and the dry line. Since this region usually has ample low level moisture it is an area of strong convective instability.

As a follow-up to the previous study, Moore (1985) expanded on the concepts presented by the above authors. He developed five diagnostic charts based on isentropic surface data. They include charts depicting:

(1) Montgomery streamfunction isopleths and isobars,
(2) Adiabatic vertical motion isopleths and isohumes (specific humidity),
(3) Horizontal moisture convergence field and low level static stability,
(4) Low level stability flux field, and
(5) A composite of key features--pressure ridges, upper level jet axis, and centers of upward vertical motion, minimum stability, moisture convergence, and stability flux convergence.

In his study Moore found that the threat area for AVE-SESAME I was characterized by:

(1) thermal riding (pressure axis);
(2) relatively low static stability;
(3) proximity to a moist axis;
(4) proximity to a moisture convergence maximum;
(5) strong adiabatic upward vertical motion;
(6) strong positive stability flux (destabilization) and,
(7) being along the upper level jet axis, preferentially in the exit region.

The charts used in this study are shown in Fig. 37a-g. Figure 37b shows the cross section used to choose the representative isentropic surfaces. Figures 37c-g are the charts described above. Note how the juxtaposition of the key thermo- and hydrodynamic features described above help depict the strong convection 3 hours later in the Texas panhandle. This was the center of the most severe activity. The west-east line of activity in Oklahoma formed north of the best "overlap" region of the parameters but was suggested by the west-east axes of adiabatic vertical motion, moisture convergence and low level stability flux.

It should be noted that these techniques are most useful during the spring and fall months when the thermo- and hydrodynamic features on isentropic surfaces are well-defined and of significant strength.

### E. Additional Applications

There are other applications associated with isentropic analyses which have not been discussed up to this point. These applications are in the area of diagnosing and forecasting the freezing level and Clear Air Turbulence (CAT) for aviation and the overrunning convective instability for thunderstorm forecasting.

#### 1. Freezing Level and Icing

Anderson (1984) describes a simple method for diagnosing the pressure level of the freezing level for the aviation community. From the Poisson equation (17) one

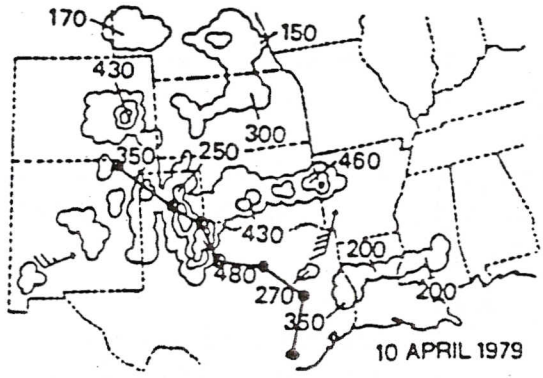


Figure 37a. National Weather Service radar summary for 2035 UTC 10 April 1979. The line shown is the cross section depicted in Figure 37b (Moore, 1985).

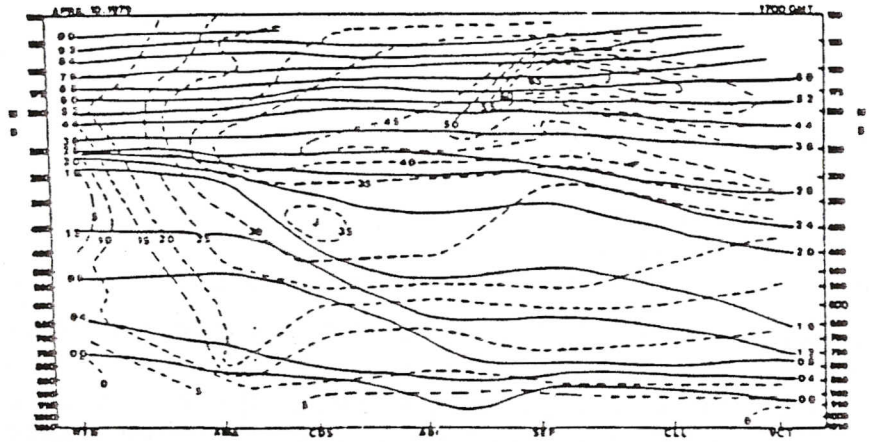

Figure 37b. Isentropic cross section for 1700 GMT 10 April 1979. The solid lines are isentropes in °K with the preceding 3 or 4 omitted. The dashed lines are isotachs of the normal wind component in m $s^{-1}$ (Moore, 1985).

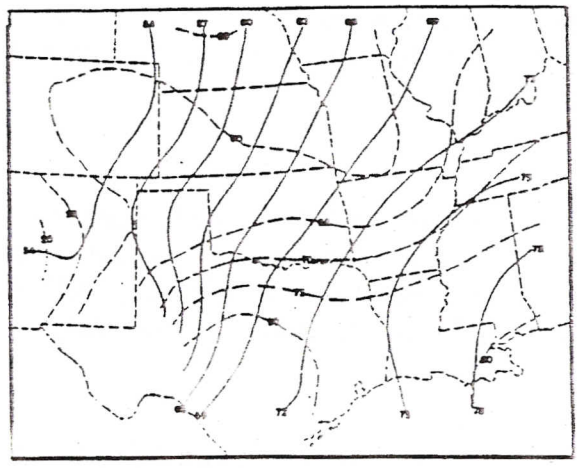

Figure 37c. The Montgomery streamfunction for 30[illegible] K surface at 1700 GMT 10 April 1979. The Montgomery streamfunction (solid) is in $10^3$ ergs/gm with the preceding 3( missing. Isobars (dashed) are in tens of mb (Moore, 1985).

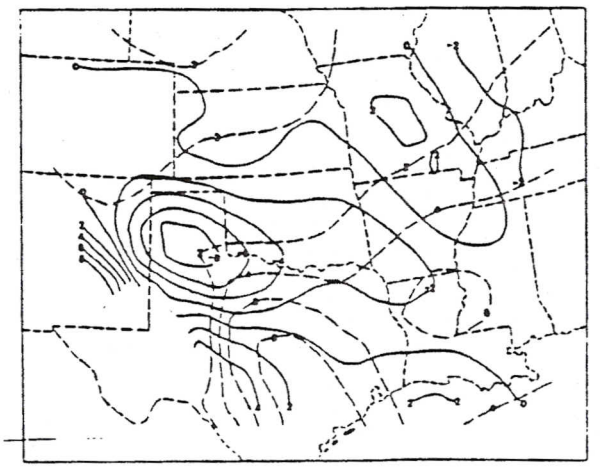

Figure 37d. Adiabatic vertical motion in microbars/s (solid) and specific humidity in gm/kg (dashed) for the 306 K surface at 1700 GMT 10 April 1979 (Moore, 1985).

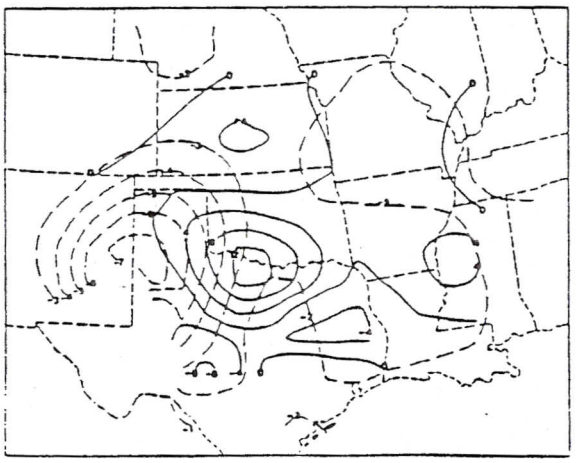

Figure 37e. Horizontal moisture convergence in gm/kg x 10 (solid) and low level stability for the 306 K surface at 1700 GMT 10 April 1979 (Moore, 1985).

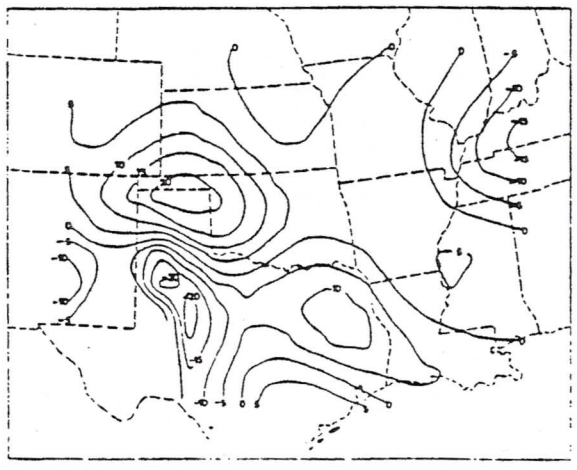

Figure 37f. Low level stability flux (x $10^5$ mb $K^{-1}$ $s^{-1}$) for the 304-308 K layer at 1700 GMT 10 April 1979 (Moore, 1985).

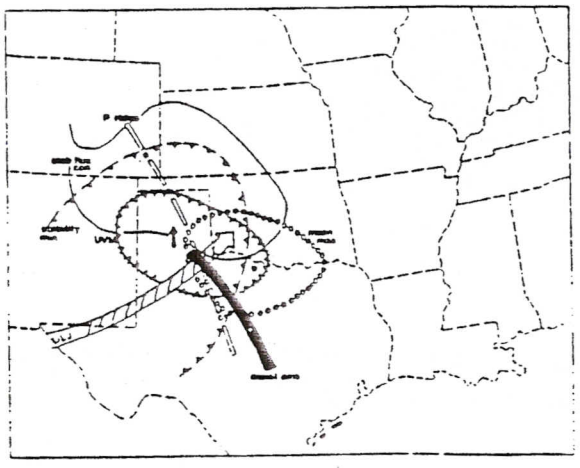

Figure 37g. Composite chart for 1700 GMT 10 April 1979 (Moore, 1985).

can easily compute the pressure value of the O°C isotherm on any isentropic surface. These pressure values are printed in Table 1 for $\theta$ = 290-320 K. On an isentropic chart the freezing pressure isobar could be colored blue for easy reference.

If aviation forecasters referenced this isobar to a chart showing the condensation ratio *or* to one showing condensation pressure and pressure, they could determine areas of possible icing conditions. Since moisture transport is more realistically depicted on an isentropic surface, these icing regions should display better continuity in space-time than on constant pressure surfaces. Even in areas of low condensation ratios, one may forecast increases in condensation ratios where significant isentropic lifting is taking place.

**2. Clear Air Turbulence**

Shapiro (1974, 1976, 1980) and Gidel and Shapiro (1979) have described and discussed CAT in relation to the level of maximum wind and the tropopause. Figure 38 shows where CAT is favored to occur with respect to a wind maximum and upper level frontal zone. The CAT region is not only found within the downward sloping frontal zone but also above the wind maximum in the upward sloping isentropic surfaces. In both regions horizontal and vertical wind shears can be quite strong. Shapiro (1974) measured, using rawinsonde data and data from a meteorologically instrumented aircraft, vertical and horizontal wind shears of 15 m $s^{-1}$ $km^{-1}$ and 25 m $s^{-1}$ (40 km)$^{-1}$, respectively, at about 450 mb. He states, "...though the turbulence is confined to short bursts over horizontal distances of tens of kilometers, it is encountered at several vertical levels, thus suggesting a large-scale (hundreds of kilometers) extent of the CAT patch when the turbulent-scale measurements are made along a surface contained within sloping shear layers rather than on constant pressure surfaces."

These ideas suggest that isentropic cross sections with normal wind components should be useful in diagnosing CAT. Numerical model data in an isentropic format can be used to forecast CAT conditions. Cross-sectional analyses can be used to qualitatively evaluate the potential for CAT while actual horizontal and vertical shears with respect to $\theta$ could be computed to assign threshold criteria.

An important consideration is that upper level frontal zones are not always easy to diagnose on constant pressure surfaces because their horizontal extent is quite limited, especially when compared to their vertical extent. Also, as Shapiro (1974) has documented, often there is a multiple structured frontal zone — jet stream system which can be resolved using cross-section analysis. Figure 39 shows an example of such a complex between Albuquerque, New Mexico (ABQ) and Oklahoma City, Oklahoma (OKC). Both frontal zones are associated with horizontal and vertical wind shear. They are easier to diagnose using the isentropic cross section than by depending upon constant pressure analysis. This diagnosis exploits the fact that isentropic surfaces slope with the frontal zone rather than cut across it as do constant pressure surfaces. Thus, frontal characteristics, such as thermal gradients, moisture gradients, and wind shears are easier to diagnosis with a large scale data set (e.g., U.S. rawinsonde data) using an isentropic framework. On constant pressure surfaces these gradients are often poorly resolved since they can take place over mesoscale distances.

Table 1. Pressure values of 0°C isotherm for various isentropic surfaces (Anderson, 1984)

| Potential Temperature (°K) | Pressure of Freezing Level (mb) |
|---|---|
| 290 | 809 |
| 291 | 800 |
| 292 | 790 |
| 293 | 781 |
| 294 | 772 |
| 295 | 762 |
| 296 | 752 |
| 297 | 745 |
| 298 | 736 |
| 299 | 727 |
| 300 | 719 |
| 301 | 711 |
| 302 | 702 |
| 303 | 694 |
| 304 | 686 |
| 305 | 678 |
| 306 | 671 |
| 307 | 663 |
| 308 | 656 |
| 309 | 648 |
| 310 | 641 |
| 311 | 634 |
| 312 | 627 |
| 313 | 620 |
| 314 | 613 |
| 315 | 606 |
| 316 | 599 |
| 317 | 593 |
| 318 | 586 |
| 319 | 580 |
| 320 | 576 |

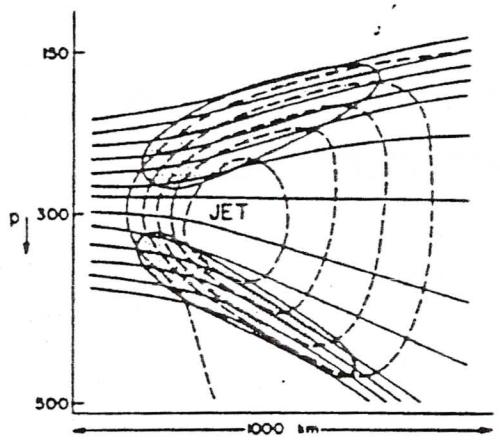


Figure 38. Schematic illustration of regions of clear-air turbulence (stippled) in the vicinity of an upper-level jet core and frontal zone. Solid and dashed lines respectively indicate potential temperature and wind speed (Shapiro, 1976).

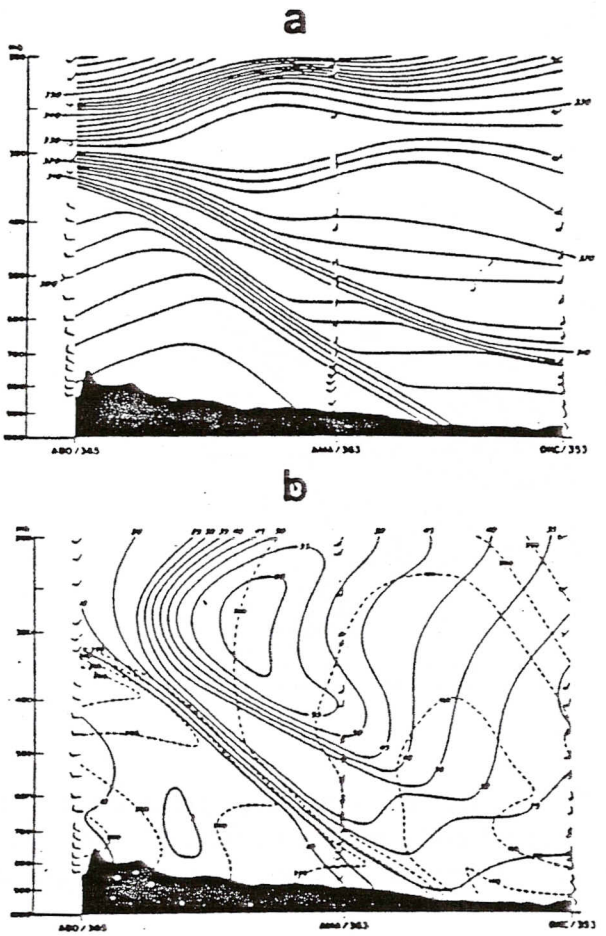


Figure 39. Cross sections of potential temperature (a) and wind speed and direction (b) at 0000 GMT 20 April 1971. Isentropes (°K), solid lines; isotachs (m/s), solid lines, isogons (°), dashed lines; positions of the Albuquerque, NM, Amarillo, TX, and Oklahoma City, OK rawinsonde ascents are marked along the abscissa, (Shapiro, 1974).

### 3. Overrunning Convection

When warm, moist unstable air (e.g., lifted indices < 0) lies to the south of a warm frontal or similar boundary in the presence of significant low level winds (e.g., > 10-15 m $s^{-1}$) elevated convection is likely to take place north of the boundary. Standard stability indices (e.g., lifted index, Showalter index) are unable to diagnose or even hint at this elevated instability region. An isentropic cross section with specific humidity can be useful in illustrating the presence of moisture aloft in a region of less stable air seen as a large separation of adjacent isentropes. Otherwise these elevated regions of low stability are difficult to diagnose with constant pressure analysis techniques.

A second method of diagnosing these cases of overrunning convection is through a cross section of equivalent potential temperature $\theta_e$. A typical case of overrunning convection can be diagnosed by noting regions where $\theta_e$ isopleths "fold" over producing regions where $\theta_e$ decreases with height. Typically warm, moist air overrides the frontal boundary at or around 800 mb and is associated with high $\theta_e$ values. Above this layer, cooler and drier air above the frontal zone is associated with low $\theta_e$ values. If decreases of $\theta_e$ with height exceed 5-10 degrees K it is often significant. In the presence of isentropic uplift this instability will be released, forming embedded convection. This kind of activity took place over Missouri and Illinois during a warm advection type snowstorm and enhanced snow totals to greater than 1 foot along a zone north of a frontal boundary. An equivalent potential temperature cross section with *parallel* wind components is shown in Fig. 40 for this case. Note that low level convergence in the plane of the cross section is collocated with the stippled region above Salem, Illinois (SLO) to indicate convective instability. Areas south and west of SLO received heavy rain with convection while heavy snow and embedded convection took place to the north in the cold air.

## V. CONCLUDING COMMENTS

The basic tools and physical concepts for using isentropic analysis techniques in the operational setting have been presented. It is now up to the reader to implement them in his/her forecasting environment so that an appreciation for how an isentropic viewpoint can help form a diagnosis may be gained. As always, experience is the best teacher. Undoubtedly one will find situations where these techniques can offer considerable insight into understanding why certain meteorological events are taking place. At other times, they may only *cloud* the issue. There are no cure-alls or quick fixes in this business. However, when used judiciously and interpreted properly it is the author's experience, shared by many others, that isentropic analysis can be used effectively *together with standard pressure analyses* to create a three-dimensional picture of atmospheric motions.

With the advent of faster computers and interactive graphic capabilities in the forecast office, the time seems right to re-introduce the isentropic viewpoint to the forecaster community. With patience and experience they will see its utility in the diagnosis and forecast process. The PC-GRIDDS software will accelerate the use of isentropic analysis in the operational setting.

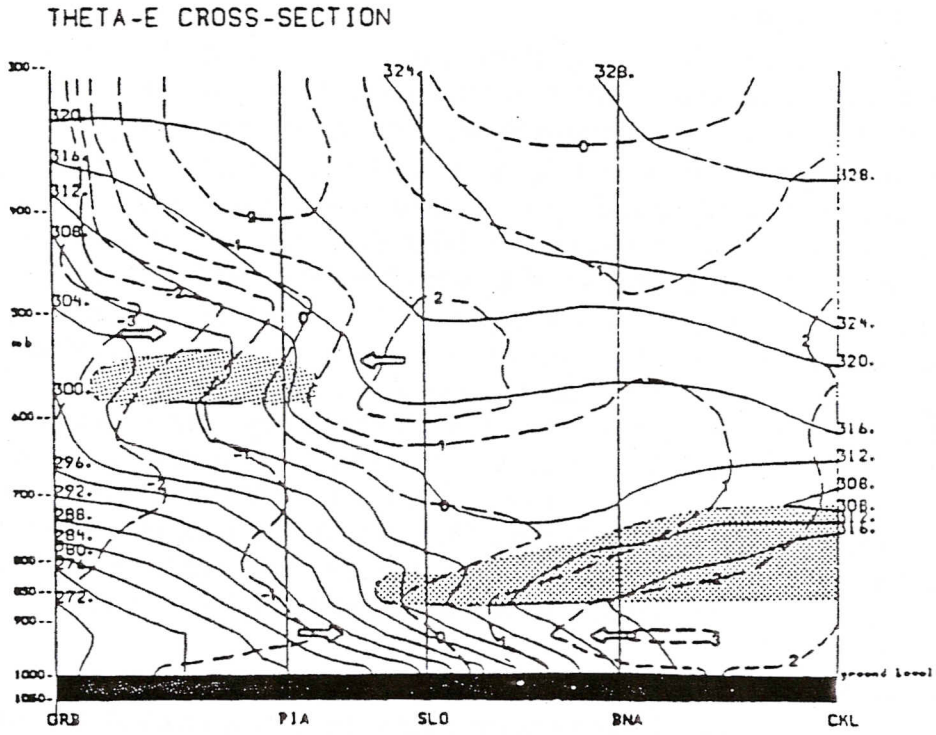


Figure 40. Cross section of equivalent potential temperature (solid lines, ° K) and wind components parallel to the plane of the cross section (dashed lines, knots). Positive values denote winds from right to left and negative values denote winds from left to right. GRB = Green Bay, WI; PIA = Peoria, IL; SLO = Salem, IL; BNA = Nashville, TN; CKL = Centerville, AL. Stippling denotes convective instability (Moore and Blakley, 1988).

## VI. ACKNOWLEDGEMENTS

The author would like to thank Saint Louis University for offering a sabbatical leave during which time he was able to work on this manuscript. The people at the NSSFC were also very supportive and offered ideas on strengthening the text. The author is also indebted to Dr. Joe Schaefer, Director of the National Weather Service Training Center (NWSTC), Dr. Richard McNulty, Chief of the Hydrometeorology and Management Division of the NWSTC, and Mr. Pete Chaston, Technical Project Leader at the NWSTC, who have enthusiastically endorsed and actively supported the author's work in the meteorological community and especially within the NWS. Also, Dr. Dale Meyer, Mr. George Taniguchi, and Mr. Michael Squires of the Air Weather Service are to be thanked for their proofreading of the text. Dr. Charles Graves wrote the software used to create the beautiful cover graphic of a three-dimensional isentropic surface. Last, but not least, the expert typing of Ms. Juanita Ryles, Ms. Jeanne Mueller and the assistance of Dr. Richard Molinaro are deeply appreciated.

## VII. REFERENCES


Abbott, E. A., 1952: Flatland, A Romance of Many Dimensions. Dover Publications Inc., New York, N.Y., 103 p.

Anderson, J. F., 1984: The Use and Interpretation of Isentropic Analysis. NOAA Tech. Memo. NWS WR-188, National Weather Service Western Region, Salt Lake City, UT, 84147-0188, 40 p.

Anthony, R. W., W. E. Carle, J. T. Schaefer, R. L. Livingston, A. L. Siebers, F. L. Mosher, J. T. Young, and T. M. Whittaker, 1982: The Centralized Storm Information System at the NOAA Kansas City Complex. Preprints - Ninth Conference on Weather Forecasting and Analysis, Seattle, WA, Amer. Meteor. Soc., 40-43.

Barnes, S. L., 1973: Mesoscale Objective Analysis Using Weighted Time-Series Observations. NOAA Tech. Memo ERL NSSL-62 National Severe Storms Laboratory, Norman, OK 73069, 60 p. [NTIS Com-73-10781]

Bennetts, D.A. and B.J. Hoskins, 1979: Conditional Symmetric Instability -A Possible Explanation for Frontal Rain Bands. *Quart, J. Roy. Meteor. Soc.*, **105**, 945-962.

Blackadar, A. K., and J. Dutton, 1970: Tracers in the Air. *Weather Wise*, **23**, 182-185.

Bleck, R., 1973: Numerical Forecasting Experiments Based on the Conservation of Potential Vorticity on Isentropic Surfaces. *J. Appl. Meteor.*, **12**, 737-752.

Bluestein, H., 1986: Fronts and Jet Streaks: A Theoretical Perspective. Chap. 9 - Mesoscale Meteorology and Forecasting, edited by Peter S. Ray, Amer. Meteor. Soc., pp. 173-215.

Browning, K. A., 1986: Conceptual Models of Precipitation Systems. *Weather and Forecasting*, **1-2**, 23-41.

Burger, D., 1965: Sphere Land, A Fantasy About Curved Spaces and an Expanding Universe. Barnes and Noble Books, Harper and Row Publishers, New York, 208 p.

Byers, H. R., 1938: On the Thermodynamic Interpretation of Isentropic Charts. *Mon. Wea. Rev.*, 66, 63-68.

Carlson, T. N., 1980: Airflow Through Midlatitude Cyclones and the Comma Cloud Patterns. *Mon. Wea. Rev.*, **108**, 1498-1509.

Carr, F. H., and J. P. Millard, 1985: A Composite Study of Comma Clouds and Their Association with Severe Weather over the Great Plains. *Mon. Wea. Rev.*, **113**, 370-387.

Danielsen, E. F., 1959: The Laminar Structure of the Atmosphere and Its Relation to the Concept of the Tropopause. *Arch. Meteor. Geophys., BioKlim, Atol., Ser. A*, **11**, 232-293.

_____, E. F., and E. R. Reiter, 1960: Bemerkungen zu E. Kleinschmidt: Nichtadiabatische Abkuhlung im Bereich des Jet-Stream. *Beitr. Phys. Atmos.*, 32, 265-273.

_____, E. F., 1961: Trajectories: Isobaric, Isentropic and Actual. *J. Meteor.*, 18, 479-486.

_____, E. F., 1966: Research in Four-Dimensional Diagnosis of Cyclonic Storm Cloud Systems. Rep. No. 66-30, Air Force Cambridge Research Lab., Dept. 66-30, Bedford, MA, 53 p. [NTIS AD 632 668].

_____, E. F., and R. Bleck, 1967: Moist Isentropic Flow and Trajectories in a Developing Wave Cyclone. Rep. No. 67-0617, Air Force Cambridge Research Lab., Dept. 67-0617, Bedford, MA, 34 p. [NTIS AD 670 847].

_____, E. F., 1968: Stratospheric-Tropospheric Exchange Based on Radioactivity, Ozone and Potential Vorticity. *J. Atmos. Sci.*, 25, 502-518.

Doswell, C. A., 1986: The Human Element in Weather Forecasting. *Nat. Wea. Dig.*, 11, 6-18.

Duquet, R. T., 1964: Data Processing for Isentropic Analysis. Tech. Report No. 1, Contract AT (30-1)-3317, Pennsylvania State University, State College, PA, 33 pp. [Available from Pennsylvania State University, Dept. of Meteorology, University Park, PA 16802].

Dutton, J. A., 1976: The Ceaseless Wind. McGraw-Hill, Inc., New York, 579 p.

Edson, H., 1966: Technique Development Reports - 1966. Technical Report 188, Air Weather Service (MAC), USAF, 135-143.

Eliassen, A., and E. Raustein, 1968: A Numerical Integration Experiment with a Model Atmosphere Based on Isentropic Coordinates. *Meteorologist Annale*, 5, 45-63.

Emanuel, K. A., 1983: On Assessing Local Conditional Symmetric Instability from Atmospheric Soundings. *Mon. Wea. Rev.*, 111, 2016-2033.

_____, 1985: Frontal Circulations in the Presence of Small Symmetric Instability. *J. Atmos. Sci.*, 42, 1062-1071.

Gidel, L. T., and Shapiro, M. A., 1979: The Role of Clear Air Turbulence in the Production of Potential Vorticity in the Vicinity of Upper Tropospheric Jet Stream Frontal Systems. *J. Atmos. Sci.*, 36, 2125-2138.

Gyakum, J. R., 1987: Evolution of a Surprise Snowfall in the United States Midwest. *Mon. Wea. Rev.*, 115, 2322-2345.

Haagenson, P. and M. A. Shapiro, 1979: Isentropic Trajectories for Derivation of Objectively Analyzed Meteorological Parameters. NCAR Technical Note NCAR/TN-149+STR, Boulder, CO, 30 p.

Haltiner, G. J. and R. T. Williams, 1980: *Numerical Prediction and Dynamic Meteorology*. John Wiley and Sons, New York, NY, 312-313.

Hess, S. L., 1959: Introduction to Theoretical Meteorology. Holt, Rinehart and Winston, New York, p. 30-34.

Hirschberg, P. A. and J. M. Fritsch, 1991a: Tropopause Undulations and the Development of Extratropical Cyclones. Part I: Overview and Obervations from a Cyclone Event. *Mon. Wea. Rev.*, **119**, 496-517.

_____, and _____, 1991b: Tropopause Undulations and the Development of Extratropical Cyclones. Part II: Diagnostic Analysis and Conceptual Model. *Mon. Wea. Rev.*, **119**, 518-550.

Holton, J. R., 1979: An Introduction to Dynamic Meteorology. Academic Press, New York, p. 87-92, 215-216, 237-240.

Homan, J. H., and R. A. Petersen, 1985: The Use of a Simplified Isentropic Model for Nowcasting Convective Development. Preprints - Fourteenth Conference on Severe Local Storms, Indianapolis, IN, Amer. Meteor. Soc., 394-397.

_____ and L. W. Uccellini, 1987: Winter Forecast Problems Associated with Light to Moderate Snow Events in the Mid-Atlantic States on 14 and 22 February 1986. *Weather and Forecasting*, 2, 206-228.

Hoskins, B. J., and F. P. Bretherton, 1972: Atmospheric Frontogenesis Models: Mathematical Formulation and Solution. *J. Atmos. Sci.*, 29, 11-37.

Koch, S. E., M. DesJardins, P. J. Kocin, 1983: An Interactive Barnes Objective Map Analysis Scheme for Use with Satellite and Conventional Data. *J. of Climate and Appl. Meteor.*, 12, 1487-1503.

Kocin, P. J., L. W. Uccellini, and R. A. Petersen, 1981: The Role of Jet Streak "Coupling" in the Development of the 10-11 April Wichita Falls Tornado Outbreak. Preprints - Twelfth Conference. Severe Local Storms, San Antonio, TX, Amer. Meteor. Soc., 560-563.

Little, C. D., 1985: Isentropic Plotter. NOAA Eastern Region Computer Programs and Problems, NWSA ERCP-No. 29, NOAA, U.S. Dept. of Commerce, 10 p.

Lussky, G. R. 1989: Heavy Rains and Flooding in Montana: A Case for Operational Use of Symmetric Instability Diagnosis. *Wea. and Forecasting*, 4, 186-201.

Moore J. T. and M. F. Squires, 1982: Ageostrophic Winds and Vertical Motion Fields Accompanying Upper Level Jet Streak Propagation During the Red River Valley Tornado Outbreak. Preprints - Ninth Conference on Weather Forecasting and Analysis, Seattle, WA, Amer. Meteor. Soc., 424-429.

_____, 1985: A Diagnostic, Isentropic Analysis Package for the Short Term Prediction of Severe Convective Threat Areas. Preprints - Fourteenth Conference on Severe Local Storms, Indianapolis, IN, Amer. Meteor. Soc., 127-130.

_____, 1986: The Effect of Diabatic Heating/Cooling on Vertical Motions in the Severe Storm Environment. Preprints - Eleventh Conference on Weather Forecasting and Analysis, Kansas City, MO., Amer. Meteor. Soc., 211-216.

———, and P. D. Blakley, 1988: The Role of Frontogenetical Forcing and Conditional Symmetric Instability in the Midwest Snowstorm of 30-31 January 1982. *Mon. Wea. Rev.*, **116**, 2155-2171.

Montgomery, R. B., 1937: A Suggested Method for Representing Gradient Flow in Isentropic Surfaces. *Bull. Amer. Meteor. Soc.*, **18**, 210-212.

Namias, J., 1938: Thunderstorm Forecasting with the Aid of Isentropic Charts. *Bull. Amer. Meteor. Soc.*, **19**, 1-14.

———, J., 1939: The Use of Isentropic Analysis in Short Range Forecasting. *J. Aeronaut. Soc.*, **5**, 295-298.

———, J., 1940: An Introduction to the Study of Air Mass and Isentropic Analysis. Amer. Meteor. Soc., Boston, MA, edited by Robert G. Stone, 232 p.

Oliver, V. J., and M. B. Oliver, 1951: Meteorological Analysis in the Middle Latitudes. Compendium of Meteorology, Amer. Meteor. Soc., Boston, MA, 715-727.

Orlanski, I., 1975: A Rational Subdivision of Scales for Atmospheric Processes. *Bull. Amer. Meteor. Soc.*, **56**, 527-530.

Palmen, E., and C. W. Newton, 1969: Atmospheric Circulation Systems. Academic Press Inc., New York, Vol. 13, 195-227 p.

Petersen, R. A. and L. W. Uccellini, 1979: The Computation of Isentropic Trajectories Using a "Discrete Model" Approach. *Mon. Wea. Rev.*, 107, 566-574.

———, R. A., 1986: Detailed Three-Dimensional Isentropic Analysis Using an Objective Cross-Sectional Approach. *Mon. Wea. Rev.*, **114**, 719-735.

Rasmussen R., M. Politovich, J. Marwitz, W. Sand, J. McGinley, J. Smart, R. Pielke, S. Rutledge, D. Wesley, G. Stossmeister, B. Bernstein, K. Elmore, N. Powell, E. Westwater, B. B. Stankov, and D. Burrows, 1992: Winter Icing and Storms (WISP). *Bull. Amer. Meteor. Soc.*, **73**, 951-974.

Reed, R. J., 1955: A Study of a Characteristic Type of Upper-Level Frontogenesis. *J. Meteor.*, **12**, 226-237.

Reiter, E. R., 1972: Atmospheric Transport Processes, Part 3: Hydrodynamic Tracers. Atomic Energy Commission Critical Review Series, [NTIS TID-25731/LA] Springfield, VA 22161, 212 p.

———, E. R., 1975: Stratospheric-Tropospheric Exchange Processes. *Review of Geophysics and Space Physics*, **13**, 459-474.

Reuter, G. W. and M. K. Yau, 1990: Observations of Slantwise Convective Instability in Winter Cyclones. *Mon. Wea. Rev.*, **2**, 447-458.

Rossy, C. G., *et al.*, 1937: Isentropic Analysis. *Bull. Amer. Meteor.* **18**, 201-209.

Sanders, F. and L. F. Bosart, 1985: Mesoscale Structure in the Megalopolitan Snowstorm of 11-12 February 1983. Part I: Frontogenetical Forcing and Symmetric Instability. *J. Atmos. Sci.*, **42**, 1050-1061.

———, 1986: Frontogenesis and Symmetric Stability in a Major New England Snowstorm. *Mon. Wea. Rev.*, **114**, 1847-1862.

Saucier, W., 1955: Isentropic Analysis. Chap. 8 in Saucier, W., Principles of Meteorological Analysis, Chicago, IL, Univ. of Chicago Press, 438 p.

Shapiro, M. A., 1974: A Multiple Structured Frontal Zone-Jet Stream System as Revealed by Meteorologically Instrumented Aircraft. *Mon. Wea. Rev.*, **102**, 244-253.

———, M. A., 1976: The Role of Turbulent Heat Flux in the Generation of Potential Vorticity of Upper Level Jet Stream Systems. *Mon. Wea. Rev.*, **104**, 892-906.

———, M. A., 1980: Turbulent Mixing within Tropopause Folds as a Mechanism for the Exchange of Chemical Constituents between the Stratosphere and Troposphere. *J. Atmos. Sci.*, **37**, 994-1004.

———, M. A., A. J. Krueger, and P. J. Kennedy, 1982: Nowcasting the Position and Intensity of Jet Streams Using a Satellite-Borne Total Ozone Mapping Spectrometer. *Nowcasting*, K. A. Browning, Ed., Academic Press, 137-145.

Snook, J. S., 1992: Current Techniques for Real-Time Evaluation of Conditional Symmetric Instability. *Wea. and Forecasting*, **7**, 430-439.

Spilhaus, A. F., 1938: Isentropic Airplane Flights—A Suggestion. *Bull. Amer. Meteor. Soc.*, **19**, 279-280.

Staley, D. O., 1960: Evaluation of Potential Vorticity Changes near the Tropopause and the Related Vertical Motions, Vertical Advection of Vorticity, and Transfer of Radioactive Debris from Stratosphere to Troposphere. *J. Meteor.*, **17**, 591-620.

Uccellini, L.W., 1976: Operational Diagnostic Applications of Isentropic Analysis. *Nat. Wea. Dig.*, **1**, 4-12.

———, L. W., and D. R. Johnson, 1979: On the Coupling of Upper and Lower Level Jet Streaks and Implications for the Development of Severe Convective Storms. *Mon. Wea. Rev.*, **107**, 682-703.

———, L. W., D. Keyser, K. F. Brill and C. H. Wash, 1985: The President's Day Cyclone of 18-19 February 1979: Influence of Upstream Trough Amplification and Associated Tropopause Folding on Rapid Cyclogenesis. *Mon. Wea. Rev.*, **113**, 962-988.

Wallace, J. M., and P. V. Hobbs, 1977: *Atmospheric Science: An Introductory Survey*. Academic Press, New York, N.Y., 467 p.

Wilson, L. J., Siok, S. and B. Marois, 1980: Operational Application of Isentropic Analysis to the Diagnosis of Severe Convective Weather Threat Areas. Preprints - Eighth Conference on Weather Forecasting and Analysis, Denver, CO, Amer. Meteor. Soc., 166-173.

———, L. J., 1985: Isentropic Analysis - Operational Applications and Interpretation. Third edition, edited for Training Branch by James Percy. Atmospheric Environment Service, Canada, 35 p.